Contract No:

This document was prepared in conjunction with work accomplished under Contract No. 89303321CEM000080 with the U.S. Department of Energy (DOE) Office of Environmental Management (EM).

Disclaimer:

This work was prepared under an agreement with and funded by the U.S. Government. Neither the U.S. Government or its employees, nor any of its contractors, subcontractors or their employees, makes any express or implied:

1) warranty or assumes any legal liability for the accuracy, completeness, or for the use or results of such use of any information, product, or process disclosed; or
2) representation that such use or results of such use would not infringe privately owned rights; or
3) endorsement or recommendation of any specifically identified commercial product, process, or service.

Any views and opinions of authors expressed in this work do not necessarily state or reflect those of the United States Government, or its contractors, or subcontractors.

FY22
LABORATORY DIRECTED RESEARCH & DEVELOPMENT
ANNUAL REPORT

Savannah River National Laboratory®

Disclaimer

This work was prepared as an account of work sponsored by an agency of the United States Government. Neither the United States Government nor any agency thereof, nor any of their employees, nor any of their contractors, subcontractors or their employees, makes any warranty, express or implied, or assumes any legal liability or responsibility for the accuracy, completeness, or any third partys use or the results of such use of any information, apparatus, product, or process disclosed, or represents that its use would not infringe privately owned rights. Reference herein to any specific commercial product, process, or service by trade name, trademark, manufacturer, or otherwise, does not necessarily constitute or imply its endorsement, recommendation, or favoring by the United States Government or any agency thereof or its contractors or subcontractors. The views and opinions of authors expressed herein do not necessarily state or reflect those of the United States Government or any agency thereof, its contractors or subcontractors.

Message from the Laboratory Director and the Deputy Laboratory Director for Science & Technology

The mission of the Energy Department is to ensure America's security and prosperity by addressing its energy, environmental and nuclear challenges through transformative science and technology solutions. As DOE's Environmental Management (EM) stewarded national laboratory, the Savannah River National Laboratory (SRNL) supports the entire DOE complex in the safe cleanup of its environmental legacy resulting from nuclear weapons development and government-sponsored nuclear energy research. SRNL also supports DOE's National Nuclear Security Administration (NNSA) as it maintains the nation's nuclear stockpile and reduces the threat of nuclear proliferation around the world.

SRNL's Laboratory Directed Research and Development (LDRD) program invests in high-risk, potentially high-payoff activities foundational to our programmatic innovation for EM, NNSA and other offices of DOE. Specifically, our LDRD program supports the development of people and advancement of mission critical technologies through exploratory research.

This year, the laboratory established the Laboratory Director's Postdoctoral Research Fellow, a new postdoctoral researcher position supported through the LDRD program. These named postdoctoral fellows are driving SRNL's scientific and technical core competencies forward through their dedication to research and advancement of technologies.

The LDRD program continues to support postdoctoral researchers, a pipeline for exceptional research talent, through the distinguished Dwight D. Eisenhower Postdoctoral Research position. This report spotlights both the Dwight D. Eisenhower and Laboratory Director's Postdoctoral Research Fellows.

Demonstrated through publications and issued patents, research supported by the LDRD program once again yielded significant contributions to the SRNL's technical contributions to the global scientific community.

We invite you to learn more about the innovative science and engineering contributions of SRNL researchers described in this year's LDRD Annual Report.

Dr. Vahid Majidi
Laboratory Director

Dr. Sue Clark
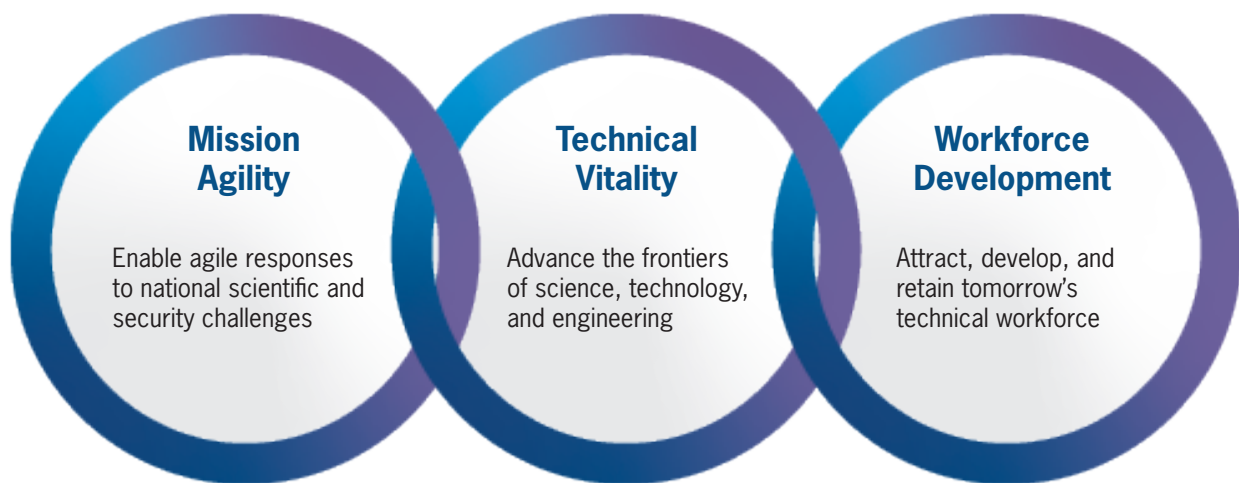Deputy Director, Science and Technology

Overview

The Laboratory Directed Research and Development (LDRD) program yields foundational scientific research and development (R&D) essential to growing SRNL's core competencies, in alignment with SRNL's Strategic Plan to provide long-term benefits to the Department of Energy (DOE), the National Nuclear Security Administration (NNSA), and other customers and stakeholders. Five strategic goals are outlined in SRNL's strategic plan:

1) Provide applied science and engineering for EM's active clean-up sites and LM's post closure management sites

2) Provide science-based solutions for gaps identified in nonproliferation strategic vision and support the government in activities impacting national security

3) Lead ST&E as the central technical authority for processing tritium loaded reservoirs and support production of plutonium pits

4) Align science and energy security programs by focusing modern modeling, simulation, and data analytics tools on materials engineering and performance applications

5) Build a workforce for the future

To fully achieve these strategic goals, SRNL must build upon its technical core competencies. SRNL's seven core competencies underpinning the laboratory's strategic goals include:

▸ Accelerating remediation, minimizing waste, and reducing risk

▸ Enabling next-generation nuclear material processing and disposition

▸ Creating manufacturing solutions for EM, NNSA, and energy security

▸ Assuring production and supply of strategic materials and weapons components

▸ Sensing, characterizing, assessing, and deterring nuclear proliferation

▸ Engineering new materials and their applications with data-driven modeling and simulation

▸ Securing connected control systems and associated data

SRNL has focused LDRD Program investments to expand and strengthen the SRNL core competencies. Each project aligns with one or more of the technical core competencies. In addition to supporting the SRNL's core competencies, each LDRD investment aligns with one or more of three overall program objectives:

Mission Agility

Enable agile responses to national scientific and security challenges

Technical Vitality

Advance the frontiers of science, technology, and engineering

Workforce Development

Attract, develop, and retain tomorrow's technical workforce

LDRD BY THE NUMBERS FY22

TOTAL PROJECTS

28

TOTAL PROGRAM COST

$6.55M

POSTDOCS FUNDED

29

PROJECTS LED BY EARLY-CAREER STAFF

17

POSTDOCS CONVERTED TO STAFF HIRES

3

PROJECTS INVOLVING POSTDOCS

22

PEER-REVIEWED PUBLICATIONS

28

PATENTS ISSUED

4

PATENT APPLICATIONS

8

INTELLECTUAL PROPERTY DISCLOSURES

9

PARTNERSHIPS & EXTERNAL ENTITIES ENGAGED

1) University of South Carolina
2) Georgia Institute of Technology
3) Clemson University
4) University of Georgia
5) Naval Research Laboratory
6) New Mexico Tech
7) Virginia Polytechnic Institute and State University
8) University of Nevada - Las Vegas
9) Coastal Carolina University

Contents

Developing the Future Workforce

The LDRD Program strengthens SRNL's future workforce pipeline by supporting postdoctoral researchers. Many postdoctoral researchers in the laboratory apply their scientific skillsets to solve complex technical challenges on LDRD projects. In turn, postdocs develop their professional research skills and build their scientific reputations through publication of their research findings.

Postdoctoral researchers are directly hired into the SRNL through named postdoctoral positions, specifically the Laboratory Director's Postdoctoral Research Fellow and the distinguished Dwight D. Eisenhower Postdoctoral Research Fellow.

SRNL's named postdoctoral fellows supported by LDRD during FY22 are highlighted below.

The Laboratory Director's postdoctoral research opportunity was established this year. Laboratory Director's postdoctoral researchers are experts in their field with a strong publication record. Individuals are hired into SRNL to support a specific project defined by their SRNL research advisor. Laboratory Director's postdoctoral researchers bring a high level of expertise to the LDRD research project, while learning from experienced researchers on how to succeed in the national laboratory R&D environment.

ALEX BRETAÑA
Laboratory Director's Postdoctoral Research Fellow, 2022-2024
Physics, University of Missouri

"I have learned more about how science gets done in the last 6 months than I did in the 6 years it took to get my Ph.D. I have learned how to write proposals in order to fund my ideas and future projects as well as conduct my research in a safe and responsible way. I have the opportunity to work with world class scientists and the facilities here at SRNL."
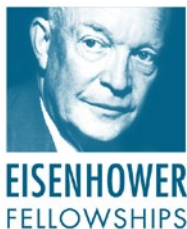
SRNL's Dwight D. Eisenhower postdoctoral research opportunity is the singular distinguished postdoctoral position. Candidates submit a proposal to pursue an independent research idea as part of the application process. The candidate selected for this highly competitive position is supported by LDRD funding to perform their proposed research.

"The Eisenhower fellow should be an expert in their field, dynamic and engaged with their lab community, ready and willing to offer their expertise and leadership where needed. The research I am conducting will be used to engineer lighter and better radiation detectors to keep our emergency responders, soldiers, and country safer."

JONATHON BAKER
Dwight D. Eisenhower Postdoctoral Research Fellow, 2021-2023
Materials Science and Engineering, NC State University

"My work as an Eisenhower Fellow kickstarted my career aiming to develop novel photochromic optoelectronic technologies. This research would not be possible elsewhere as it relies on the unique resources only available at SRNL."

COREY MARTIN
Dwight D. Eisenhower Postdoctoral Research Fellow, 2022-2024
Chemistry and Materials Science, University of South Carolina

Expanding Scientific Vitality

The Laboratory Directed Research and Development Program supported establishment of a mini arc melter capability at SRNL in FY22. This experimental investment was installed to specifically support the technical goals of project LDRD-2022-00132, *Topological magnetic textures in lanthanide- and actinide-based quantum materials*.

Equipped with a copper crucible and able to reach temperatures up to 3,500°C, this new capability expands the researcher's ability to study higher melting point alloys . and the range of future research opportunities at SRNL. Similar techniques, like induction melters, are limited to only 2000°C. Possible materials to synthesize include permanent magnets, topological quantum materials, and high-entropy alloys.

The MAM-1 mini arc melter is designed for melting samples up to 20 g. It has reliable contactless ignition of the arc and a small melting chamber. The arc melter has a built-in pumping system for evacuation of the melting chamber and argon gas connections to flush the chamber, allowing operation in an inert atmosphere.

Binod Rai and Alex Bretaña

The small melting chamber ensures fast evacuation and low gas consumption. Furthermore, the MAM-1 has molds of various shapes and sizes, allowing the user to cast different shaped alloys to support experiments on a wide range of materials of various shapes and sizes.

This state-of-the-art instrument expands SRNL's capabilities and SRNL's ability to address future high temperature materials mission needs.

FY22 FUNDED PROJECTS

Theoretical Evaluation of Point Defect Induced Charge Trapping Mechanisms in CdZnTe and CdZnTeSe

Jonathon N. Baker

Cadmium zinc telluride selenide is a promising next-generation material for room temperature semiconductor radiation detectors. This research uses advanced computational materials science to deeply understand performance limiting factors of this system, and their relationship with processing. In turn, this will enable a deep level of materials engineering on this system.

Introduction

Techniques for accurately calculating the concentrations and ionization states of point defects in compound semiconductors have advanced rapidly in the past 10 years. However, these methods have yet to be applied in any kind of systematic way to materials of interest for radiation detection, due to difficulties in curating the large scale of hybrid exchange-correlation functional DFT (Density Functional Theory) data required to inform the necessary thermodynamics calculations. Additionally, the already extreme computational expense of performing these types of simulations for line compound materials is exponentially increased when considering alloys.

Simultaneously, substantial improvements have been made to the CdZnTe (CZT) material system by adding selenium, especially in terms of crystal quality. These improvements and work to overcome fundamental hurdles facing CZT (e.g. substantial reduction of large amounts of sub-grain boundary networks and tellurium inclusions, and issues controlling alloy composition) have culminated in the development of CdZnTeSe (CZTS). However, point defect derived trap states and their relation to processing remain, at best, poorly understood. This research seeks to systematically apply the advances in computational techniques for studying point defects to current state of the art methods for producing CZT and CZTS. This will fill the void of information on defect chemistry in CZTS while also allowing for very detailed analysis of particular defects of interest and is expected to advance both defect science in CZT and CZTS, and computational science for the study of point defects.

Approach

Hybrid exchange correlation functional density functional theory (DFT) calculations (an advanced, high fidelity, and high computational expense method of treating the electron self-interaction in density functional theory) were performed for a large number of native and selenium-containing defects and defect complexes in ZnTe and CdTe, for use in projecting defect properties into lightly Se-doped CZT alloy, **Figure 1**. Alongside this effort, a thermodynamic model was derived for Traveling Heater Method growth of CZT and CZTS. The full set of point defect calculations and the thermodynamics model are taken together to calculate defect chemistry versus various processing and doping parameters via statistical mechanics methods. The vibrational properties of high population defects from these models were then calculated and fed back in to refine the statistical mechanics calculations. Additionally, special quasi-random structure (SQS) simulations were performed on various CZTS compositions to study alloy disorder effects versus changing composition.
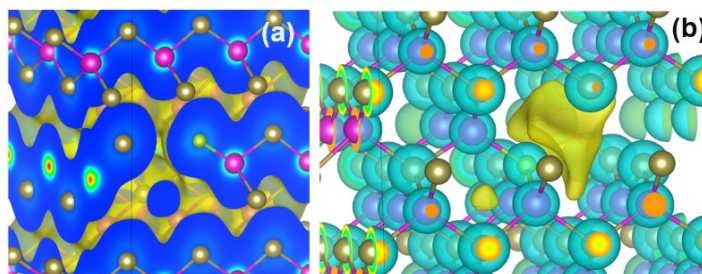
Figure 1: Hybrid functional DFT simulation of charge field (a) and potential field (b) in and around a v_{Cd}-Se_{Te} complex (Cd atoms shown in violet, Te atoms shown in tan, Se shown in green).

All DFT calculations were performed using VASP 6. The HSE06 exchange-correlation functional was used with the exact exchange amount tuned to CdTe and ZnTe for defect calculations, bandstructure calculations, and thermodynamic ground state reference calculations, while the PBE exchange-correlation functional was used to calculate the force constant matrices for defect vibrational properties, and for the SQS simulations. Force constant

matrices were post-processed using the Asphalt Minimal Phonon Library module, while data management and statistical mechanics analysis were enabled by the Asphalt Database and Point Defects Virtual Workbench modules. Initial preparation of SQS supercells was performed with the AT-AT Monte Carlo SQS module. Together, these approaches are being used to study the defect chemistry and property changes of CdTe, ZnTe, and CdZnTe with selenium concentrations varying between light doping and light alloying.

Accomplishments

- Vibrational properties of all high concentration native and selenium related point defects in CdTe and ZnTe were completed.
- High priority impurity defect simulations and their associated vibrational simulations were initiated
- Alloy projection of end-member datasets into alloy composition is currently in progress.
- Defect chemistry of THM-grown ZnTe and CdTe has been analyzed as a function of selenium content.

- A manuscript documenting the effects of selenium alloying on $Cd_{0.9}Zn_{0.1}Te$ host matrix lattice parameter variations and associated HR-XRD data was published and selected as a featured article.

Peer-reviewed Publications

Roy, U.N.; Baker, J.N.; Camarda, G.S.; Cui, Y.; Yang, G.; James, R.B.; Evaluation of crystalline quality of traveling heater method (THM) grown $Cd_{0.9}Zn_{0.1}Te_{0.98}Se_{0.02}$ crystals. *Appl. Phys. Lett.* 2022, *120*, 242103, **Figure 2**. https://doi.org/10.1063/5.0093255

Baker, J.N.; Roy, U.N.; Effects of Selenium Doping in Zinc Telluride from First Principles; *in press*

Intellectual Property

Invention Disclosure and Copyright submitted for BLAST software (Bond Length Analysis and Statistics Tool)

Team Members

Utpal Roy

Figure 2: (Figure and caption are a pre-publication version of Fig 3. of *Appl. Phys. Lett.* 2022, *120*, 242103, listed in Publications section above) Representative statistics of $Cd_{0.9074}Zn_{0.0926}Te$ and $Cd_{0.9074}Zn_{0.0926}Te_{0.9815}Se_{0.0185}$ alloy SQS simulations shown as ideal (110) interplanar spacing binned into 0.01 Å bins. Counts are of bonds of atoms within this simulation volume corresponding to the given (110) spacing bin. (a) Calculated interplanar spacings showing Cd–Te, Cd–Se, and Zn–Te sublattice spacings. Vertical dashed lines show the bond lengths in pure ZnTe and pure CdTe. Here, the sublattice interplanar spacing statistics are broken out by composition (columns) and sublattice type (rows). (b) and (c) Cd–Te sublattice statistics and (d) and (e) Zn–Te sublattice statistics.

Functionalized Cellular Magmatics

Cory Trivelpiece

Engineered cellular magmatics are an evolution of traditional foam glass technology. These materials are synthesized from post-consumer waste glass mined from landfills. This program is focused on leveraging Savannah River National Laboratory's (SRNL) core competencies in glass science and biotechnology to develop advanced ECMs for applications such as wastewater filtration and hydrocarbon remediation.

Introduction

SRNL has led the DOE national laboratory complex in the development of glass science and technology related to nuclear waste disposal. We are now using these skill sets to create novel materials, known as ECMs, which are a transformative advancement of traditional foam glass technology. Over 4 million tons of glass are disposed of in landfills annually in the United States including up to 85% of the post-consumer glass that is curbside "recycled" by citizens. Our program seeks to end this waste by upcycling the infinitely recyclable material that is glass into novel products that have wide-ranging applications.

We have two main areas of interest: 1) the fundamental science of ECM materials, and 2) biotechnological applications of ECMs. In terms of the fundamental ECM science, our efforts have centered on ECM fabrication and post-synthesis functionalization. Our interest in coupling biotechnology to ECMs stems from the need for advanced remediation and biomining technology. Efforts in this area focused on the growth of various species of biofilms on ECM substrates and processes to deploy these "biomagmatics" at industrial scales.

Successes in both areas have advanced our understanding of ECM technology significantly. Most importantly, this project has laid the groundwork for ending the disposal of "recycled" glass in landfills and developed novel materials for advanced applications.

Approach

We approached this program by simultaneously investigating both the inorganic (fundamental glass science) and organic (biotechnology) aspects of ECMs. Our inorganic track draws from glass science, geochemistry, and materials characterization to elucidate various aspects of fundamental ECM science. We employ characterization techniques such as differential scanning calorimetry, X-ray diffraction, and scanning electron microscopy coupled with advanced modeling based on machine learning to understand the mechanistic phenomena controlling foaming reactions and post-synthesis functionalization. Since the program inception, we have been interested in understanding the various mineralogical phases that form during synthesis and as a result of post-synthesis treatments. Primarily, we have focused our attention on the growth and characterization of zeolitic minerals for advanced filtration applications.

Our biotechnology track started by asking, "Can we grow biofilms on ECM substrates?" Since the beginning of the program, we have focused our biotechnology efforts on understanding the optimal conditions, including time, temperature, glass composition, etc., under which various biological species grow and proliferate on ECM surfaces. In addition, we have developed techniques to preserve and deploy these coupled systems at industrial scales. We also tested optimized combinations of ECMs and biofilms in specific applications to gauge the fundamental efficacy of the materials as well as the commercialization potential of the combinations.

From an organizational standpoint, many individuals have contributed to the success of these programs. A major organizational goal of this program was to include efforts from post-doctoral scholars. To date, we have supported the efforts of three post docs and one summer intern.

Accomplishments

The following list highlights some of the most significant achievements:

ECM fundamental science:

- Demonstrated the ability to reduce the concentration of NO - contamination in aqueous solution by approximately 20% with a starting concentration of 100 ppm using tailored ECMs – significantly higher than most environmental contamination levels
- Reduced the concentration of Ba^{2+} in a contaminated solution by 99% through what appears to be a co-reaction of precipitation and ion exchange
- Discovered potential mechanistic evidence indicating that ECM synthesis, in particular "foamability," is as dependent on batch mixture surface tension as viscosity, which was previously believed to be the main controlling factor of pore development
- Used post-synthesis treatment to grow targeted mineral phases on a variety of ECM compositions as well as delineated the compositional dependence of mineral phase development

Biotech:

- Developed an industrially scalable method for the growth, preservation, and deployment of biofilms on ECM substrates

Peer-reviewed Publications

Wilkinson, C.J.; Trivelpiece, C.L.; Mauro, J.C. Statistical Mechanical Modeling of Glass-forming Systems: A Practical Review Considering an Example Calcium Silicate System. Curr. Opin. Solid State Mater. Sci. 2022, 26 (5), 101018. DOI: 10.1016/j.cossms.2022.101018

Wilkinson, C.J.; Trivelpiece, C.L.; Hust, R.; Welch, R.S.; Feller, S.A.; Mauro, J.C. Hybrid Machine Learning/Physics-Based Approach for Prediction Oxide Glass-Forming Ability. Acta Mater. 2021, 221, 117432. DOI: 10.1016/j.actamat.2021.117432

Kugler, A., Brigmon, R., Trivelpiece, C. Foamed Glass Ceramics – an Upcycled Scaffold for Microbial Film Development. Biotechnol. Lett. Submitted – Under Review (SRNL Primary and Corresponding Author)

Trivelpiece, C.L.; Hsieh, M.C.; Stanfield, A.D.; Jolin, W.C.; Smith, R.J.; Missimer, D.M.; Housley, C.E.; Wilkinson, C.J.; Hust, R.M. A Novel Approach to Zeolite Synthesis and Support Using Upcycled Waste Glass. Mater. Today Sustainability. Submitted – Under Review (SRNL Primary and Corresponding Author)

Invited Presentation

Trivelpiece, C.L. From Nuclear Waste to Glass Sustainability: How SRNL is Saving the World Again. Glass Sustainability Conference. Alfred University, Alfred, NY. September 8-9, 2022

Intellectual Property

- POROUS GLASS-BASED MICROBIAL STORAGE AND DELIVERY SYSTEM (SRS-22-011) – patent pending
- METHODS AND ACTIONS OF MINERALIZING ENGINEERGED CELLULAR MAGMATICS (SRS-22-012) – non-provisional patent being drafted

Team Members

Austin Stanfield, Alex Kugler, Eric McCaslin, William Jolin, Madison Hsieh, Robin Brigmon, Catherine Housley, Whitney Riley, Jackson DeVault[a], Collin Wilkinson[b]

[a]Ohio University
[b]Alfred University

Fundamental U-235 Nuclear Resonance Spectroscopy

Jonathan Christian

Enriched uranium (U-235) is ubiquitous in the nuclear industry yet many of its fundamental properties have never been studied using magnetic resonance. To remedy this, we built a high frequency nuclear quadrupole resonance spectrometer that can measure the very high quadruple resonance signals of U-235.

Introduction

Conventional nuclear magnetic resonance techniques are ill-suited for characterizing U-235 due to the small gyromagnetic ratio and extremely large quadrupole moment of this spin $^7/_2$ isotope. Thus, we have designed and built a high-frequency nuclear quadrupole resonance spectrometer for measuring the quadrupole resonance of this important isotope. Our detection system uses a solenoid coil and capacitor design to produce and measure resonance frequencies as low as 500 kHz and as high as 3 GHz. To date, we have performed successful NQR measurements of several non-uranium materials that have quadrupole resonance signals as high as several hundred gigahertz. We continue to search for the quadrupole resonance signal of U-235, and we are hopeful the signal will be uncovered soon.

A successful nuclear quadrupole resonance measurement of ^{235}U would be a significant accomplishment and could yield valuable physical parameters such as chemical shifts, local electric field gradients, and through-bond and through-space internuclear couplings, all of which are directly related to local structure. These terms can be used to understand structural details of poorly characterized uranium materials and can improve computational models of uranium for which accurate reference data is lacking.

Approach

Because the quadrupole moment of nuclei is orientation-dependent, we first developed robust synthetic techniques for producing high quality single crystals of different uranium compounds with varying levels of U-235. We also produced crystals of uranyl nitrate that contained up to 50% N-15 to support NMR analysis. We then designed and built a high frequency NQR spectrometer with a robust solenoid coil detection system. The NQR spectrometer was installed within SRNL's Category II Nuclear Facility in FY22. After functional and benchmark testing of our NQR spectrometer using chemical standards, enriched uranium-containing samples were analyzed and are still undergoing analysis as of the end of FY22. Some follow-on funding has been acquired to support additional development of this research program.

Accomplishments

- Designed and built a novel high frequency NQR spectrometer capable of measuring resonance signals up to several gigahertz
- Performed functional and benchmark tests of the high frequency NQR spectrometer up to several hundred gigahertz using validated chemicals
- Published two peer-reviewed manuscripts on uranium tetrafluoride
- Performed extensive N-15 NMR measurements of depleted uranyl nitrate hexahydrate crystals
- Performed preliminary N-15 NMR measurements of enriched uranyl nitrate hexahydrate crystals
- Found that N-15 NMR measurements should aid in understanding how U-235 affects the NMR spectra of neighboring nuclei; prepared a draft manuscript on this subject
- Delivered a presentation at the 22nd International Society of Magnetic Resonance Conference
- Installed and operated our high-frequency NQR spectrometer in SRNL's Category II Nuclear Facility in FY22
- Designed a solenoid and capacitor high frequency generation and detection system that delivers significant operational flexibility for a variety of zero-field spectroscopic experiments

- Equipped multiple radiological laboratory spaces for chemical synthesis
- Developed robust methods for the synthesis of multiple uranium-bearing single-crystals
- Procured depleted and highly enriched uranium certified reference materials

Peer-reviewed Publications

Christian, J. H.; Klug, C. A.; DeVore, M.; Villa-Aleman, E.; Foley, B. J.; Groden, N.; Baldwin, A. T.; Wellons, M. S., Characterizing the solid hydrolysis product, UF4(H2O)2.5, generated from neat water reactions with UF4 at room temperature. *Dalton Transactions* **2021,** *50* (7), 2462-2471

Foley, B. J.; Christian, J. H.; Klug, C. A.; Villa-Aleman, E.; Wellons, M. S.; DeVore, M.; Groden, N.; Darvin, J., Probing the hydrolytic degradation of UF4 in humid air. *Dalton Transactions* **2022,** *51* (15), 6061-6067

Team Members

Jason Darvin, Bryan Foley, Garret Gothelf and Nicholas Groden, Christopher Klug[a]

[a] United States Naval Research Laboratory

Figure 1: Savannah River National Laboratory new NQR spectrometer installed in a radiological laboratory to facilitate measurements with enriched uranium and other radioactive materials.
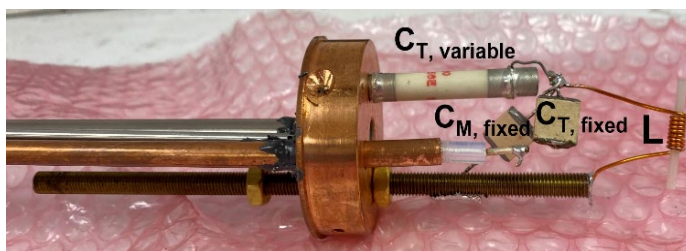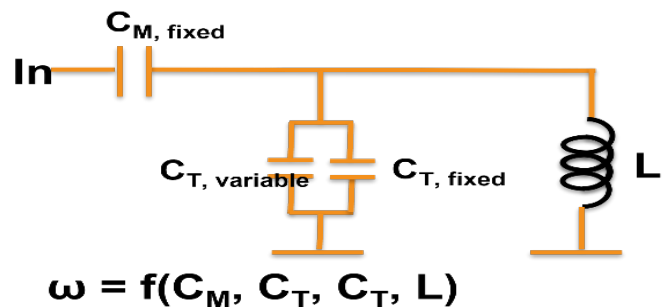

$$\omega = f(C_M, C_T, C_T, L)$$

Figure 2: *Top:* Electrical diagram demonstrating the design of the high frequency NQR solenoid and capacitor system; *Bottom:* A photograph of the high frequency NQR solenoid and capacitor system with a sample placed inside a tube inside the solenoid coil (labeled L)

Figure 3: SRNL researchers evaluate newly created uranium-containing single crystal compounds in a radiological laboratory.

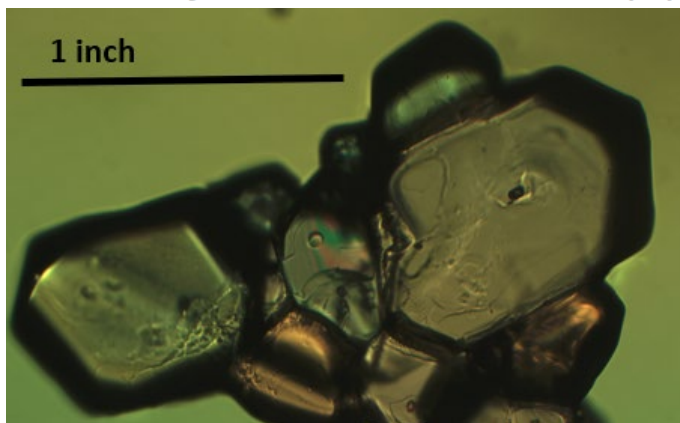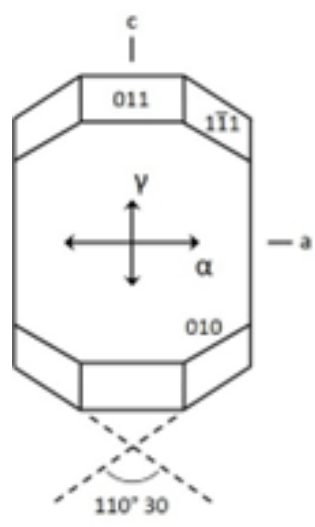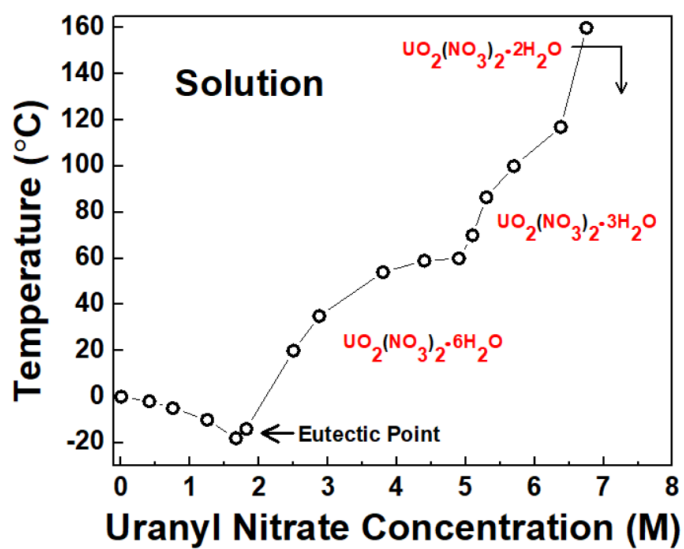**Figure 4.** *Top left*: The phase diagram of uranyl nitrate was used to develop a robust method for producing high quality single crystals of $UO_2(NO_3)_2{\cdot}6H_2O$; *Bottom left*: Micrograph of multiple single crystals of $UO_2(NO_3)_2{\cdot}6H_2O$; *Top right*: Illustration of the crystallographic shape and axes for $UO_2(NO_3)_2{\cdot}6H_2O$ crystals.


Kori McDonald

Microbially Influenced Separation of Uranium Isotopes

Beth Lewczyk

The main objectives of this project are to explore the possibility of microbially mediated isotopic separation through means of dissimilatory metal reducing microorganisms and to adapt that process to high assay low enriched uranium production through the use of spent nuclear fuel, which would be accomplished via the removal of the neutron poison, U-236.

Introduction

Currently, many studies of uranium isotopic separation focus on the separation of U-235/U-238 without taking into consideration U-236. By looking at separating U-236 there is added technical difficulty as U-236 is generally seen concentrating alongside U-235. Moreover, U-236 is found only in spent nuclear fuel (SNF) and reprocessed uranium, giving the Savannah River National Laboratory (SRNL) a unique opportunity to use its available reserve of materials to perform microbiological separations of U-236 from SNF. The methods of uranium isotopic separation currently in place are limited while demands for high assay low enriched uranium (HALEU) are expecting to reach almost 600 MT by 2030 as estimated in **Figure 1** from a letter from the Nuclear Energy Institute (NEI) to Energy Secretary Perry in 2018.
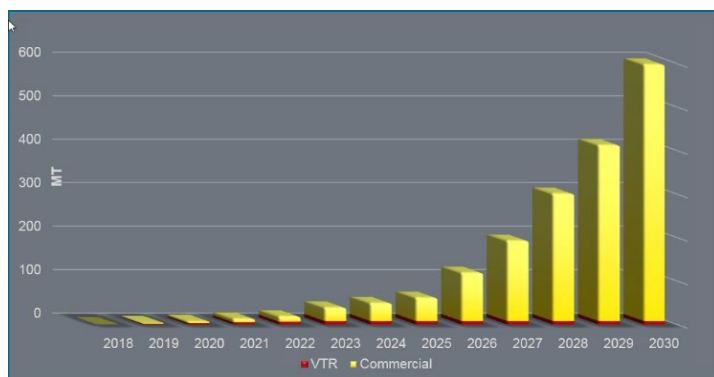
Source for Industry Demand: Nuclear Energy Institute's letter to Secretary Perry, DOE (July 5, 2018)

Figure 1: Estimated Commercial HALEU Market Needs by 2030

Having an additional method of HALEU production is imperative for SRNL as the electrochemical processing is only estimated to deliver approximately 5 MT of 19.75% U – 10 wt% Zr fuel by 2023, and by 2020 the hybrid zirconium extraction process (ZIRCEX) is only at a ¼ scale facility, leaving a wide margin of need left unfulfilled. Leveraging the ability of select microorganisms to separate uranium isotopes is a way to help alleviate the increasing need for HALEU production while advancing SRNL's potential in the field of microbial heavy metal reduction, by looking specifically at U-236, then applying the process to reactor fuel production. This project aims to determine potential for U-236 separation using microorganisms.

Approach

Dissimilatory metal reducing microorganisms (DMRM) are being looked at more frequently for environmental remediation in water sources to decrease metal ion mobility, and it has been found that a large category of microorganisms can assist in bioremediation through heavy metal ion adsorption and metal reduction capabilities. Bacterial reduction of soluble U(VI) to insoluble U(IV) leads to preferential partitioning of U-238 in the U(IV) solids. To our knowledge, the use of DMRM for the intended application of removing U-236 from SNF is a novel approach. Selected microorganisms were cultured and tested for iron reduction as a surrogate test prior to using uranium. The microorganisms were then incubated at 30°C for a period of 96 hours in a specially formulated media solution under anaerobic conditions with uranium in the form of uranyl nitrate or uranyl acetate. A diagram of the testing apparatus is shown in **Figure 2**. The uranyl nitrate was made using highly enriched uranium, while the uranyl acetate was made using depleted uranium. The media solution provides proper nutrients for the microorganisms' survival and encourages metal reduction. At different time points, samples were taken in triplicate to determine at what time in the metal reduction process the most fractionation is occurring. In this environmental condition, the microorganisms are expected to reduce the soluble uranium, creating a precipitate with a degree of isotopic fractionation due to the nuclear volume effect.

The precipitate will ideally be enriched with the lighter isotope, compared to the starting material. Samples are being analyzed using inductively coupled plasma mass spectrometry to determine the isotopic ratio at each time point.

Figure 2: Testing Apparatus Diagram

Accomplishments

- Completed iron reduction testing with a crystalline iron oxide in two different media solutions for *Shewanella sp.* Results in **Figure 3** from the iron reduction test show that the formulated media for uranium reduction testing is appropriate and does not inhibit metal reduction.
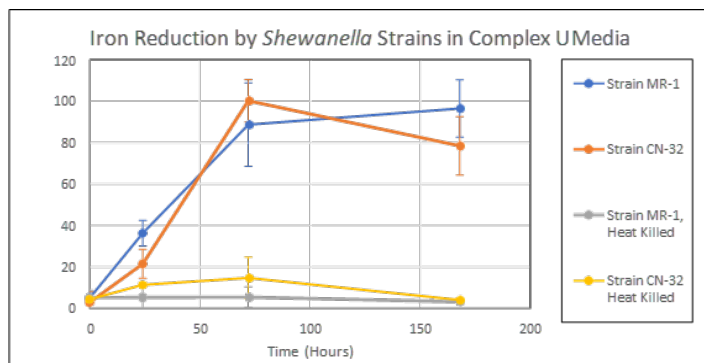
Figure 3: Iron Reduction by *Shewanella* Strains in Complex U Media

- Determined that uranium metal reduction and subsequent isotopic fractionation was undetectable when using uranyl nitrate as an electron acceptor for *Shewanella sp.* This result is in line with existing literature and the iron reduction test.
- Achieved uranium metal reduction with the use of uranyl acetate as an electron acceptor for *Shewanella sp.*

- Preliminary analytical results with uranyl acetate show no isotopic fractionation between timepoints 10 hours and 24 hours using a U235/U238 isotopic ratio.
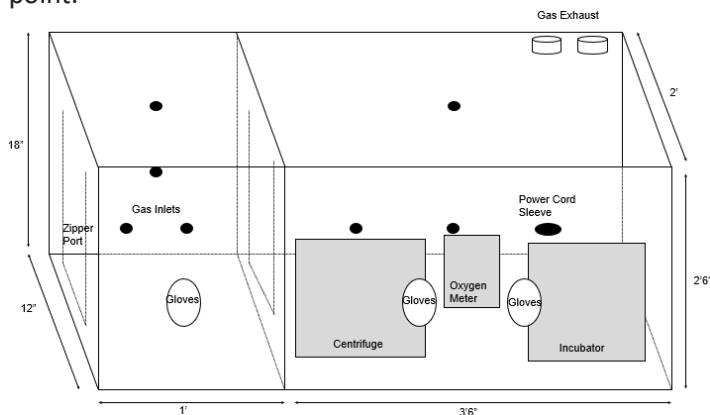
Team Members

Nathanial Losey and Alex Kugler

Unraveling the Mysteries of "Magic" Ionization: A Basic Science Approach to Understand Ionization Matrix

Danielle Mannion

Matrix-Assisted Ionization is a new and highly promising mass spectrometry technique for rapid analysis of uranium; however, the chemistry and physics underlying this ionization mechanism are largely unknown. This effort seeks to understand the fundamental ionization phenomena by characterizing both ionization matrix materials themselves and analyte chemistry ionization trends.

Introduction

Ambient mass spectrometry is a collection of methods for the rapid detection and characterization of trace inorganic analytes with minimal sample preparation. Matrix-Assisted Ionization (MAI) is one of the most recently discovered ambient mass spectrometry techniques, wherein ions are produced without the application of heat, photons, electrons, or high voltage as required for conventional mass spectrometry, *Figure 1*).[1, 2] Although SRNL was the first to demonstrate that this technique could be used to ionize inorganic compounds in aqueous solutions, [3] the underlying ionization phenomena remains uncharacterized.[1, 4-10] This effort seeks to examine fundamental aspects of MAI via a combination of mass spectrometry experiments, x-ray diffraction of MAI matrix chemicals, and modeling/simulation. This research will shed light on this fascinating ionization phenomena and could lead to sensitivity and accuracy gains to inform future development of fieldable mass spectrometry methods.

The first year of the project encompassed 1) instrument familiarization and parameter optimization for inorganic analytes, 2) mass spectrometry studies to investigate the origin of previously identified matrix derived ions, and 3) procurement and light microscopy of various MAI matrix compounds. The second year of the project focused on understanding the effect of periodic table trends on ionization through mass spectrometry comparison studies of the lanthanides. MAI matrix chemicals were screened for their ability to ionize cerium to determine matrix impact on ion production. The impact of matrix crystal size on ion abundance was also investigated.

Lastly, the crystal structure of one MAI matrix was solved and modeling/simulation was undertaken to identify intermolecular interactions.
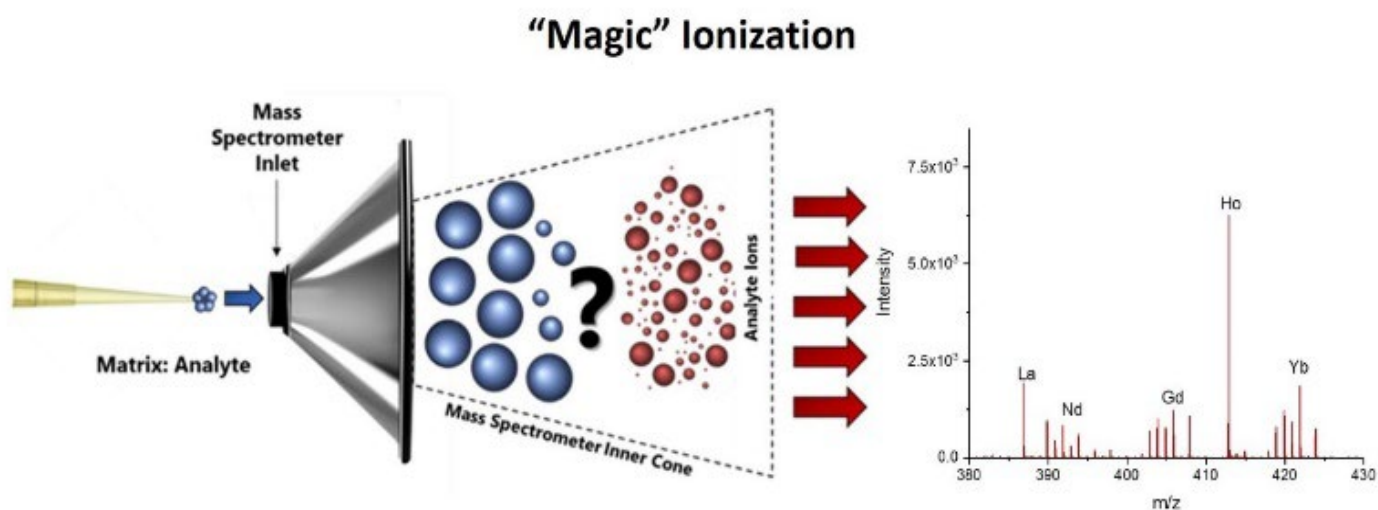

Figure 1: Schematic of matrix-assisted ionization (i.e., magic ionization) showing how introducing a matrix-analyte mixture into the mass spectrometer orifice results in analyte ion production.

Approach

The objective of this project was to investigate the MAI inorganic ionization mechanism through systematic experimentation and to develop a testable theory for the inorganic ionization process. A key part of developing an ionization theory is to develop and understand the factors of an MAI formalization equation as shown in *Equation 1*. The main investigative avenues of this project are to characterize the influence of matrix and analyte properties on MAI ionization. Initial instrument optimization was performed to determine the parameters and sample introduction methods that resulted in high reproducibility and ion sensitivity. Additionally, an RStudio data processing suite was developed to standardize and expedite data analysis.

Equation 1: Concept of the MAI formalization equation, with key investigative factors that are the focus of this work in brackets.

$$\frac{N_+}{N_0} \propto E_{MS} \, [M_F] \, DF \, [A_F]$$

E_{MS} is Mass Spectrometer Ion Transmission Efficiency
M_F is the Matrix Factor
DF is the Driving Force
A_F is the Analyte Factor

To investigate the matrix factor, the chemical matrix 3-nitrobenzonitrile (3-NBN) was studied as a model matrix. This chemical was examined via mass spectrometry analysis using three ionization methods, *Figure 2*, and collision induced dissociation (CID) to determine the origin of matrix-derived ions. Single-crystal X-ray diffraction (SC-XRD) was performed to determine crystal structure, *Figure 3,* and subsequent modeling/simulation was done to determine intermolecular contacts. Mass spectrometry experiments were also conducted to 1) investigate the impact of matrix crystal size on ion production and 2) examine other MAI matrix chemicals for cerium ionization, *Table 1*. To investigate the analyte factor, the lanthanide series of elements were selected for spectrometric analysis due to their well characterized physical and chemical trends. Comparative MAI and electrospray ionization (ESI) analysis was performed on solutions of single element lanthanide nitrates to determine if similarities exist between the two ionization methods.
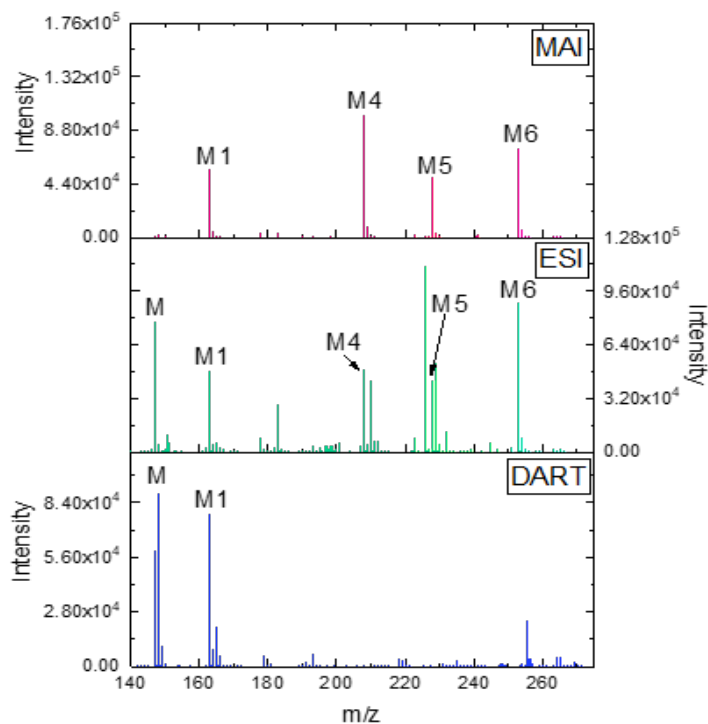

Figure 2: Mass spectra generated from 3-NBN using three mass spectrometry methods: (*Top*) matrix-assisted ionization, (*Middle*) electrospray ionization, and (*Bottom*) direct analysis in real time.
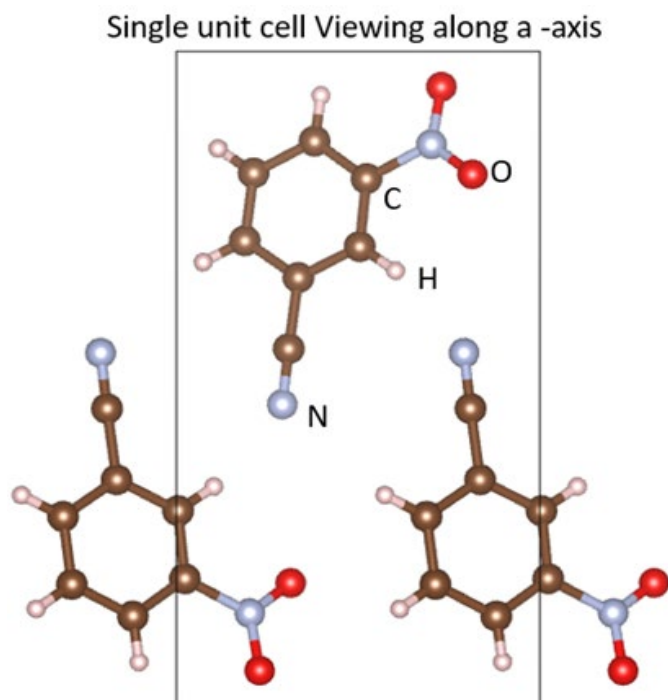

Figure 3: Single unit cell of the 3-NBN crystal structure based on SC-XRD crystallographic data.

MAI Matrix Name	Cerium Detected (+ mode)	Cerium Detected (- mode)
1,2-Dicyanobenzene	Yes	Yes
1,2-Dinitrobenzene	No	Yes
1,4-Dihydroxy-2,6-dimethoxybenzene	No	No
2-Bromo-2-nitro-1,3-propanediol	No	No
2-Bromo-3-nitroacetophenone	No	No
2-Hydroxy-5-nitroacetophenone	Yes	No
2-Methyl-2-nitro-1,3-propanediol	No	Yes
2-methyl-5-nitrobenzonitrile	No	Yes
2-Napthol	No	Yes
2-Nitrobenzontrile	No	Yes
3,6-Dibromocarbazole	No	Yes
3-Nitrobenzoyl chloride	No	No
4-Aminophthalonitrile	No	No
4-Hydroxy-3-nitrocoumarin	No	No
4-Methyl-3-nitroaniline	No	Yes
4-methylphthalonitrile	No	No
5-Bromo-3-nitropyridine-2-carbonitrile	No	No
5-Nitroindole	Yes	Yes
9-vinylcarbazole	No	No
Coumarin	No	Yes
Methyl-2-methyl-3-nitobenzoate	Yes	No
Phthalic anhydride	Yes	No

Table 1: Results of MAI matrix screening test to assess for cerium ionization in positive and negative ionization modes.

Accomplishments

- Demonstrated that 3-NBN matrix-derived ions are formed within the first few centimeters of the instrument and are created from the MAI process.
- Resolved the crystal structure of 3-NBN using SC-XRD, a previously unknown structure.
- Discovered that two matrix-derived ions are detected in ion complexes with lanthanides using MAI. There is no evidence that these complexes form in solution.
- Demonstrated that various MAI matrix chemicals ionize cerium in both positive and negative ion modes.

- Analyzed and detected a selection of transition metals using MAI in negative ion mode (copper, cobalt, nickel, palladium, scandium, yttrium, zinc, and zirconium).
- Determined that MAI ion abundance of the lanthanides correlates with various chemical properties in a similar manner to complimentary ESI studies, **Table 2**.

Linear Correlation Analysis

Ionization Technique	Ratio of Interest	Atomic Number	(Ln–O) Dissociation Energy	Nitrate Solubility	Ionic-Radius	Electro-Negativity
ESI-MS	$[Ln(NO_3)_4]^-$ /$[^{153}Eu(NO_3)_4]^-$	0.95	-0.82	-0.93	-0.94	0.94
MAI-MS	$[Ln(NO_3)_4]^-$ /$[^{153}Eu(NO_3)_4]^-$	0.83	-0.81	-0.62	-0.84	0.80

Table 2: Results of a linear correlation analysis to examine correlations between lanthanide ionization trends and periodic table trends. ESI data shows clear correlation between lanthanide ionization and periodic table trends, but no significant correlation is observed with MAI. Legend: The numerical value is r calculated with the Person method. All data exhibits a p-value < 0.001.

- Produced convincing evidence that inorganic ion formation using MAI is driven by a different mechanism than in ESI ion formation.
- Demonstrated that inorganic ion abundance appears inversely related to matrix crystal size suggesting a matrix crystal surface area impact, **Figure 4**.

Peer-reviewed Publications

- Understanding Matrix-Assisted Ionization Through an Investigation of the Lanthanides. Submitting to *Journal of the Analytical Chemical Society,* 2022.
- Uranium Isotopic Analysis with Matrix-Assisted Ionization. Submitting to *Analytical Chemistry,* 2022.
- Characterization of 3-Nitrobenzonitrile as a Model Matrix-Assisted Ionization Matrix. Submitting to *Chemistry of Materials*, 2022.
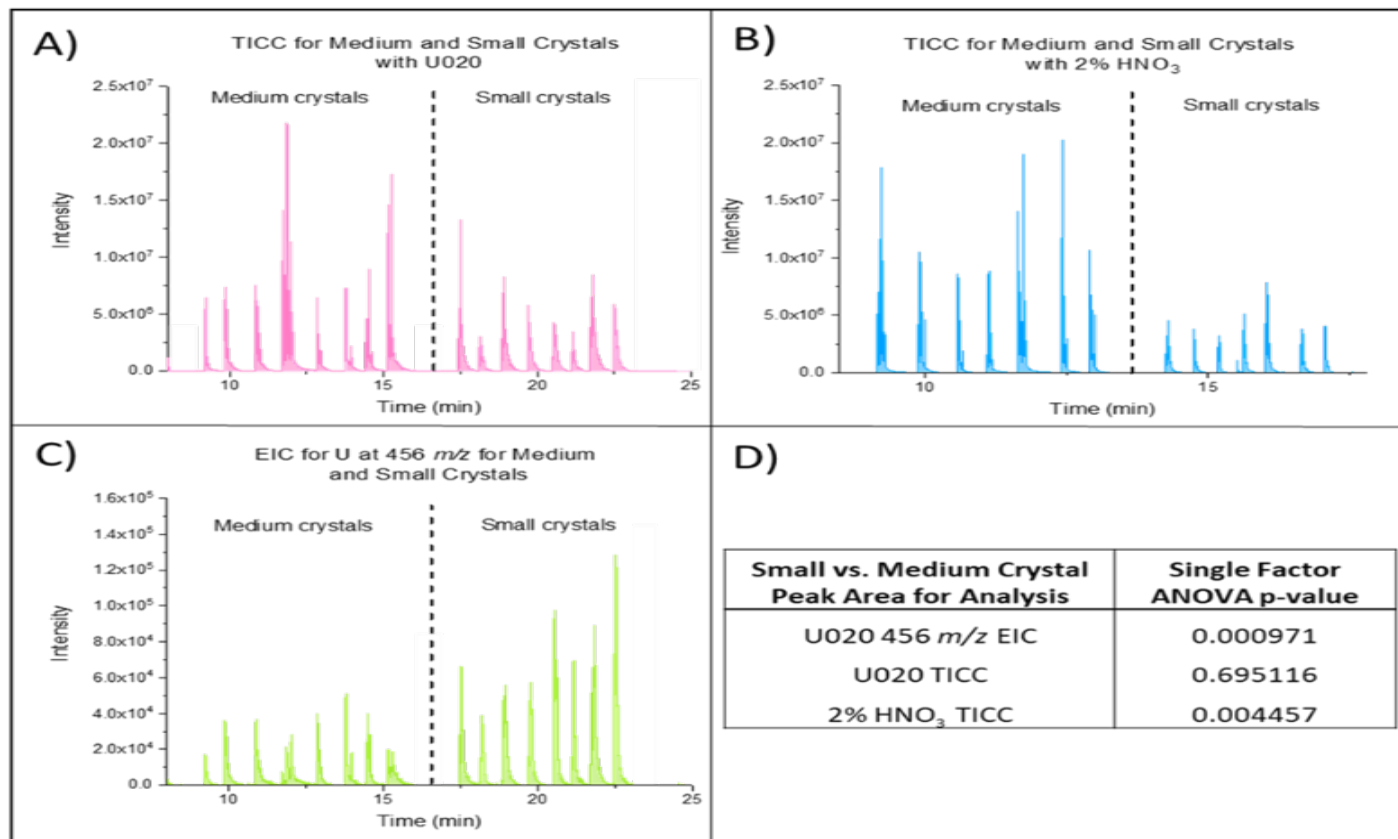
Figure 4: Experimental results of the impact of crystal size on inorganic analyte ionization: A) total ion current chromatogram (TICC) produced by two crystal sizes with a uranium spike, B) TICC produced by two crystals with a 2% nitric acid spike, C) extracted ion chromatogram (EIC) of the primary uranium peak produced from analysis A, and D) single-factor ANOVA results for peak areas generated from A, B, and C to determine if the difference between crystal size populations is significant.

Conference Presentations

- Matrix-Assisted Ionization Mass Spectrometry for the Detection and Characterization of Uranium Species. The Great Scientific Exchange (SciX) 2021 Conference, Providence, RI September 26-October 1, 2021. Invited Oral Presentation.
- Matrix-Assisted Ionization and Quantitative Analysis of Uranium Isotopic Composition and Assay by AccuTOF Time-of-Flight Mass Spectrometry. 69th American Society for Mass Spectrometry (ASMS) Conference on Mass Spectrometry and Allied Topics, Philadelphia, PA October 31-November 4, 2021. Oral Presentation.
- Matrix-Assisted Ionization Mass Spectrometry for Uranium Measurement in Field Environments. 12th International Conference on Methods and Applications of Radioanalytical Chemistry (MARC), Khona, HI April 3-8, 2022. Oral Presentation.

- Matrix-Assisted Ionization Time-of-Flight Mass Spectrometry of Lanthanides. 70th American Society for Mass Spectrometry (ASMS) Conference on Mass Spectrometry and Allied Topics, Minneapolis, MN June 5-9, 2022. Poster Presentation.

Funding Agency Presentations

- Matrix-Assisted Ionization Mass Spectrometry for the Detection and Characterization of Uranium Species. NA-22 Brown Bag Seminar, Virtual Presentation, November 16, 2021. Invited Oral Presentation.
- Matrix-Assisted Ionization Mass Spectrometry for the Detection and Characterization of Uranium in Austere Environments. NA-24 Research Seminar, Virtual Presentation, June 22, 2022. Invited Oral Presentation.

Team Members

Abigail (Abby) Waldron and Elizabeth (Betsey) Pettit

References

Trimpin, S.; Inutan, E. D., Matrix assisted ionization in vacuum, a sensitive and widely applicable ionization method for mass spectrometry. *Journal of The American Society for Mass Spectrometry* 2013, *24* (5), 722-732.

Trimpin, S., "Magic" ionization mass spectrometry. *Journal of the American Society for Mass Spectrometry* 2016, *27* (1), 4-21.

Mannion, D. R.; Mannion, J. M.; Kuhne, W. W.; Wellons, M. S., Matrix-Assisted Ionization of Molecular Uranium Species. *Journal of the American Society for Mass Spectrometry* 2020, *32* (1), 8-13.

Inutan, E. D.; Trimpin, S., Matrix assisted ionization vacuum (MAIV), a new ionization method for biological materials analysis using mass spectrometry. *Molecular & Cellular Proteomics* 2013, *12* (3), 792-796.

Lee, C.; Inutan, E. D.; Chen, J. L.; Mukeku, M. M.; Weidner, S. M.; Trimpin, S.; Ni, C. K., Toward understanding the ionization mechanism of matrix-assisted ionization using mass spectrometry experiment and theory. *Rapid Communications in Mass Spectrometry* 2019.

Trimpin, S.; Lutomski, C. A.; El-Baba, T. J.; Woodall, D. W.; Foley, C. D.; Manly, C. D.; Wang, B.; Liu, C.-W.; Harless, B. M.; Kumar, R., Magic matrices for ionization in mass spectrometry. *International Journal of Mass Spectrometry* 2015, *377*, 532-545.

Trimpin, S.; Lu, I.-C.; Rauschenbach, S.; Hoang, K.; Wang, B.; Chubatyi, N. D.; Zhang, W.-J.; Inutan, E. D.; Pophristic, M.; Sidorenko, A., Spontaneous charge separation and sublimation processes are ubiquitous in nature and in ionization processes in mass spectrometry. *Journal of The American Society for Mass Spectrometry* 2018, *29* (2), 304-315.

Trimpin, S.; Lee, C.; Weidner, S. M.; El-Baba, T. J.; Lutomski, C. A.; Inutan, E. D.; Foley, C. D.; Ni, C. K.; McEwen, C. N., Unprecedented ionization processes in mass spectrometry provide missing link between ESI and MALDI. *ChemPhysChem* 2018, *19* (5), 581-589.

Trimpin, S.; Inutan, E. D.; Karki, S.; Elia, E. A.; Zhang, W.-J.; Weidner, S. M.; Marshall, D. D.; Hoang, K.; Lee, C.; Davis, E. T., Fundamental studies of new ionization technologies and insights from IMS-MS. *Journal of The American Society for Mass Spectrometry* 2019, *30* (6), 1133-1147.

McEwen, C. N.; Inutan, E. D.; Moreno-Pedraza, A.; Lu, I.-C.; Hoang, K.; Pophristic, M.; Trimpin, S., Sublimation driven ionization for use in mass spectrometry: mechanistic implications. *Journal of the American Society for Mass Spectrometry* 2020, *32* (1), 114-123.

Molecular Radiation Resistance Markers in Microorganisms

Brady Lee

Research will help with understanding of microbiological response mechanisms with respect to radiation resistance and associated genetic loci for response to radiation in individual prokaryotes and microbial communities. Environmental isolates involved in radionuclide biotransformation will also be tested for radiation resistance, in efforts to understand how metabolism in these environments can be improved through higher survival rates in the presence of ionizing radiation. Identification of important genetic determinants and microbes with a range of radiation resistance will allow for future development of biosensors for application for nonproliferation, environmental, and medical purposes.

Introduction

Radiation resistance is a trait common across all domains of life, yet molecular resistance mechanisms are not well understood. The objective of the proposed work is to understand how expression of single-stranded deoxyribonucleic acid binding proteins are central to radiation resistance. Expression of single-stranded deoxyribonucleic acid binding proteins in a highly-radiation resistant microorganism is hypothesized to be a model of radiation resistance across the three domains of life. Expression of genes encoding these proteins and associated regulators was analyzed in the radiation resistant prokaryote, *Halobacterium salinarum* NRC-1. In addition, radiation resistance in environmental isolates used for radionuclide transformation will also be determined. Signatures that are part of this mechanism are important to the Department of Energy because the information can then be used as a signature for radiation biology, non-proliferation, and improved remediation processes, and preventing corrosion in nuclear storage environments.

Approach

Research goals were accomplished using a combined molecular biology and microbial growth approaches. In order to determine the effect of this large insertion on the expression of three RPA homologs in *Halobacterium*, these

regulators and the region containing the mutation were deleted, **Figures 1 and 2,** and analyzed for changes in the expression of *rfa1*, *rfa2*, and *rfa3* through quantitative PCR. In addition, experiments were performed to monitor changes in growth characteristics associated with gene deletion. Strain designation keys are shown in **Table 1**. Plasmids constructed are shown in **Table 2**. Known strains of metal and radionuclide reducing bacteria were exposed to varying levels of ionizing radiation and then grown to determine levels of radiation resistance in these species.
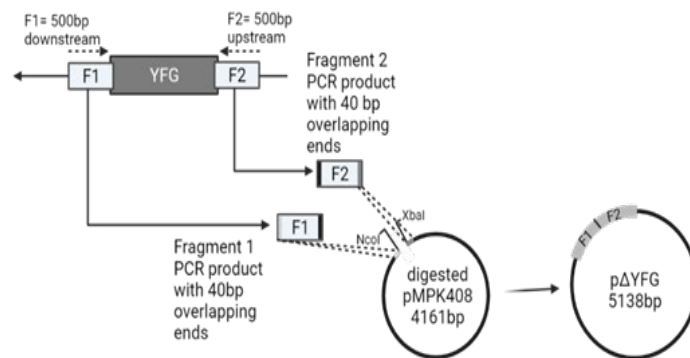

Figure 1: Schematic outlining the creation of deletion plasmids. The suicide vector pMPK408 was used in a Gibson Assembly. "YFG" is a placeholder for the gene/region of interest.
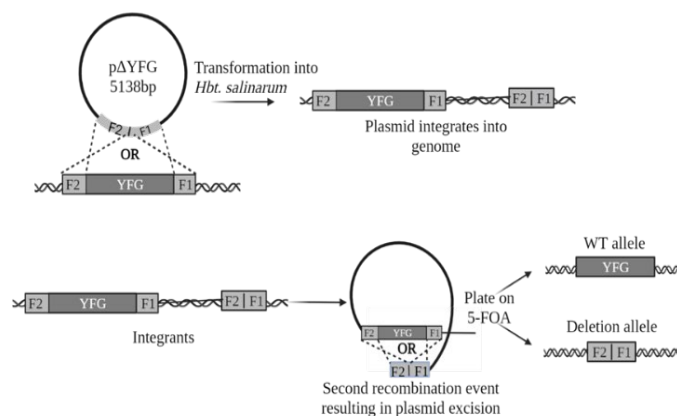

Figure 2: Schematic of the homologous recombination events in the established pop-in-pop-out method of gene replacement (Peck et al, 2000). This method can result in either the retention of the wild-type allele or the replacement by the deletion allele.

Hbt. salinarum strain	Genotype	Source
NRC-1	Wild type	Gift from S. DasSarma
LH101	As NRC-1, but Δura3	Laboratory stock
LH102	Δura3 derivative of radiation resistant mutant LH5	Laboratory stock
LH103	Δura3 derivative of radiation resistant mutant LH6	Laboratory stock
LH 184	As LH103, but Δvng155	This study
LH185	Isogenic to LH184, but vng155+	This study
LH186	As LH101 but Δecp	This study
LH187	Isogenic to LH186, but ecp+	This study
LH188	As LH102 but Δecp	This study
LH189	Isogenic to LH188, but ecp+	This study
LH190	As LH103 Δecp	This study
LH191	Isogenic to LH190, but ecp+	This study
LH192	As LH101 but Δerc	This study
LH193	Isogenic to LH192, but erc+	This study
LH196	As LH101, but Δvng155-160	This study
LH197	Isogenic to LH192, but vng155-160+	This study
LH198	As LH103, but Δvng155-160	This study
LH199	Isogenic to LH194, but vng155-160+	This study

Table 1: Strains used in studies for **Tables 4-5** and **Figures 3-6**.

Plasmid	Description	Source
pMPK408	Litmus 28 (NEB)-based plasmid containing ura3; suicide vector for Halobacterium	Peck et al., 2000
pKQP1	pMPK408 containing Δerc allele	This study
pKQP2	pMPK408 containing Δecp allele	This study
pHTL150	pMPK408 containing Δprtr1 allele	This study
pHTL155	pMPK408 containing Δvng41 allele	This study
pHTL156	pMPK408 containing Δvng41 - tnp1	This study

Table 2: Plasmids used to knockout selected genes in *Halobacterium*. Construction is shown in **Figure 1**. Resulting strains are listed in **Table 1**.

Accomplishments

- Tools were developed using Gibson Assembly, **Figure 1**, and established methods, **Figure 2**, to generate knockout alleles of loci potentially involved in radiation resistance in *Halobacterium*
- Demonstrated the co-transcription of two potential regulatory genes in *Halobacterium* and the extent of leader transcript, **Figure 3**.
- Microbes known to metabolize and concentrate radionuclides demonstrated varying levels of radiation resistance, **Table 3**.
- Determined that radiation resistance may be attributed to multiple factors working in unison and that regulators for single-stranded DNA binding proteins are likely located in other areas of the genome, **Figure 4; Tables 4 and 5**.
- A deletion in the gene encoding an ATP-dependent RNA helicase homolog caused changes in growth along with changes in expression of RPA genes, **Figures 5-7**.
- Isolated new halophilic species for additional testing and genome sequencing
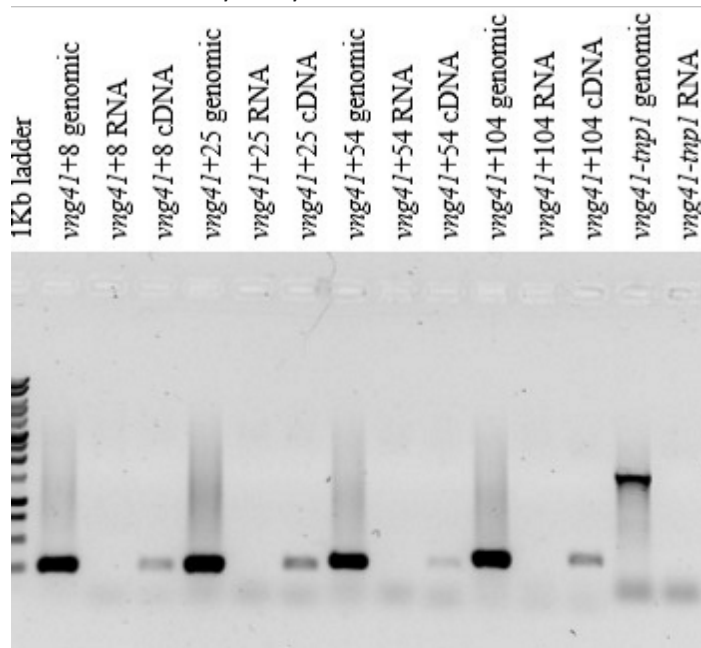- Isolated microbial DNA from hypersaline environments for community analysis

Figure 3: Determination of co-transcription and analysis of start of transcription of genes in the *prtr1-vng41* region. All isolated strains transcribe the region between the start of *prtr1* and 104 bp upstream of the start of *vng41* amplified from cDNA. LH101 genomic DNA was used as a control.

Microbial Species	D10 (Gy)
Cellulomonas ES-6	80 - 320
Cupriavidus basilensis SRS	20 - 80
Shewanella algae BRY	20 - 80
Shewanella oneidensis MR-1	20 - 80

Table 3: Ionizing radiation resistance in metal and radionuclide reducing bacteria. D10 is the radiation dose required to inactivate 90% of a viable microbial population or reduce the population by a factor of 10.
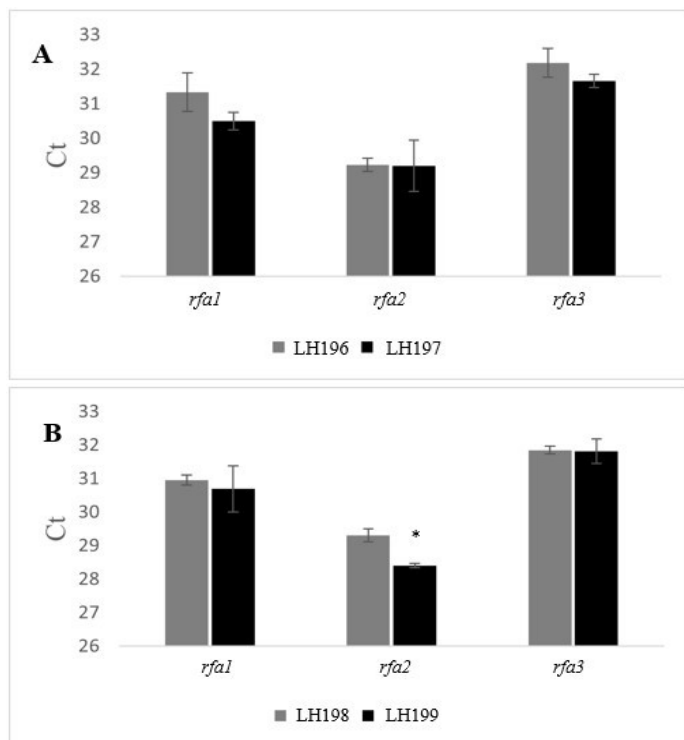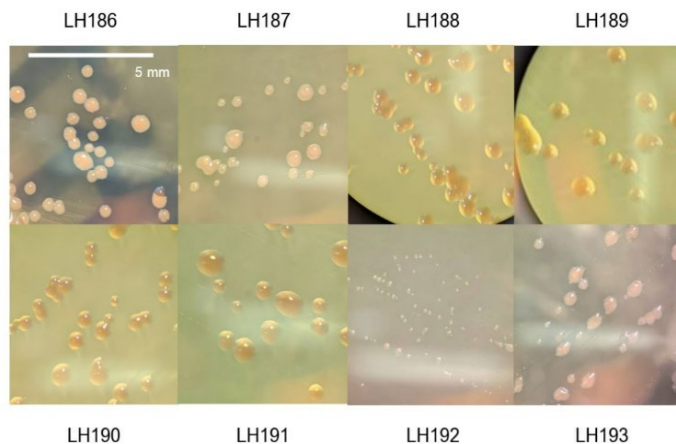

Figure 5: *Halobacterium salinarum* deletion and isogenic strains LH186-LH193. Strains were grown on solid CM+ media for 7 days and viewed under a light microscope. See **Table 1** for genotypes of strains.
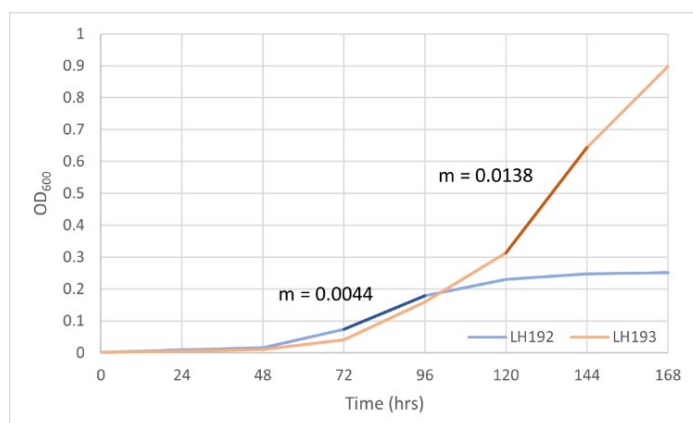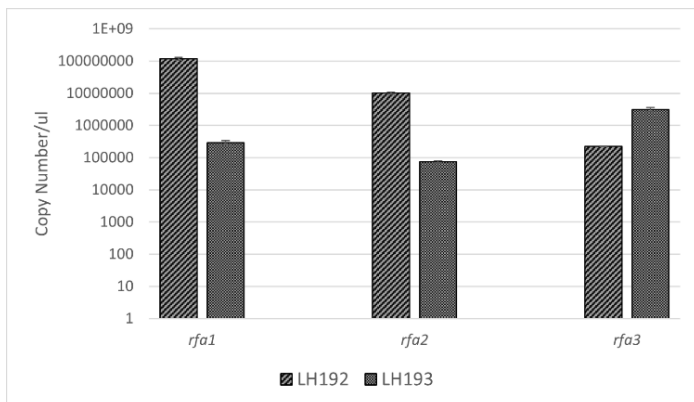

Figure 6: Effect of *erc* deletion on growth kinetics of *H. salinarum*. *Erc* deletion LH192 (blue line) and isogenic strain LH193 (orange line). Exponential phase for each is highlighted in the corresponding darker color.

Figure 4: Effect of deletion of *vng41-tnp1* on *rfa* gene expression. Deletion of the *vng41-tnp1* intergenic region confers a significant change in Ct (cycle threshold) values in background strain LH103 (B), but not in background strain LH101 (A). Ct values are shown for each target gene.

Strain	Copy# *rfa1*	Copy# *rfa2*	Copy# *rfa3*
LH184	1.49e6	1.62e6	5.9e6
LH185	1.27e6	1.9e6	6.87e6
LH196	6.55e5	7.95e5	4.69e6
LH197	1.13e6	8.10e5	6.87e6
LH198	8.42e5	7.54e5	6.0e6
LH199	9.99e5	1.36e6	6.17e6

Table 4: Absolute expression of *rfa* genes in strains deleted for potential regulatory regions for *rfa3* compared to their isogenic counterparts

Strain	*rfa1*	*rfa2*	*rfa3*
LH101	4.79×10^5	7.56×10^4	3.1×10^6
LH102	5.80×10^5	7.59×10^4	7.28×10^6
LH103	4.4×10^5	7.51×10^4	9.82×10^6

Table 5: Copy number of *rfa* gene transcripts in *H. salinarum* strains in the absence of irradiation

Gene	Relative Change	p-value
rfa1		
	400.018	3.82E-06
rfa2		
	133.670	3.15E-07
rfa3		
	0.07233	0.0084

Figure 7: Copy number of *rfa1*, *rfa2*, and *rfa3* in *erc* deletion (LH192) and *erc*+ (LH193) strains. (A) Expression of RPA homologs. (B) Relative change of RPA homolog expression in LH192 as compared to LH193.

Peer-reviewed Publications

Meeks, H.N., R.P. Oates, H. Cui, G. M. Hwang, R.P. Volpe, R. B. Hayes, T.Y. Steen, R.T. Agans, C.E. Turick, R. Brigmon, B. Liebeskind, K. Ganduly, M.R. Sussman, B.D. Lee, A. Lewis, D. Schabacker, and W.L. McKendred. 2022. Harnessing the Environment to Identify Nuclear Processes: Biologically - Mediated Approaches. Countering WMD J. 24: 60-85

Perea, K., L. DeVeaux, R. Brigmon, B.D. Lee. Draft Genome Sequence of *Halomonas estuarii* isolated from … Microbiology Resource Announcement. *In prep*.

Team Members

Nate Losey[a], Linda DeVeaux[b], Hannah Lambertson[b], Katheryn Perea[b], Katherine Persinger[b]

[a]*Environmental and Legacy Management*
[b]*New Mexico Institute of Mining and Technology*

Application of Machine Learning Techniques to Meteorological Forecasting

David Werth

Fog occurs frequently at Savannah River Site (SRS), impacting on-site operations. We developed a process to forecast fog using machine learning techniques which make predictions of fog after being trained on past events at SRS. The techniques all have greater forecasting skill when compared to the existing fog forecast tool.

Introduction

Among the adverse weather conditions that occur at the Savannah River Site (SRS), fog occurs several days per month and has a strong impact on SRS operations; decreased visibility will mandate restrictions on aviation and transportation and can curtail outdoor work. SRS personnel therefore require accurate forecasts of these events, which are difficult to forecast using traditional techniques. This is largely due to the sensitivity of fog to small-scale variability not resolved in numerical weather models. It is therefore desirable to develop a new process to forecast fog that leverages the resolved model processes rather than unresolved small-scale variability.

Machine learning (ML) is the process by which a computer algorithm analyzes a series of matched inputs and outputs and derives the best relationship to relate each input to each output. For weather forecasting, this takes the form of a predictor/predictand relationship, in which potential precursors serve as input, and the subsequent occurrence or non-occurrence of the targeted weather event is the output. By applying ML algorithms to large datasets, precursor events that are highly correlated with a specific weather event can be identified, thereby allowing for a forecast to that effect when those precursor events occur in the future. Multiple ML techniques – the random forest (RF), logistic regression, a neural network, and the CatBoost – have been trained on meteorological datasets collected from weather towers at the SRS. The benefit of the algorithms will be judged based on their performance relative to the Savannah River Site's current fog forecasting approach.

Approach

For each day, we develop a set of observed and model-based predictors, along with a single fog predictand. To define the predictand, we selected as our goal the prediction of fog occurring anytime on SRS between 0600 UTC and 1200 UTC, when it is most likely. 'Fog' was defined in various ways (e.g., visibility falls below 1.6km in B area) when training the different algorithms, and the algorithms are trained by assuming either a continuous visibility or binary (fog/no fog) predictand. The predictors comprise both observed meteorological data and model weather forecasts for the period in question. The fog forecast is assumed to be issued at 1200 UTC on the previous day (i.e., the forecast is issued on January 1st at 1200 UTC for the occurrence of fog between 0600 UTC and 1200 UTC on January 2nd.) Therefore, the predictor for each day will comprise data that is available at that time. As with the visibility, we aggregate the meteorological data to yield a single set of daily predictor values. For example, the overnight (0000 UTC – 1200 UTC) low temperature represents one predictor for forecasting the 0600-1200 UTC fog occurrence on the next night. The ML algorithms were scored and compared to current fog forecast, **Figures 1-4**, – the Model Output Statistics (MOS) forecasting tool, which includes a visibility forecast. The accuracy scores of the two were similar, but the equitable threat score, which cannot benefit from true negatives (correctly predicting no fog), shows much better values for the ML algorithms.

Two skill metrics applied – the Equitable Threat Score (ETS) and the Accuracy, both defined in terms of the number of True Positive (TP), False Positive (FP), False Negative (FN) and True Negative (TN) values.

Equitable Threat Score (ETS) =

$$\frac{TP - TP_{random}}{TP + FN + FP - TP_{random}}$$

Accuracy = $(TP+TN)/(TP+FN+FP+TN)$

	RF	MOS
ETS	0.25	0.17
Accuracy	0.77	0.86

Figure 1: Equitable threat score (ETS) and Accuracy scores for the Random Forest using a binary predictand (Fog = The minimum visibility on site falls below 1.6km), along with the scores for the MOS tool.

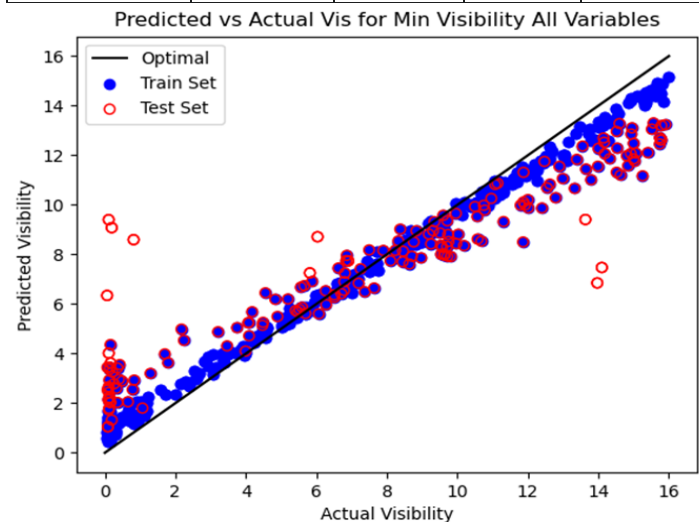| Fog Threshold	RF 1.6 km	RF 3.2km	MOS 1.6 km	MOS 3.2km
Accuracy	0.74	0.88	0.86	0.84
Avg Abs. Error	2.29km	2.18km		
ETS	0.03	0.52	0.17	0.19

Figure 2: *Top*- Scatter plot comparing observed to predicted minimum site visibility when forecasted with the random forest using a continuous predictand. *Bottom*- Equitable threat score (ETS), absolute average errors and accuracy scores for the Random Forest when the predicted visibility is converted to a binary predictand (1.6km or 3.2km), along with the scores for the MOS tool.

	L Tower	H Tower
ETS	0.37	0.33
MOS ETS	0.14	0.15
Accuracy	0.91	0.86
MOS Accuracy	0.88	0.88

Figure 3: Equitable threat score (ETS) and accuracy scores for the logistic regression using a binary predictand (Fog = Visibility falls below 1.6km at L or H tower), along with the scores for the MOS tool.

	Neural Net	Cat Boost	MOS
ETS	0.37	0.60	0.17
Accuracy	0.84	0.90	0.86

Figure 4: Equitable threat score (ETS) and accuracy scores for the neural network and cat boost algorithms using a binary predictand (Fog = Site Minimum Visibility falls below 1.6km), along with the scores for the MOS tool.

Accomplishments

- Established that ML algorithms can discern precursors of fog in meteorological datasets and use them to predict day-ahead fog occurrence.
- Established that ML algorithms can be used to predict actual visibility values on site over a shorter (3 hour) timescale, with a ~0.90 correlation between the predicted and observed values.

Peer-reviewed Publications

The Application of Machine Learning Techniques to Fog Forecasting at the Savannah River Site, in preparation (led by SRNL)

Team Members

Tom Danielson, Stephanie Gamble, Ajay Kumar Gogineni[a], Eric Hoar, Elizabeth LaBone, Brian Mayer[a], Stephen Noble, Naren Ramakrishnan[a]

[a]*Virginia Polytechnic Institute and State University*

Biomining Rare Earth Elements (REEs) Through Bioextraction

Robin Brigmon

Rare earth elements (REEs) are crucial to many high-tech devices and maintaining a competitive modern economy, thus they are of critical and strategic importance. Currently, mining approaches include rock grinding, strong acid or base extraction, separation, and concentration. The objective of this project was to develop cost-effective, environmentally friendly technologies for bioextracting REEs from mined materials.

Introduction

Problem: The United States government has identified that the REEs are critical elements, used extensively in consumer electronics, and military and national security hardware, which are in short supply. **Relevancy:** In response to increasing geopolitical tensions with key critical element producers, several agencies are issuing funding opportunity announcements related to improved recovery of these elements. **Objective.** Here we tested biomining, the process of microbiologically extracting REEs from water, rock ores, and mine waste to fill this need. Currently, these elements are mined by mineral grinding, followed by solvent extraction, separation, and then reconcentration. This work aimed to develop technologies for bioextracting these REEs from mined ores. Bio extraction technology focused on 1) utilizing natural microbes that generate exudates that enhance the extraction of elements, 2) evaluating microbes to dissolve the materials, and 3) and biosurfactant producing microbes. **Results.** Electrochemical impedance spectroscopy and voltametric techniques were combined with molecular analysis to determine optimum microbe-mineral interactions for critical element bio recovery. Select microorganisms were tested and proved useful for REE uptake. REEs were successfully extracted at the part per million level from select mined materials. A partnership has been developed with Mosaic, a mining company with REE rich mine tailings tested by Savanah River National Laboratory (SRNL), and they have requested a proposal for future work based on our results. The study culminated in a proof-of-concept demonstration, manuscripts, partnership with a major mining company to move forward, and the data needed to develop proposals for scaled-up biomining of critical elements.

Approach

REEs are an essential part of many high-tech devices, thus of critical and strategic importance. Currently, the major mining approach of REEs is and creates large waste streams. The objective of this project is to develop cost-effective, environmentally friendly technologies for bioextracting and bioaccumulating REEs from mined bastnaesite (Ce, La)CO_3F), rhyolite (silica rich felsic volcanic rock), and apatite ($Ca_5(PO_4)_3(OH,F,Cl)$) and phosphogypsum using microorganisms. Microorganisms tested for bioextraction include *Bacillus cereus* (ATCC 14579), *Cupriavidus basiliensis* SRS, a bacterium isolated from the Savannah River Site, and BioTiger®, a microbial consortium patented by SRNL. *B. cereus* and BioTiger® exude biosurfactants (e.g., rhamnolipids) that enhance the extraction of multivalent cations. With the bastnaesite *C. basiliensis* SRS extracted REEs cerium (Ce), lanthanum (Ln), neodymium (Nd), significantly higher (>20ppb) than the other cultures compared to uninoculated samples using biostimulation. Bioextracting worked better using the natural mined material rather that autoclaved mining material, suggesting a potential role for the native microbiota of the material in biomining success. Next-generation sequencing of 16S rRNA genes was used to monitor microbial population changes associated with biomining. When added in combination with nutrient broth to natural (unautoclaved) mining material, the isolate *Cupriavidus* SRS was highly competitive, dominating 99% of the microbial population in the extracted material. In biosorption studies, *C. basiliensis* SRS sorbed >90% Ce and Ln from solution over controls. Using bioaugmentation along with heat treatment, it was demonstrated that *Cupriavidus* SRS can bioextract select REEs from mined materials at ppm concentrations from two different materials.

Accomplishments

- Non-Disclosure Agreement (NDA-2021-00032) and a Mutual Confidentiality Agreement were made with the Mosaic Company to work on their mining materials and exchange information.
- Screening of microbes with biomining potential demonstrated that *Cupriavidus basilensis SRS*, a novel microbe isolated from SRS, was the strongest candidate.
- Of the minerals/mining materials tested, Bastnaesite Ore from MP Materials, Mountain Pass CA, and the Apatite & Phosphogypsum from Mosaic Company, Plant City, FL, showed the greatest potential for bioextraction of REEs up 200 ppm, **Figures 1-3**. This was a significant improvement over Year 1 where we only got to the ppb level of REE bioextraction efficacy.
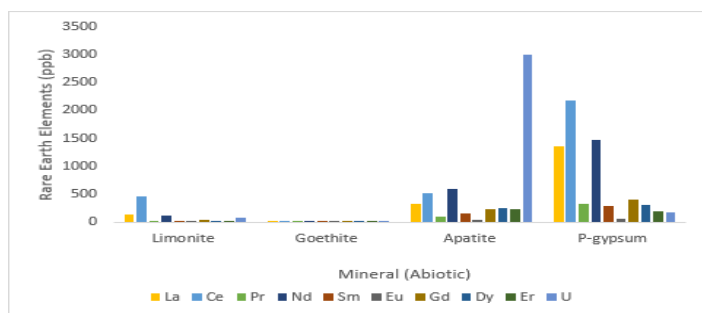
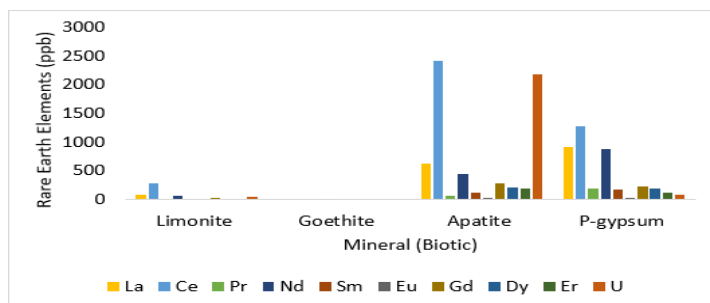**Figure 1:** Extraction of REES with heating alone.

Figure 2: Bioextraction of REEs with combined heating and *Cupriavidus basilensis SRS*.
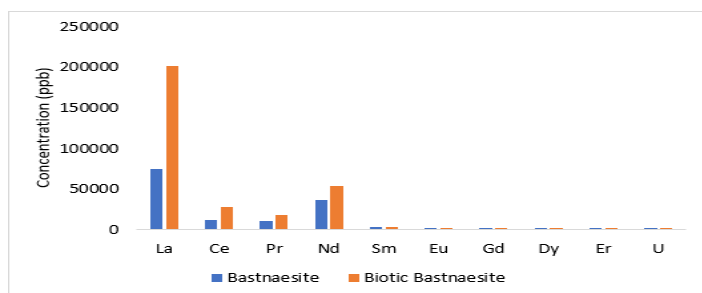

Figure 3: Bioextraction of REES from Bastnaesite with heating and *Cupriavidus basilensis SRS*.

- Heating the material before bioextracting REEs gave the most productive results.
- Characterization of *Cupriavidus basilensis SRS* demonstrated its novelty, **Table 1** and **Figure 4**.

Size	G+C content (%)	No. of Contigs	N50 (bp)	Coverage (x)	CheckM Completeness (%)	CheckM Contamination (%)
8.92 Mb	65.2	176	123,203	411	99.94	2.68

Table 1: General features of the draft genome of *Cupriavidus basilensis* SRS
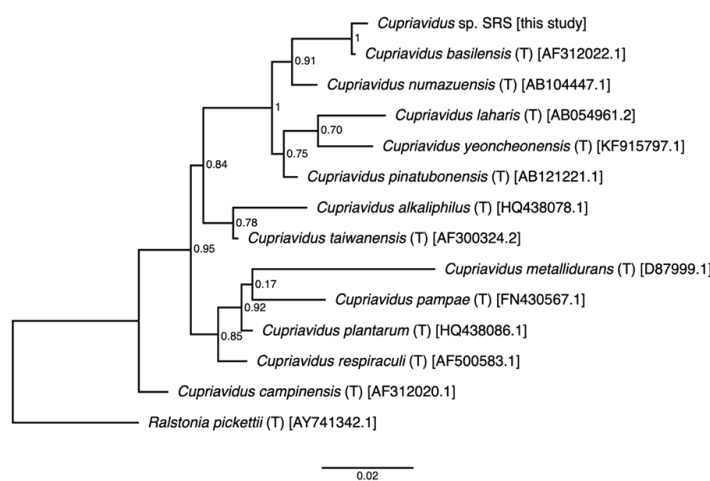

Figure 4: Phylogenetic tree of 16S rRNA relating *Cupriavidus basiliensis SRS* to other closely aligned Cupriavidus spp, resulting from a near-full length nt sequence indicating a near 100% confidence that the *Cupriavidus basiliensis SRS* belongs to the *Cupriavidus* genus.
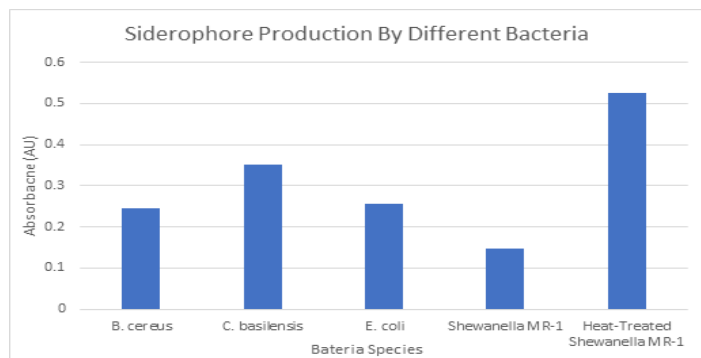

Figure 5: Siderophore presence in different bacteria as measured by absorbance

- *C. basilensis* SRS was shown to produce siderophores that can facilitate biomining REEs, **Figure 5**. Siderophores are low-molecular-weight molecules that chelate metals with a very high and specific affinity.
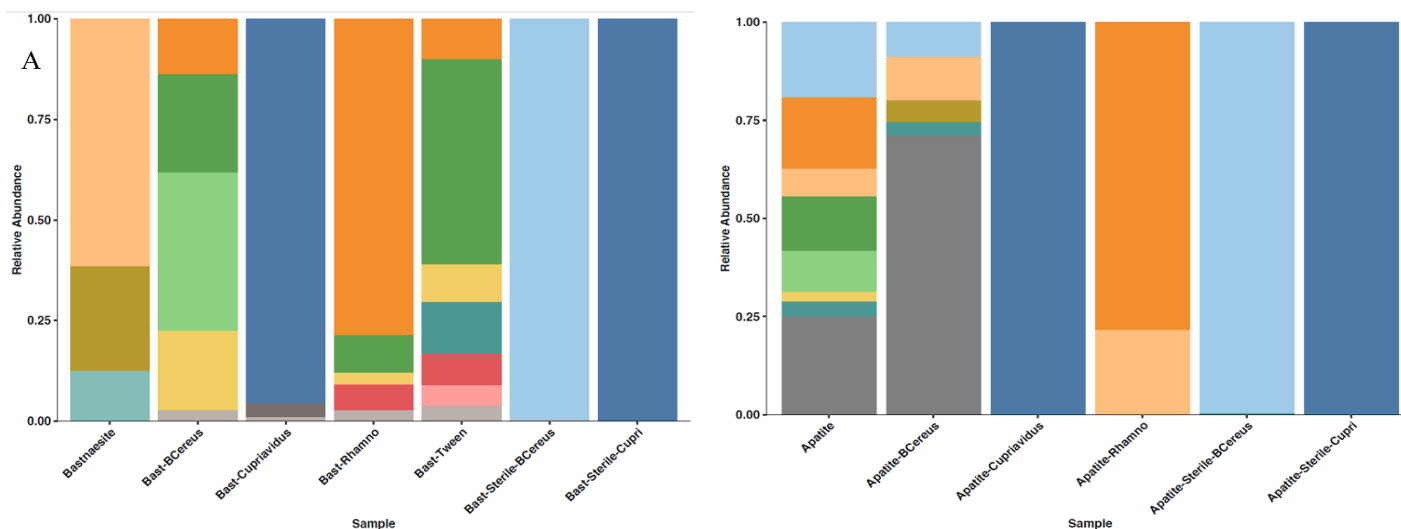
Figure 6: Relative abundance of genera following a 2-week incubation. Bast=Bastnaesite, shown in A and apatite is shown in B. Sterile indicates substrate autoclaved prior to incubation.
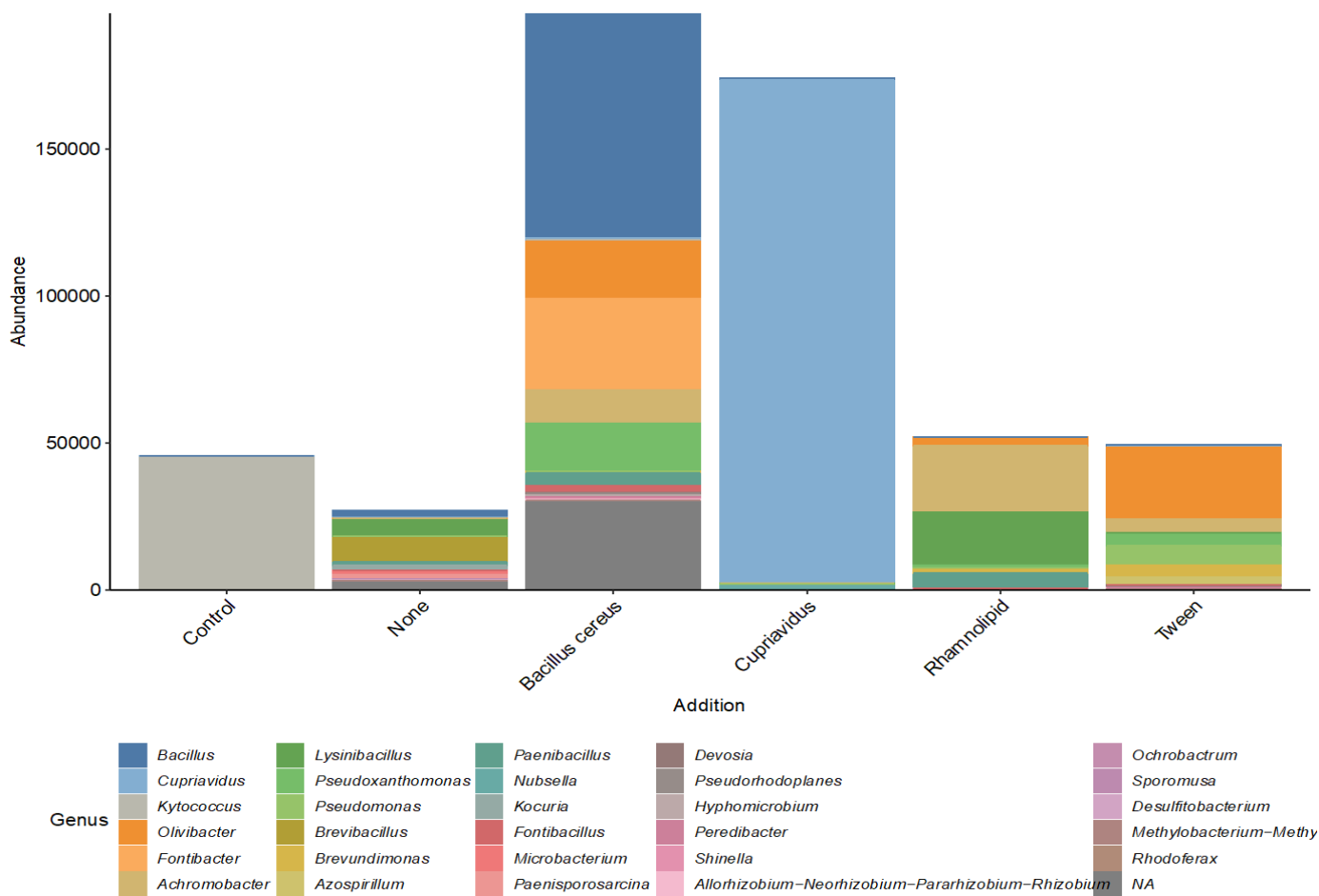

Figure 7: Shifts of bacterial profile based on experimental surfactant treatment. Bc=Bacillus cereus, Cup=Cupriavidus, Rh=rhamnolipid, Tw=Tween 20, Rf=Reference culture of Bacillus cereus and Cupriavidus, NA=non added.

- When added to mine materials in REE extraction experiments, *C. basiliensis* dominated showing a competitive edge over indigenous microorganisms using molecular techniques, **Figures 6** and **7**.
- We developed techniques to monitor bacterial biomining activity in real time using the cost-effective technique that links electronic signals to physiological status of cells, **Figure 8**.
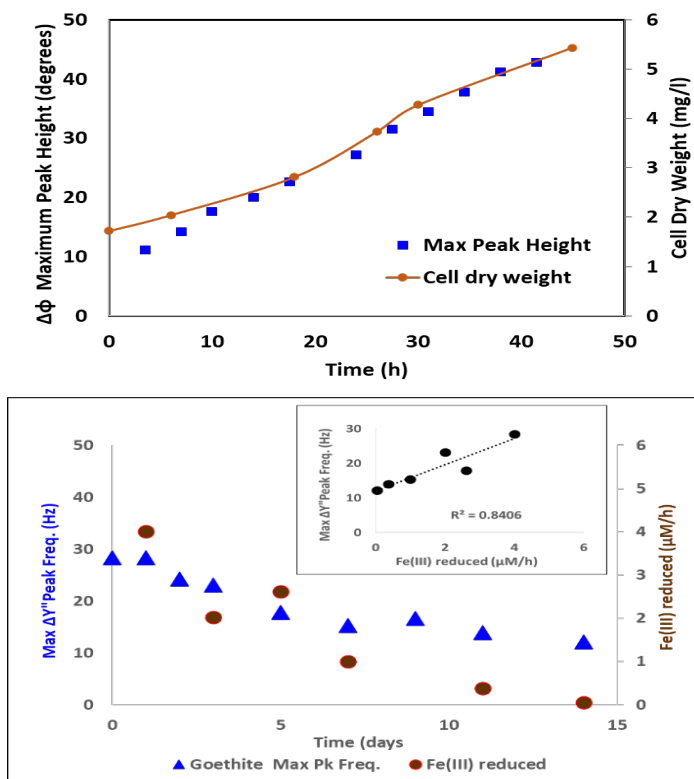- Mosaic Company has expressed interest in future work with Savannah River National Laboratory (SRNL).

Figure 8: Remote, in-situ detection of bacterial growth (left) and Fe(III) oxide reduction (right). Bacterial cells are surrounded by lipid membranes that have a relatively high electrical resistance. The change in the phase angle ($\Delta\phi$) reflects increased resistance (impedance in an AC signal) and the increase in $\Delta\phi$ correlates well to increased cell density during growth. The bacteria we used send electrons extracellularly to Fe(III) minerals in order to grow and is reflected in the rates of Fe(III) mineral reduction.

Peer-reviewed Publications

Fu, H., A. Kugler, P.Huyck, R. L. Brigmon, E. Ottesen. 2022. Draft Genome Sequence of *Cupriavidus basilensis SRS*, a Bacterium Isolated from Stream Sediments. *Microbiology Resource Announcements*. Vol. 11, No. 10

Kugler, A., F. M. Coutelot, A. Friedman, S. W. Polson, . C. Seaman, W. Simpson, and R. L. Brigmon. 2021. Bioremediation of Metals in Constructed Wetland Sediments with *Cupriavidus SRS*. *Nature Scientific Reports.* 12:17615

Teel, H.R., K. Likit-anurak, S. Shimpalee, C. E. Turick. 2022. Imaginary admittance and charge transfer resistance correlate to the physiological status of *Shewanella oneidensis* cultures in real time. *Bioelectrochemistry*. 147, 108210

Electrochemical Impedance Spectroscopy Correlates Microbial Growth Status to Mineral Reduction. 2022. Teel, H.R., S. Shimpalee, A. J. Kugler, C. E. Burckhalter, R. L. Brigmon, and C. E. Turick. *Journal Industrial Microbiology & Biotechnology*. In prep.

Teel, H.R., S. Shimpalee, A. J. Kugler, C. E. Burckhalter, R. L, Brigmon, and C. E. Turick. 2022. Electrochemical Impedance Spectroscopy Correlates Microbial Growth Status to Mineral Reduction. In prep.

Kugler, P., Fu, H., A. Kugler, D. Kaplan, R. L. Brigmon, A.N. Depoy, E. Ottesen. 2022. Solubilization of Critical Elements from Unprocessed Ores by Bacterial Processes. *Frontiers in Microbiology: Microbiological Chemistry and Geomicrobiology.* In prep.

A.N. Depoy, Fu, H., A. Kugler, P. Huyck, D. Kaplan, R. L. Brigmon, E. Ottesen. 2022. Regulation od Siderophores Bioprocessing Rare Earth Elements. Applied Environmental Microbiology. In prep.

Presentations

Teel, H.R., S. Shimpalee, A. J. Kugler, C.E. Turick, and C. E. Burckhalter. 2021. Use of Dielectric Spectroscopy to Correlate Admittance and Charge Resistance to Microbial Growth Status. Poster. Geophysical Union Annual Meeting. New Orleans, LA

Brigmon, R.L., A. Kugler, D. Kaplan, J. Seaman, H. Fu, E. Ottesen. 2022. Bioextraction of Rare Earth Elements with Novel Bacteria. American Society for Microbiology Meeting. Washington, DC.

Manager presentation: *Biomining – Critical Minerals and Materials Recovery Using Microorganisms* – SRNL L3000 Managers Meeting Presentation, 16Dec2021 (Talk)

Team Members

Yasmi Chibber[a], Amber Depoy[b], Jackson DeVault[c], He Fu[b], Patrick Huyck[b], Alex Kugler, Daniel Kaplan, Harris Teel[d]

[a]University of Maryland
[b]University of Georgia
[c]University of Toledo
[d]University of South Carolina

Madison Hseih and Alex Kugler

Study of Ionic Mass Transport in Non-Conventional Electrolytes for Energy Storage Applications

Nathaniel Hardin

To lessen societies dependance on fossil fuels to mitigate climate change, advances in energy storage technologies are required. The work highlighted herein describes advances in non-conventional electrolytes for lithium-ion and redox flow batteries for electric vehicle and grid storage applications.

Introduction

The primary technology currently used for energy storage is lithium-ion batteries. Conventional rechargeable lithium-ion batteries are ubiquitous in daily life, being the battery of choice for phones, laptops, and, more recently, electric vehicles (EVs). However, lithium-ion battery research is primarily focused on using conventional organic solvents as the supporting electrolyte such as dimethyl carbonate and ethylene carbonate. Carbonate based electrolytes have numerous downsides such as safety and stability. This project focused on the development of non-conventional electrolytes to address these shortfalls. During this project, a novel deep eutectic electrolyte (DEEs) was developed and demonstrated for potential use as a lithium-ion battery, **Figure 1**.

Figure 1: Coin call setup used for electrochemical tests.

The developed electrolyte has shown low temperature operation al capability and provides insight for new pathways in the development of novel non-conventional

lithium electrolytes. The understanding gained from this research can also be applied to non-lithium-based systems such as sodium, potassium, aluminum, magnesium, and calcium, **Figure 2**.
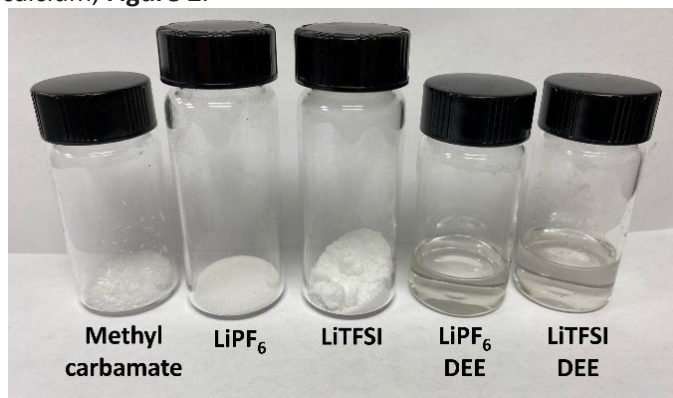

Figure 2: Picture of starting materials and formed DEEs

Leveraging knowledge gained in this research, strategies for the development of DEEs for grid storage applications were formulated. Redox flow batteries, as compared to a standard battery, use redox active electrolytes as the catholyte and anolyte in the battery. Electroactive DEEs could offer an interesting alternative to the industry standard acidic-aqueous based vanadium electrolytes. Compared to aqueous systems, DEEs can have higher concentrations (also yielding higher capacities), less corrosive environments, and provide a large electrochemical stability window.

Approach

The approach used in this project leveraged our scientific capabilities in non-conventional eutectic electrolytes to engage in a multifaceted and systematic study of the target materials. Specifically, it allowed for the study of molecular interactions between hydrogen bond donors (in this case methyl carbamate) and acceptors with lithium salts, and their ability to form a eutectic. The formulated eutectic is then evaluated using various electrochemical and spectroscopic characterization techniques to identify the mechanistic behavior influencing the performance of the
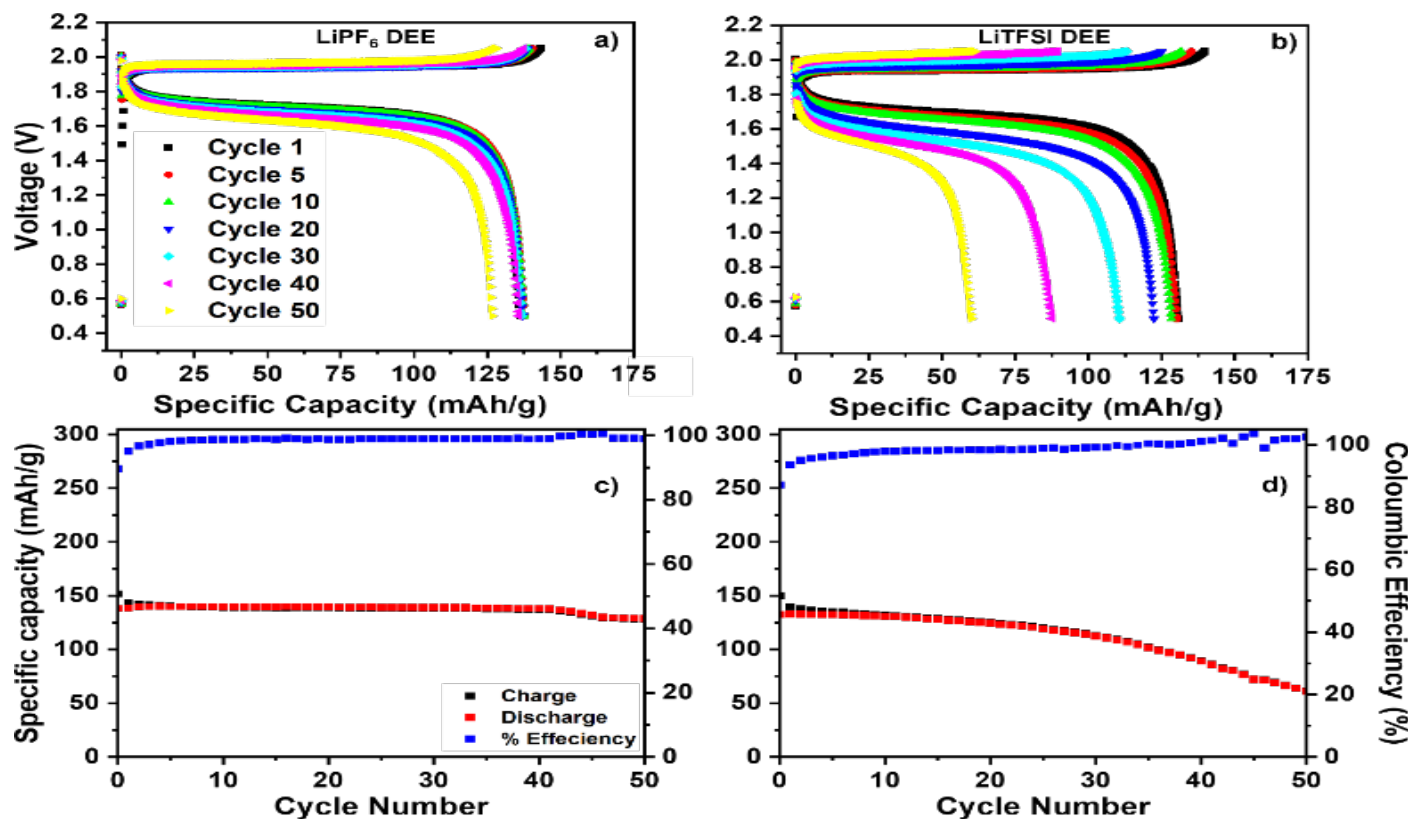
Figure 3: a-b) Voltage profiles of (a) LiPF6 DEE and (b) LiTFSI DEE, c-d) Cycling performance and efficiency of (c) LiPF6 DEE and (d) LiTFSI DEE.

system. Various electrochemical measurements such as cyclic voltammetry (CVs) and galvanostatic cycling provide a tool to study the properties of eutectic electrolytes. Ionic conductivity was evaluated by electrochemical impedance measurements to directly measure and compare the influence of cycling and temperature on the ionic conductivity of the DEE.

Accomplishments

- Designed novel DEEs for lithium-ion batteries based on methyl carbamate, lithium hexafluorophosphate (LiPF$_6$), and lithium bis (trifluoromethanesulfonyl)imide (LiTFSI), **Figure 3**.
- Achieved 93% capacity retention after 50 cycles with a voltage stability between ~1 V to 5 V
- Demonstrated operational feasibility of a lithium-ion battery at less than -45 °C by powering a light emitting diode (LED)
- Developed eutectics based on Iron, Chromium, and Manganese salts for redox flow batteries
- Iron, Chromium and Manganese eutectics showed to be electrochemically reversible from cyclic voltammetry (CV) measurements
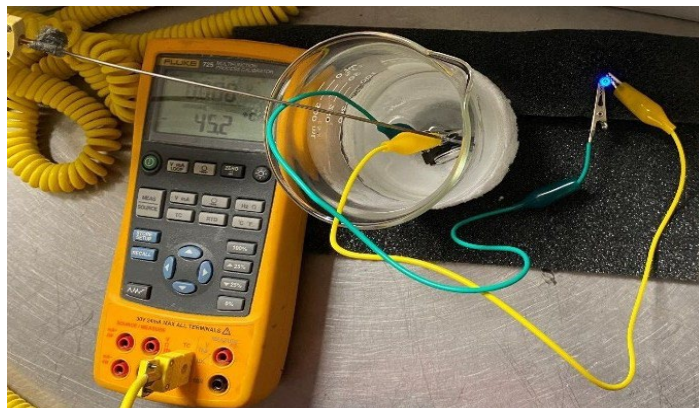

Figure 4: Low temperature operation of a blue LED

Peer-reviewed Publications

N. Z. Hardin, Z. Duca, A. Imel, P. A. Ward, Methyl Carbamate-Lithium Salt Deep Eutectic Electrolyte for Lithium-Ion Batteries. *ChemElectroChem* 2022, *9*, e202200628.

Team Members

Zachary Duca

Biosensor FRET Based Detection

Steven Demers

The goal of this project was to develop a novel multifunctional fluorescence-based sensor for the simultaneous detection of biological, chemical, and nuclear threats with high selectivity, high confidence, and reduced false positives. Using the sensor, a sarin metabolite was identifiable at levels comparable to complex, laboratory-based instruments.

Introduction

The development of a multifunctional portable fluorescent sensor with high selectivity for the simultaneous detection of specific chemical, biological, and nuclear threats (CBRN) is extremely valuable for various entities and situations, including emergency responders, forensics, and environmental sampling. Current detection techniques for CBRN threats are generally complex and require highly specific and ultra-sensitive methods in which a laboratory environment is necessary. Alternatively, fluorescence based Förster Resonance Energy Transfer (FRET) sensors for CBRN threats are much faster, with real-time response time and a simpler signal readout. FRET sensors are ideal for in field detection due to the low detection limits, miniature size, and low power requirements. In FRET, an excited donor molecule transfers energy to an acceptor through nonradiative dipole-dipole interactions.[1-5] Upon a biological, chemical, or radionuclide target analyte binding, a decrease in transfer efficiency occurs due to a change in the distance between the covalently bound donor and acceptor, **Figure 1**. For the detection of the sarin metabolite, methylphosphonic acid (MePA),[6] FRET pairs that consist of energy donors (organic dyes or quantum dots (QDs)) and energy acceptors (gold nanoparticles (AuNPs) or fluorescent quenchers) are used. The donors and acceptors were bound together by single-stranded or double-stranded DNA aptamers that have been found to be selective for MePA binding.[6, 7] This same approach would then be applied to other CBRN threats, where a multiplexed system would be created for simultaneous CBRN detection capabilities.

Approach

In this project, FRET clusters were developed to target one analyte in each CBRN class. QD and dye donors and AuNP
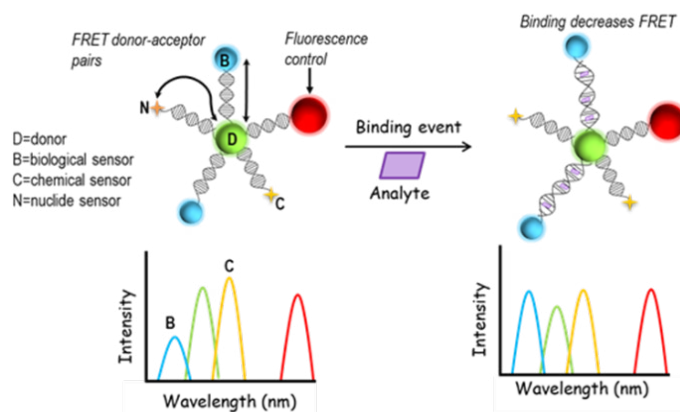

Figure 1: Possible multiplexed, multichannel FRET arrangement for detection of CBRN threats. Threats would be distinguished based off changes in particular florescence wavelength channels.

and quencher acceptors were functionalized with multiple specified targeting ligands to create FRET pairs that specifically target chemical and biological agents. Targeting agents were evaluated with a focus on DNA aptamers; however, other targeting agents include antibodies for biological agents and nuclide resin materials for nuclear material. Upon binding of the targeted analyte, a change in FRET efficiency was measured by the change in the fluorescence ratio for the donor and acceptor. This arrangement can be seen in **Figure 2**. Individual FRET pairs were created using aptamers for a sarin metabolite (MePA), with results shown in **Figure 3**. For reference, the reported detection limits using mass spectroscopy are 10–50 nM (1–4 ng/mL) in buffer[8, 9] and for gas chromatography in urine, the reported detection limit was 625 nM.[10] Trials for aptamers for anthrax protective antigen 63 were undergone and a Sr aptamer was synthesized. Once individual CBRN threats' detection limits could be quantified, a multiplexed system can be created by combining the aptamer strands
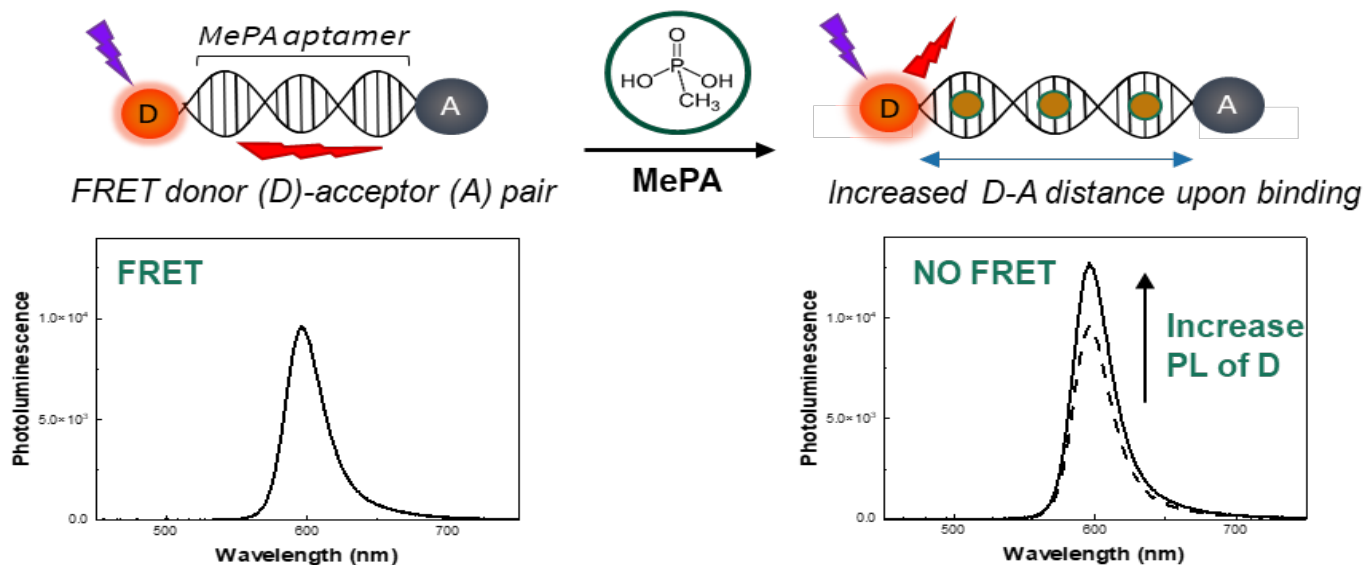
Figure 2: FRET-based biosensor composed of QD donor (D) and dye acceptor (A) bound together through a DNA aptamer. Each DNA aptamer has 3 binding sites for MePA. When MePA binds to the aptamer, a conformational change of the DNA between the donor and acceptor leads to a quantifiable change in the fluorescence (PL) signal.

and FRET pairings, depicted in **Figure 1**. Additionally, by expanding the types of metals used in nansensors allows for control over detection capabilities. Like FRET, nanometal surface energy transfer (NSET) is an energy transfer effect between a donor molecule and a metal nanoparticle; however, NSET experiences a $1/r^4$ dependence compared to FRET's $1/r^6$, leading to lower detection limits.

Accomplishments

- Two types of FRET pairs were created for a sarin metabolite, methylphosphonic acid (MePA), detection.
- Created a FRET-pair biosensor for the detection of MePA. A trend can be seen for the detection of MePA in artificial urine, **Figure 3**.
- FRET arrangement for detection of Anthrax (Anthrax Protective Antigen 63). Anthrax Protective Antigen 63 found to have negligible quenching effects on QDs in saline solution.
- FRET/NSET calculations were carried out for 6 different metal nanoparticles (Cu, Ag, Au, Ni, Pd, Pt) between 2-100 nm in diameter. The FRET/NSET efficiencies were calculated between dyes and given metal nanoparticles for interparticle distances of 4-600 Å.

- Quenching measurements for 10 and 20 nm gold nanoparticles follow the trend as described by NSET calculations. See Figure 4.
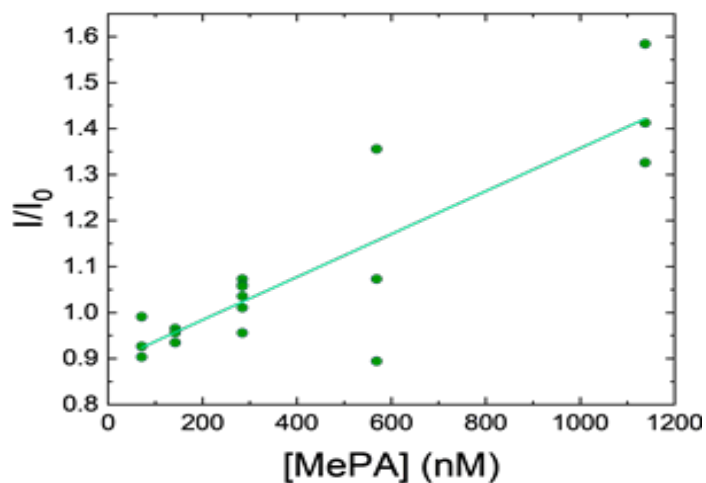

Figure 3: MePA calibration curves in artificial urine. Data collected from measurements at each concentration. The detection limit was calculated from the linear range of the data depicted.

- Conjugation techniques for thiol-DNA to silver and platinum nanoparticles were explored. A citrate conjugation method was found to work best for silver nanoparticles. A slow salt-aging process was found to work best for platinum nanoparticles.
- This work was presented as two oral presentations at APS March Meeting and ACS Spring Meeting.
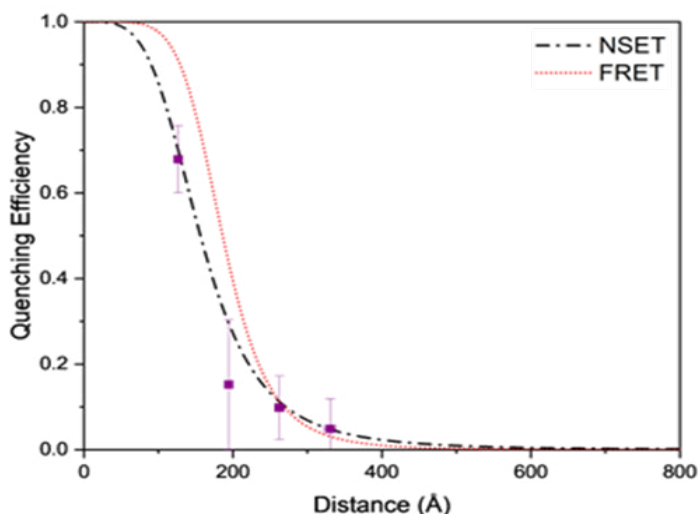
Figure 4: Calculated FRET and NSET quenching efficiency as a function of distance for r = 5 nm AuNPs. Experimentally found values for the quenching efficiency from 4 experiments.

Peer-reviewed Publications

Demers, S. M. E.; Kuhne, W. W.; Swindle, A. R.; Coopersmith, K.; Quantum Dot-DNA FRET Conjugates for Direct Analysis of Methylphosphonic Acid in Complex Media. *In submission*

Demers, S. M. E.; Coopersmith, K.; Examination of NSET Behavior of Nanoparticles of Varying Composition. *In preparation*

Intellectual Property

SENSOR FOR SIMULTANEOUS CHEMICAL, BIOLOGICAL, AND RADIOLOGICAL/NUCLEAR DETECTION
- Provisional: BSRA-305-P (63/297,361)
- Full patent: BSRA-305 (SRS-22-004)

References

Singh, M. P., and Strouse G. F., Involvement of the LSPR Spectral Overlap for Energy Transfer between a Dye and Au Nanoparticle. *J. Am. Chem. Soc.* 2010, *132*, 9383-9391.

Han, H.; Valle, V.; Maye, M. M., Probing Resonance Energy Transfer, and Inner Filter Effects in a Quantum Dot-Large Metal Nanoparticle Clusters using a DNA-Mediated Quench and Release Mechanism. *J. Phys. Chem. C* 2012, *116*, 22996-23003.

Breshike, C. J., Riskowski, R. A., and Strouse, G. F., Leaving Forster Resonance Energy Transfer Behind: Nanometal Surface Energy Transfer Predicts the Size-Enhanced Energy Coupling between a Metal Nanoparticle and an Emitting Dipole. *J. Phys. Chem. C* 2013, *117*, 23942-23949.

Chen, G.; Song, F.; Xiong, X.; Peng, X., Fluorescent Nanosensors Based on Fluorescence Resonance Energy Transfer. *Ind. Eng. Chem. Res.* 2013, *52*, 11228-11245.

Lakowicz, J. R., *Principles of Fluorescence Spectroscopy*. Second ed.; Kluwer Academic/Plenum Publishers: New York, NY, 1999.

Bruno, J. G.; Carrillo, M. P.; Phillips, T.; Vail, N. K.; Hanson, D., Competitive FRET-Aptamer-Based Detection of Methylphosphonic Acid, a Common Nerve Agent Metabolite. *Journal of Fluorescence* 2008, *18* (5), 867.

Bruno, J. G.; Carrillo, M. P.; Cadieux, C. L.; Lenz, D. E.; Cerasoli, D. M.; Phillips, T., DNA aptamers developed against a soman derivative cross-react with the methylphosphonic acid core but not with flanking hydrophobic groups. *Journal of molecular recognition: JMR* 2009, *22* (3), 197-204.

Li, B. Q.; Wei, J. N.; Kong, J. L.; Qin, M. L.; Yang, L.; Li, C. P., Rapid detection of Sarin hydrolysis products based on microextraction by packed sorbent combined with Nano-ESI mass spectrometry. *International Journal of Mass Spectrometry* 2021, *461*.

Baygildiev, T.; Zatirakha, A.; Rodin, I.; Braun, A.; Stavrianidi, A.; Koryagina, N.; Rybalchenko, I.; Shpigun, O., Rapid IC-MS/MS determination of methylphosphonic acid in urine of rats exposed to organophosphorus nerve agents. *Journal of chromatography. B, Analytical technologies in the biomedical and life sciences* 2017, *1058*, 32-39.

Minami, M.; Hui, D. M.; Katsumata, M.; Inagaki, H.; Boulet, C. A., Method for the analysis of the methylphosphonic acid metabolites of sarin and its ethanol-substituted analogue in urine as applied to the victims of the Tokyo sarin disaster. *Journal of chromatography. B, Biomedical sciences, and applications* 1997, *695* (2), 237-44.

Sea Breeze Influence on Aerosols and Convection in the Southeastern United States

Stephen Noble

Sea breezes in the southeastern United States can move inland over a large area and occur more often than previously thought. This phenomenon is sensitive to temperature differences, cloud cover, topography, and soil moisture. Sea breezes change atmospheric conditions and affect clouds, precipitation, air quality, energy production, and climate.

Introduction

In the southeastern United States, coastal sea breezes can penetrate inland more than 150 km, impacting other atmospheric processes. This complex interaction between the atmosphere, land and ocean drives marine airmasses - with generally higher moisture content, lower temperatures, and different aerosols - inland. Our research demonstrates that sea breezes are ubiquitous in the southeastern United States and can frequently penetrate inland more than 150 km, about 27% of time during the sea breeze season (March to October). The extent of the inland penetration was found to be driven by inland thermal gradients, latitude, topography, and soil moisture. A residual sea breeze layer can remain in place into the next day and impact convective and cloud processes. Thus, in the southeastern United States, the sea breeze is important in determining the drivers of convection, cloud formation, and precipitation which are influenced by changing climate forcings. The sea breeze potentially impacts renewable energies, air and water quality, and radiative forcing of climate. Due to the shallow nature and smaller scale of these circulations, earth system models may not correctly assess the importance of intruding sea breezes. This research establishes a base line for future sea breeze research related to previously mentioned areas of impact.

Approach

We utilized mesoscale modeling to test the sensitivity of the sea breeze to various influences, such as the inland thermal gradient, latitude, topography, and soil moisture. We also developed new data sets through analysis and

quality control: precipitation chemical analysis and particle size distribution measurements. These provided insight to additional characteristics of inland penetrating sea breezes. We also utilized a suite of observations and reanalysis data to identify more sea breezes in the southeastern United States region and those specifically penetrating to the Savannah River Site. With all the identified cases from 2015 to 2021, a seasonal component was identified by grouping characteristics by month. All of these sea breeze cases drove our research focused on the sea breeze influence on carbon fluxes, convection, ozone concentrations, and aerosol properties. They also provided a baseline for future sea breeze identification.

Accomplishments

- Discovered that large inland thermal gradients (differences in surface temperatures inland compared to near the coast) drives the deep penetration of sea breeze inland to the Savannah River Site, **Figure 1**.
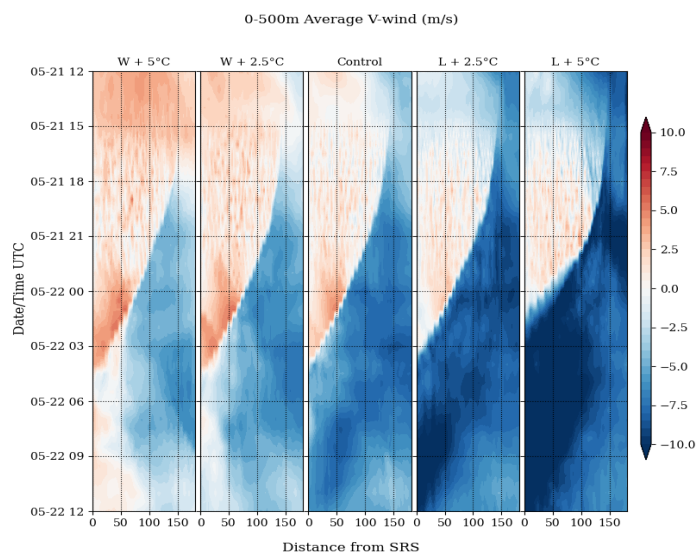

Figure 1: Average meridional wind over the lowest 500 m above the ground as a time series over a 24-h period from 21 May 2019 to 22 May 2019. Savannah River Site (left axis) is located 150 km from the coast (~150 km). Gradients were altered to be 5 or 2.5 degrees warmer towards the land (L) or ocean (W). Similar to **Figure 9** of Wermter et al. 2022.

- Numerical sensitivity studies identified that latitude and topography influenced the deep inland penetration of the sea breeze in the southeastern United States, **Figure 2**.
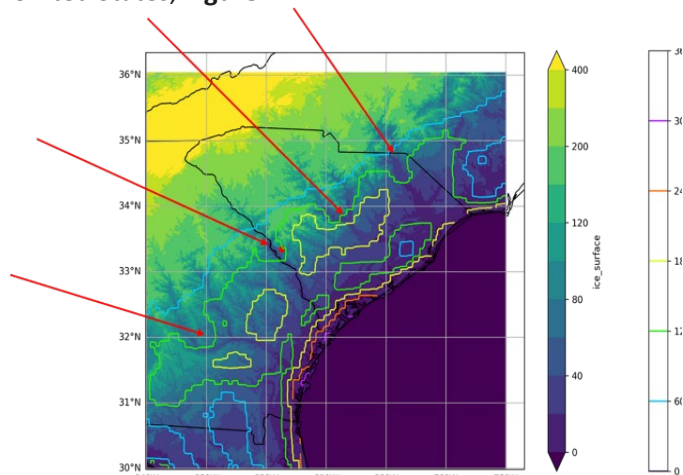

Figure 2: Surface topography with sea breeze accumulated wind contours. Red arrows indicate low river valleys with reduced sea breeze accumulated winds. From Bao et al. 2022.

- Discovered a relationship between soil moisture and sea breeze frequency during the spring dry season in the southeastern United States (soil moisture sensitivity).
- Performed Ion Chromatography (IC) and Inductively Coupled Plasma Mass Spectrometry (ICP-MS) analysis on 158 precipitation samples collected at SRS to identify components of sea breeze aerosol. Thirty-seven samples show elevated levels of chloride possibly related to scavenged sea breeze aerosols, but additional analysis is needed.
- Analyzed 122 days of particle size distributions measurements from 2021 to identify 35 sea breeze cases where aerosol changes with the sea breeze passage were related to the near surface level wind direction after the sea breeze passage.
- Used similar identification approach from previous years to identify 79 sea breezes at Savannah River Site in 2021.
- Created a new identification method with other data sources to identify 293 sea breeze cases identified at North Myrtle Beach, SC and 305 sea breeze cases at Sumter, SC from 2015 to 2021.
- Determined that sea breezes seem to have a limiting effect on nocturnal carbon respiration at the US-Aiken AmeriFlux site.
- Lightning density in the summertime indicated that convection triggering lightning tends to occur about

two to four hours earlier on days following a sea breeze than on days not related to a sea breeze, **Figure 3.**
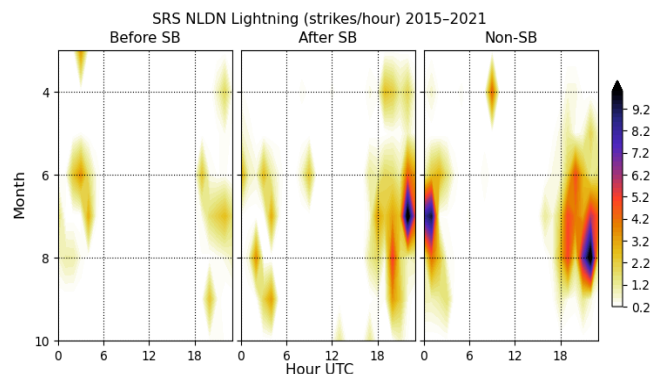

Figure 3: Lightning density at Savannah River Site by hour of day and month for day of the sea breeze initiation, the day after the sea breeze and all other non-sea breeze days. From Noble et al. 2022.

- Completed numerical modeling to illuminate how the shifting winds associated with sea breezes lead to an increase in the amount of maritime air over various South Carolina locations, **Figure 4.**
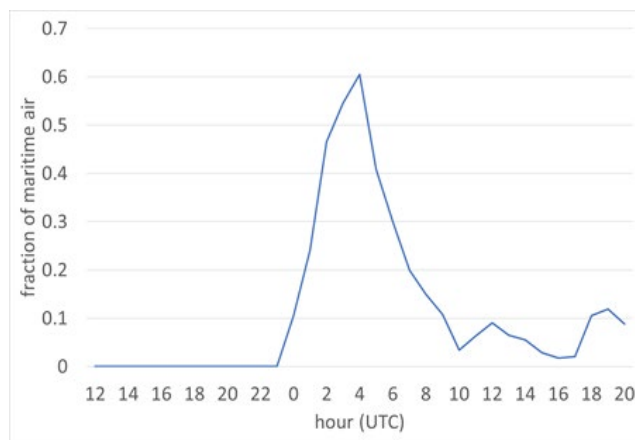

Figure 4: Time series of maritime fraction at SRS for a mesoscale simulation of the sea breeze that occurred on Mar 28-29, 2019.

- Identified a possible connection of sea breeze frequency to the North Atlantic Oscillation which indicates sea breeze sensitivity to climate.
- Identified that the precipitation analysis technique that was implemented for this project has a possible use in nonproliferation.

Peer-reviewed Publications

Savannah River National Laboratory

Wrester, J.; Noble, S.; Viner, B. Impacts of the Thermal Gradient on Inland Advecting Sea Breezes in the Southeastern United States. *Atmosphere* **2022**, *13*, 1004. https://doi.org/10.3390/atmos13071004

Viner, B.; Noble S. Analysis of the Impact of Inland Sea-Breeze Air Masses from an Eddy-Covariance Perspective. *Agricultural and Forest Meteorology*, **2022** (under review)

Noble, S.; Viner, B.; Wermter, J. Identification and Summary of Inland Penetrating Sea Breezes at the Savannah River Site from 2015-2021. *Atmospheric Science Letters*, **2022** (under review)

Noble, S.; Werth, D.; Buckley, R. Influence of sea breezes on aerosols at an inland site. *Aerosol Science and Technology*, 2022 (in preparation)

Wermter, J.; Noble, S.; Viner, B.; Werth, D.; Qian, J.; Shen, D.; Bao, S.; Pietrafesa,, L.; Gayes, P. The seasonality of soil moisture's influence on sea breezes in South Carolina. *Monthly Weather Review*, **2022** (under review)

Coastal Carolina University

Pietrafesa, L.; Bao, S.; Gayes, P.; Mitchell, G.; Burdette, S.; Viner, B.; Noble, S.; Qian, J.; Werth, D. The Anatomy of the South Carolina U.S.A. Coastal Sea Breeze 2019-2020. *International Journal of Geosciences* **2022**, *13*, 576-592. doi: 10.4236/ijg.2022.137031

Bao, S.; Pietrafesa, L.; Gayes, G.; Noble, S.; Viner, B.; Qian, J.-H.; Werth, D.; Mitchell, G.; Burdette, S. Mapping the spatial footprint of sea breeze winds in the southeastern United States. *Journal of Geophysical Research: Atmospheres*, **2022** (under review)

Team Members

Brian Viner, David Werth, Jian-Hua Qian, Joseph Wermter, Paul Gayes[a], Leonard Pietrafesa[a], Shaowu Bao[a], Grant Mitchell[a], Savannah Burdette[a], Dongliang Shen[a] and Hongyuang Zhang[a]

[a] *Coastal Carolina University*

Growth and Development of Quantum Materials

Utpal N. Roy

Topological insulators (TIs) are novel states of matter classified as quantum materials. The goal of the project is to find suitable TI materials having robust topological surface states for different dopants/impurities with the capability of tuning the Fermi level. The exotic properties of topological insulators can be used for developing dissipation-less, ultra-fast electronics and quantum computation devices.

Introduction

Topological insulators have a unique characteristic of being an insulator as the bulk property and having conducting surface states. The surface states are symmetry-protected Dirac fermions that are well isolated from the bulk valence and conduction bands. Ideally, these topological surface states and bulk electronic states would act independently. The degree to which they interact depends on the crystalline quality, material composition, and defects present in the material. The goal of this project is to find a suitable TI material with robust topological surface states against doping/impurities, plus the capability of tuning the Fermi level.

Recently, Sb_2Te_2Se was reported[1] to have a capability to tune the Fermi level and shows robustness of the topological surface states against impurity doping. Undoped Sb_2Te_2Se was reported as *p*-type, while tin-doped material is an *n*-type material.

We recently grew an undoped Sb_2Te_2Se ingot by the vertical Bridgman technique, which is melt growth technique. Tin-doped Sb_2Te_2Se is being grown by the same method. The availability of *p*- and *n*-type material will allow us to fabricate and characterize quantum devices on *p-n* junctions. A polished wafer of the as-grown material has been characterized using different tools, including single crystal x-ray diffraction, powder x-ray diffraction and energy dispersive spectroscopy (EDS), to measure the alloy composition and crystallinity. The lattice constant and the Se composition variation along the growth direction were determined to further estimate the composition along the length.

Approach

Ideally, these topological surface states and bulk electronic states would act independently. The degree to which they interact depends on the crystalline quality, material composition, and defects present in the material. The approach is to grow topological insulator materials having robust topological surface states against doping/impurities plus the capability of tuning the Fermi level. Thus, control of the material composition and the ability to grow high-quality crystals are required for developing effective topological insulators as quantum devices.

Very recently Sb_2Te_2Se has been reported[1] to have the ability of tuning the Fermi level and having the robustness of topological surface states against impurity doping. The crystals are also capable of tuning the Fermi level by doping with tin to convert the material from *p*-type to *n*-type. Undoped Sb_2Te_2Se acts as *p*-type and tin-doped (about 1 at. %) Sb_2Te_2Se behaves as *n*-type material. The goal is to grow *p*-and *n*-type high-quality Sb_2Te_2Se crystals that would allow us to fabricate quantum devices based on *p-n* junctions. We have grown un-doped Sb_2Te_2Se ingot by using the vertical Bridgman growth technique. Crystals have been characterized by single crystal X-ray diffraction and powder X-ray diffraction to analyze the crystal structure and the variation of the lattice constant along the length of the ingot. The data were used to study the extent of the compositional variation along the growth direction. The selenium content is reported to segregate along the growth direction in Sb_2Te_2Se ingot and concentrate in the last-to-freeze section, which is commonly observed. Energy dispersive spectroscopy (EDS) was also carried out along the length of the grown ingot to further understand the compositional variation and segregation of selenium. **Figure 1a** shows a photograph of the Sb_2Te_2Se ingot of diameter 22mm and about 4.8 cm long. The variation of selenium along the axial direction of the ingot is shown in **Figure 1b**. The surface defects in the image are inconsequential, the EDS measurements were carried out on the wafer cut along the length of the ingot.
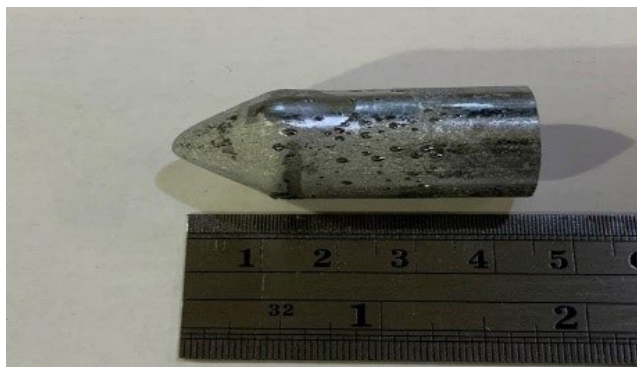
a)
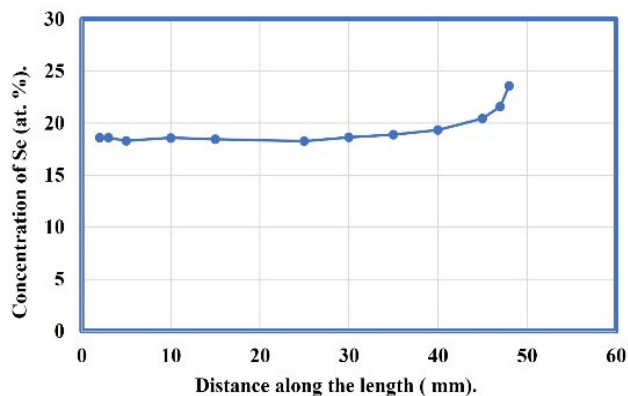
b)

Figure 1: *a)* Photograph of an undoped Sb_2Te_2Se ingot grown by the vertical Bridgman growth technique, *b)* selenium concentration along the length of the as-grown ingot.

Accomplishments

- Successfully grew an undoped $Sb_2Te_{3-x}Se_x$ (nominal value is x=1) ingot with a diameter of 22 mm by the vertical Bridgman growth technique.
- Within the accuracy of the measurement method, the EDS results showed a uniform composition along the length of the ingot up to ~4 cm from the tip. After 4 cm, the selenium segregates heavily towards the end of the ingot.
- The powder X-ray diffraction results performed at various lengths of the ingot show similar findings. For example, the calculated lattice constant ("a") at 1.6 cm from the tip and 2.5 cm from the tip were found to be 4.1816 Å and 4.1825 Å respectively, indicating good uniformity. The corresponding value for the Se composition "x" varied between ~1.00 to 0.99, again indicating good uniformity. Near the end of the ingot (last to freeze), the lattice constant ("a") was 4.1688, and the corresponding value of x was 1.132. Thus, the segregation of selenium near the end of the ingot is more prominent as compared to the rest of the ingot.

- The growth of tin-doped Sb_2Te_2Se ingot is underway to obtain *n*-type material. If successful, we will explore the future possibility of fabricating novel quantum devices based on *p-n* junctions of $Sb_2Te_{3-x}Se_x$. Other dopants will also be explored to achieve *n*-type materials.

References

D. Mallick et al. Applied Phys. Lett. 118 (2021) 154001.

Team Members

Alex Bretana, Jonathon Baker, Binod Rai, Henry Ajo, Catherine Housley, Patrick O'Rourke and Robert Lascola

Topological Magnetic Textures in Lanthanide-based and Actinide-based Quantum Materials

Binod Rai

Materials which are governed by quantum behavior display emergent phenomena, such as exotic magnetism and topological states of matter, and are potentially suitable for future energy storage. Engineering these new quantum materials while understanding their fundamental properties is essential to successfully utilizing these materials in future technologies.

Introduction

The design and development of new materials has often played a key role in discovering new physical phenomena and advancing technology. Quantum materials exhibiting exotic magnetism and topological states of matter are potentially suitable for future energy storage. Alongside the possibility of utilizing these materials in future technologies, the emergent phenomena associated with quantum materials has motivated scientists worldwide. However, the realization of exotic magnetism and topological states of matter as well as the understanding of the fundamental mechanisms of such systems are limited to only a few materials. The *f*-electron-based compounds are a promising class of materials, where RKKY interactions and spin-orbit coupling favor stabilizing such exotic magnetism and topological states of matter.

This materials-driven research program identified and synthesized several quantum materials that have the potential to exhibit exotic magnetism. The synthesized quantum materials were investigated to study the relationship between structural, magnetic, and electronic properties by establishing collaboration with universities, national labs, and DOE User facilities. Our study focuses on the fundamental science of quantum materials and found complex magnetic structures in these materials. The revelation of exotic quantum phases in new classes of materials is fundamental yet extremely crucial scientific information needed for advancing our understanding of and establishing a path from the discovery of topological materials to a final product.

Approach

The design and development of new materials for this project requires the liquid flux crystal growth lab for intermetallic- and oxide-based materials. The crystal growth lab was established for the first time at SRNL by completing safety work control documents in FY22. We have synthesized several materials in the newly established lab, such as $NdCuGa_3$ and $EuPtSi_3$. The actinide-based materials are synthesized in collaboration with other researchers at Savannah River National Laboratory (SRNL). The structural property analysis of new materials using single crystal XRD, powder XRD, and SEM are performed at SRNL. The newly established single crystal XRD at SRNL is crucial for the project to examine the microscopic details such as disorder, bond lengths, etc. in the newly synthesized non-radioactive and radioactive materials.

The physical properties of magnetic materials are essential to achieving the project's proposed objectives; however, SRNL doesn't currently have the capability. Thus, materials' magnetic and thermodynamic properties were measured at collaborator's institutes Idaho National Laboratory (INL), Los Alamos National Laboratory (LANL), and Oak Ridge National Laboratory (ORNL). To investigate the magnetic structure of materials, neutron beamtime proposals were submitted through a general Users proposal call at ORNL (DOE User facility). Four neutron beamtime proposals were awarded and neutron scattering experiments were successfully completed in FY22, **Figure 1-2.** Note, on **Figure 1**, weak magnetic satellite reflections were observed in a four-fold pattern around the nuclear Bragg peaks and can be indexed by the propagation vector (0.2, 0, 0). One of the beamtime proposals examined the magnetic properties of NpO_2 at cryogenic temperature. Two more neutron beamtime proposals have been awarded in FY23, which are scheduled for measurements in early FY23. One of the proposals is to study complex magnetic structures in actinide-based chloride materials. Our studies focusing on the fundamental science of quantum materials has found

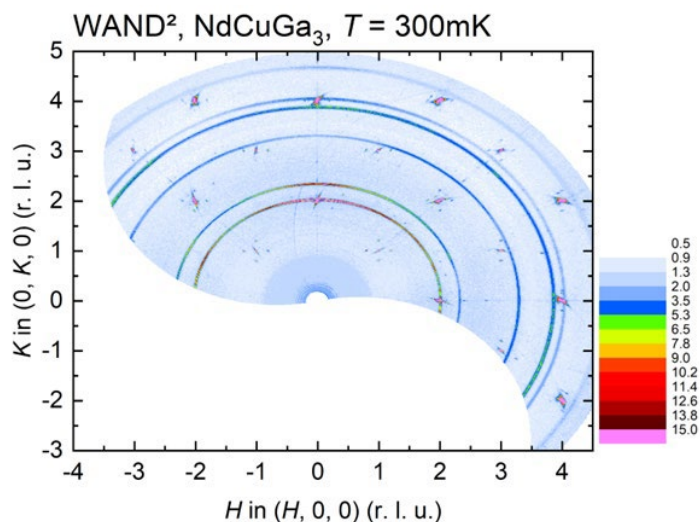interesting crystal structure details and complex magnetic structure in these materials.

Figure 1: Neutron diffraction results collected at WAND[2], ORNL. Reciprocal HK0 map of $NdCuGa_3$ measured at 300 mK.
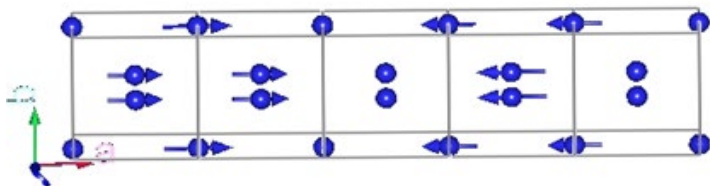

Figure 2: Sketch of the resulting magnetic structure from neutron diffraction experiments. The magnetic moment of Nd on the positions where the arrow is too short to be displayed is $0.7\mu_B$.

Accomplishments

We have published two peer-reviewed articles, prepared one manuscript draft, presented two contributed talks, and submitted one DOE full proposal for clean energy technology. The details are provided below:

- Lead a full DOE SC proposal (~$4 M for 3 years) on 16th May 2022 in collaboration with 3 co-PIs from national labs (INL and LANL) and 3 co-PIs from universities (University of South Carolina Columbia, University of Memphis, Florida A&M University) under DOE-FOA-0002676. The pre-application under this FOA encouraged the full proposal submission in April 2022.
- Invited to write an RTX3 topical review article from the IOP publication and published in the Journal Physics: Condensed Matter in May 2022 [see the journal detail in the peer-reviewed publications section].

- The review article identifies several candidate materials that have potential to exhibit exotic magnetism and topological states of matter.
- The review article was featured as a publication spotlight at SRNL in June 2022.
- Discovered complex magnetic phases for Fe-doped $NiBr_2$ based on the physical property measurements. The results are published in the Journal of Magnetism and Magnetic Materials. A neutron scattering study is underway to examine the possibility of a material's topological ground states.
- Delivered two contributed scientific talks at the American Physical Society and Materials Research Society in FY22. $NdCuGa_3$ results were presented at the conferences.
- Presented a poster Advanced Manufacturing Center (AMC) collaboration Workshop in June 2022.
- Awarded four proposals for neutron beamtime at ORNL in FY22. The neutron beamtime was requested using a general user proposal call. Powder and single crystal neutron diffractions were completed at ORNL in $NdCuGa_3$ and NpO_2 materials.
- Awarded two proposals (FY22) for neutron beamtime at ORNL , which are scheduled for measurements in FY23.
- Established a crystal growth lab for intermetallic- and oxide-based materials for the first time at SRNL.
- Synthesized several candidate materials such as $NdCuGa_3$ and $EuPtSi_3$. In addition, single crystal x-ray diffraction data were collected for synthesized materials at SRNL. For example, the crystal structure solution and neutron diffraction results of $NdCuGa_3$ are presented in **Figures 1-3**. Note, Figure 3 illustrates the single crystal XRD data characterized and analyzed using a newly installed SCXRD instrument.
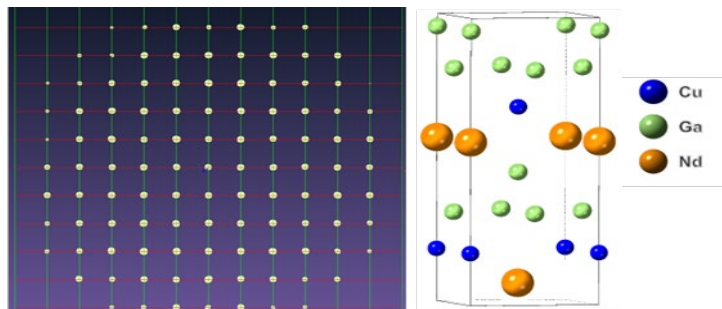

Figure 3: *Left-* Indexed Bragg reflections at the lattice sites suggest a very high-quality single crystal of $NdCuGa_3$. The size of the spots relates to the integrated intensity. *Right-* $NdCuGa_3$ atoms in a unit cell for the solved crystal structure.

- Procured an arc-melter instrument that is a new capability at SRNL to alloy metallic materials, **Figure 4**. The new capability will extend SRNL's materials growth and processing strength. The USQ writing process is underway, and the arc-melter is expected to be operational by the first month of FY23.
- Established an internal collaboration for actinide material synthesis and an external collaboration for the magnetic and physical property measurements of synthesized materials.

Figure 4: Arc-melter to alloy intermetallic materials (procured in FY22).

Peer-reviewed Publications

B. K. Rai, Patrick O'Rourke, Utpal Roy, "Review on crystal structures and magnetic properties of RTX_3 materials", *J. Physics: Cond. Matter.* 2022 34 273002 (*Invited* Topical Review Article, SRNL publication spotlight)

B. K. Rai, Shang Gao, Matthias Frontzek, Yaohua Liu, A. D. Christianson, A. F. May, "Magnetic properties of Fe-substituted NiBr2 single crystals", *J. Magn. & Magn. Mater.*, 2022 557 169452

B. K. Rai, Patrick O'Rourke, Catherine Housley, Henry Ajo, Arjun Pathak, Narayan Poudel, Firoza Kabir, Krzysztof Gofryk, Boris Maiorov, Qiang Zhang, Travis Williams and Matthias Frontzek "Magnetic structure and physical properties of $NdCuGa_3$ single crystals", *Manuscript in preparation 2022*

Team Members

Garrett Gotthelf and Ryan Greer

Software Supply Chain Attack Behavior Analysis

Dillon Tauscher

Industrial Control Systems (ICS) and Operational Technology (OT), as a unified system, are a target of foreign adversaries. They are rapidly becoming a major vulnerability for the United States. This project created a comprehensive environment for detecting and characterizing Software Supply Chain Attacks (SSCA). This environment spans the development, quality assurance, and production environments which span across physical workstations, operational technology devices, and network infrastructure. Allowing the baselining of hosts, networks, and application data while producing Indicators of Compromise (IOCs). The SSCA characterizes the IOCs while contained in a logically separated testbed. These testbeds are separated via Software Defined Networking (SDN). This capability complements existing prevention and detection efforts, placing SRNL at the forefront of securing U.S. Critical Infrastructure, including DOE.

Introduction

Following the SolarWinds attack of 2019, thousands of systems were impacted by the installation of malicious updates. These malicious updates allowed attackers to gain access to production environments, Microsoft 365, and Azure cloud environments. To successfully support and defend the rapidly merging Industrial Control Systems (ICS) and Operational Technology (OT) environment, a hybrid virtual-physical environment was created using a combination of open and closed-source software, physical network devices, physical severs, and workstations, **Figures 1-2**. This reusable environment greatly enhanced the virtualization capabilities of the GCIIC lab, making it a highly marketable platform for external customers by hosting advanced platforms for network segmentation. The enhanced capabilities of the GCIIC allow multiple virtual machines to sit on the same platform while virtualizing production, development, and quality assurance domains. Thus, allowing access from a singular physical machine, **Figure 3**.
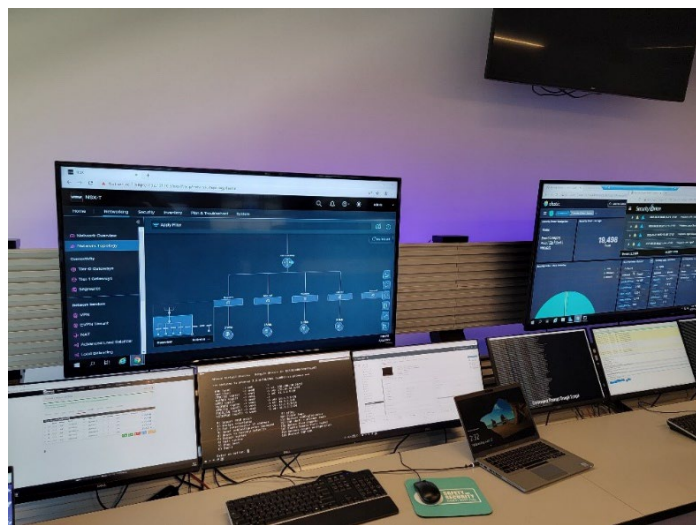

Figure 1: Servers Hosting Virtualized Environment
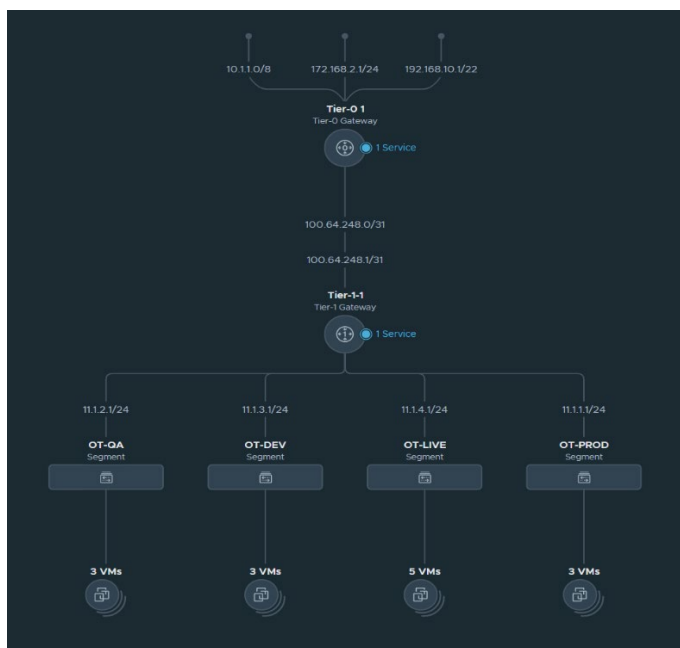

Figure 2: User Workstation and SIEM Console

Figure 3: Software Supply Chain Attack Surface

Approach

Combining existing ESXI and vCenter architecture with a VMWare virtualization platform (NSX-T), engineers focused on developing multiple environments with tailored services that would behave differently when the SSCA was released into the environment. The combination of a virtual distributed switch allowing for a flat yet intricate network where NSX-T supports specific East-West communication. The environment was successfully established and tested to ensure there would be no leakage when final approval was received to test corrupted programs and modified dynamic link libraries (DLLs) for monitoring. While a SSCA is not specifically characterized as malware, it is still a persistent threat that would be released into the controlled environment for monitoring. Beyond NSX-T related segmentation, engineers ensured virtual machines had no connectivity to the physical environment by using a virtualized PFSense firewall as an added layer of security. Combining the virtualization security of NSX-T, vCenter, and a virtualized firewall allowed for a truly isolated testbed by all definitions. From a continuous monitoring perspective, Security Onion was selected- as it is open source and has the capability to monitor a multitude of environments when utilizing NSX-T's segmentation properties, **Figure 4**. Once fully implemented, the SIEM will be used to determine if SSCAs can be characterized by behavior and respond to monitoring for IOCs.

Figure 4: Security Onion Dashboard

Accomplishments

- Created environment fully capable of low-level software monitoring with isolation properties.
- Garnered interest and funding of NNSA customers due to newly established capabilities.
- Supported Savannah River Pit Production Facility by developing capabilities to identify indicators of compromise (IOCs) in production and development environments.
- Enhanced technical rapport of SRNL Global Security Directorate.

Advanced Modeling of Tritium Embrittlement of Stainless Steel

Eric Hoar

Austenitic stainless steels are the structural material most commonly utilized in the infrastructure for storage and processing of tritium. In tritium, and hydrogen, environments many alloys undergo changes caused by the leeching of tritium into the material and lead to fracture. Therefore, understanding these changes is essential for predicting the limits of tritium infrastructure.

Introduction

Austenitic stainless steels are structural materials utilized in vessels for the storage of tritium gas. This is due to the resistance of the steel to hydrogen isotope embrittlement [1-3]. However, exposure to tritium over long periods leads to tritium uptake which decomposes to helium resulting in further synergistic embrittlement effects. **Figure 1**, obtained from Krentz, *et al.* (2021), illustrates how both the microstructure as well as the charging environment (noncharged vs hydrogen charged vs tritium charged) can change the mechanical properties of stainless steel [4].
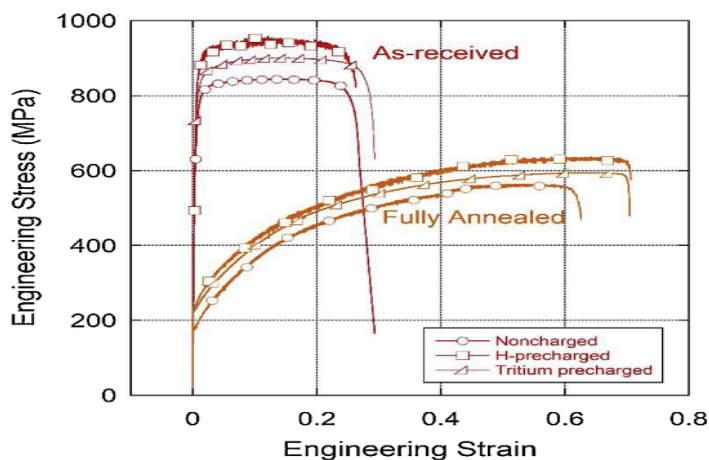
Figure 1: Comparison of stress-strain curves for stainless steel samples of the same composition charged in various environments and with different microstructures.

Due to these differences in embrittlement effects, it is important for tritium facilities to understand the material limitations of stainless steel in this environment. SRNL has been performing tritium embrittlement experiments for decades to identify these embrittlement effects. However, there has not been much effort in the development of a model capable of predicting the mechanical properties of austenitic stainless steel after tritium charging. Therefore, due to the availability of such a large dataset, machine learning algorithms provide an opportunity to model the stainless-steel embrittlement due to the ability of these algorithms to identify patterns in data sets that are difficult and costly to identify in other manners [5].

Approach

The approach of this project begins with the development of a machine learning ready dataset by pulling all of the experimental data at Savannah River National Laboratory together with literature data identified through a literature search. This dataset will then provide a foundation for the development of a machine learning model capable of predicting fracture toughness. Through discussions with experts in the field it was identified that the stainless-steel composition, hydrogen content, tritium content, helium content, initial yield strength and initial tensile strength would be key parameters of interest to the model. The machine learning algorithms will be built using python and the open source Scikit, SciPy and NumPy libraries. These libraries provide pre-built functions and reduce the number of custom-built functions required for model development. Multiple models will be developed and trained to identify the most optimal machine learning algorithm for the given dataset. These models include the use of decision tree, random forest, and gaussian process regression algorithms. **Figure 2** shows a schematic of the random forest algorithm. These algorithms each require a different amount of training data to be viable and as such it is expected that only some of these algorithms will show good predictive ability. Model performance will be described using the coefficient of determination to identify the model's ability to characterize the variability of the training data. The average percent error will identify the model's ability to accurately predict the fracture toughness of the test dataset.
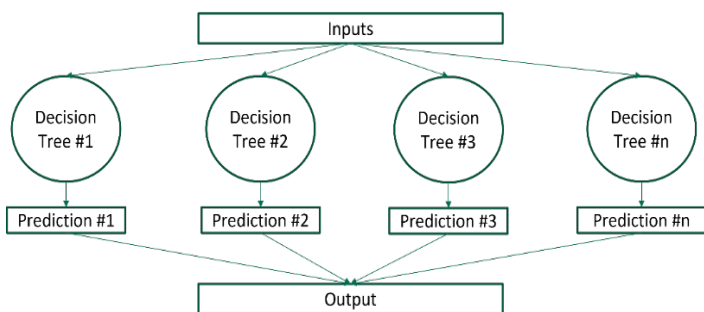
Figure 2: A schematic of the structure of a random forest machine learning algorithm.

Accomplishments

- Developed a singular data repository for all SRNL tritium embrittlement data obtained over the past 20 years.
- Performed a literature review for data which can be utilized concurrently with SRNL tritium data for a larger dataset.
- Developed multiple machine learning models utilizing several algorithms including decision trees, random forest, gaussian process regression, and multilayer perceptron.
- An analysis of the trends of prediction error vs amount of data was performed for each of the developed models to identify which models were performing well in the simulation conditions.
  - This is illustrated by **Figure 3** for the random forest model.
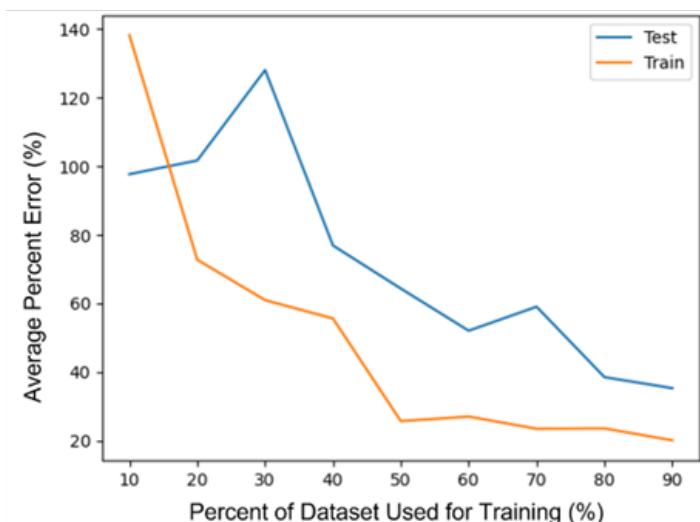
Figure 3: A plot of average percent error vs percent of data used in training showing the trends of the training error and testing error. For good models both errors should decrease to a small value as the amount of data used in training with the testing error being larger than the training error.

- Error analyses were performed on each of the developed models to identify the trained model's fit to the training data and predictive ability for new data points.
  - The random forest model was found to provide the best fit and predictive ability with the decision tree model a close second.
  - **Table 1** describes the R^2 and average percent error values for each of the developed models.

Algorithm	R_2	% Error (%)
DT	0.9591	26.6959
RF	0.9623	26.3897
GPR	0.8506	276.8863
MLP	0.4583	253.5980

Table 1: Comparison of R^2 and average percent error for each of the developed models including the decision tree (DT), random forest (RF), gaussian process regression (GPR), and multilayer perceptron (MLP) models.

- The random forest model prediction was compared to the actual fracture toughness values in **Figure 4**, where an optimal model would have all points lie on the green line. This illustrates the ability of the model to predict the fracture toughness of both the training dataset and the test dataset. The model was also compared to specific SRNL data points in fracture toughness vs content plots as shown by **Figures 5 and 6** to illustrate the predictive ability of the model.
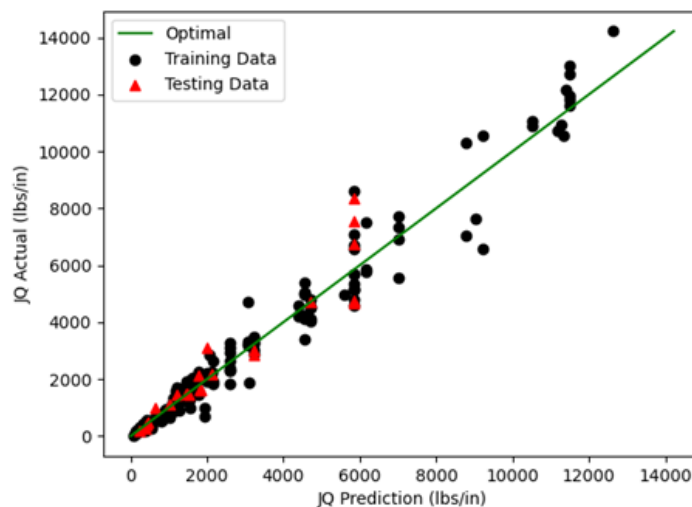

Figure 4: A comparison of actual fracture toughness values vs predicted fracture toughness values using the trained random forest model and showing the training dataset and test dataset with the green line showing an optimal result.
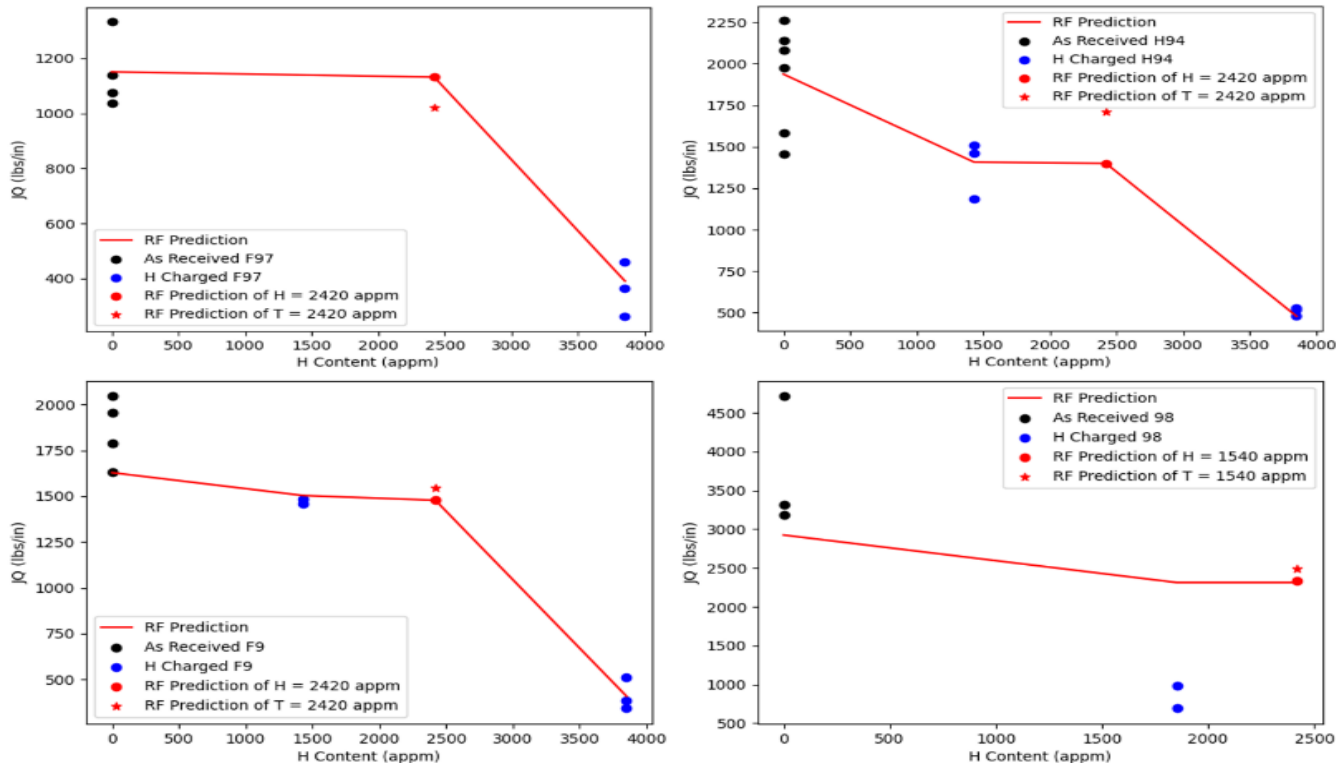
Figure 5: Fracture toughness vs hydrogen content plots showing the SRNL datapoints as well as the random forest model prediction line for the F97 (*top-left*), H94 (*top-right*), F9 (*bottom-left*) and 98 (*bottom-right*) samples identified in report WSRC-TR-2007-00244.
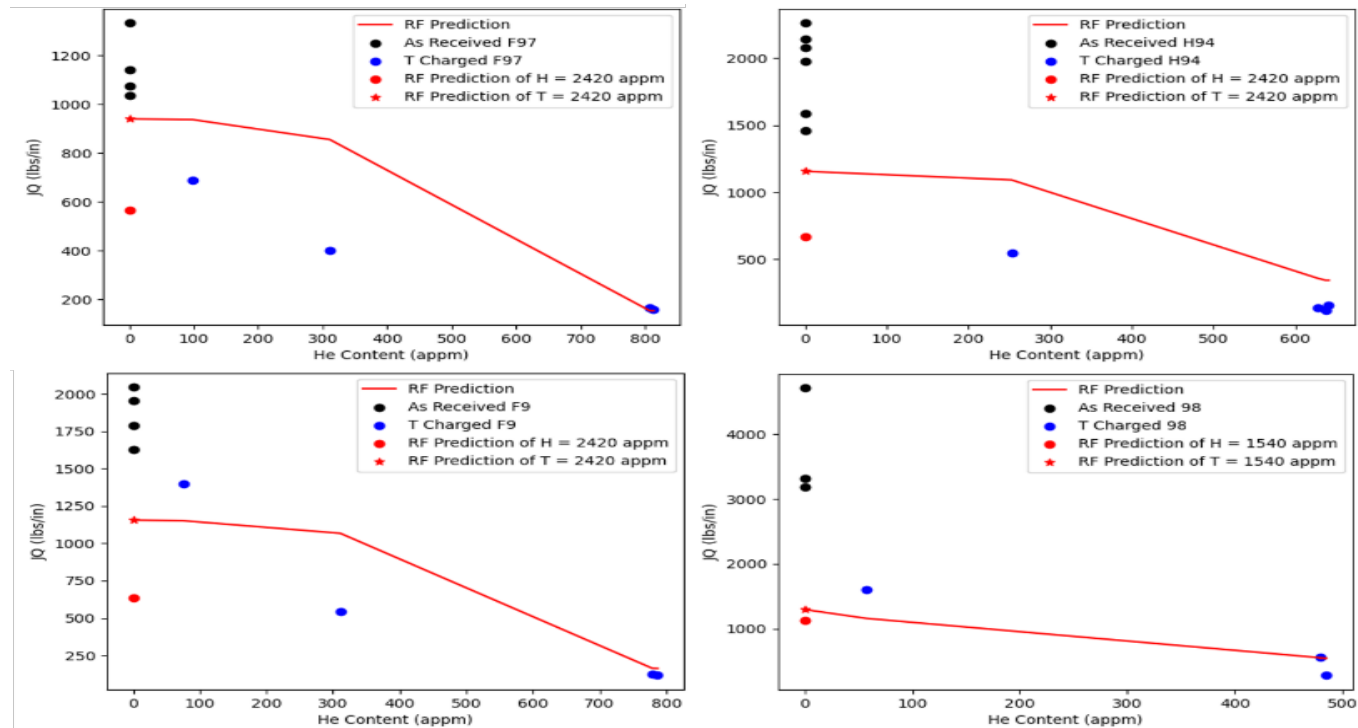

Figure 6: Fracture toughness vs helium content plots showing the SRNL datapoints as well as the random forest model prediction line for the F97 (*top-left*), H94 (*top-right*), F9 (*bottom-left*) and 98 (*bottom-right*) samples identified in report WSRC-TR-2007-00244.

- Model results were presented at the 2022 Materials Research Society Spring Meeting on May 25, 2022, in the Advanced Reactors & Modeling of Radiation Damage section.

Peer-reviewed Publications

"Advanced Modeling of H-isotope Embrittlement in Stainless Steels" Eric Hoar, Dale Hitchcock, Timothy Krentz, Lindsay Roy, *2022 Materials Research Society Spring Meeting,* May 2022. *(Oral presentation)*

Team Members

Dale Hitchcock, Timothy Krentz, and Lindsay Roy

Zach Duca

Enhancing Charge Injection Using Transition Metal Substituted Polyoxometalate-Based Photosensitizers

Lauren Hanna

A series of 3d-transition metal containing polyoxometalates have been synthesized. These materials were successfully characterized using a variety of spectroscopic and electrochemical techniques. A selected polyoxometalate was sensitized with a porphyrin-based dye to permit for more efficient solar spectrum utilization.

Introduction

The impact of Earth's reliance on fossil fuels and the climate change impacts from their combustion has created a surge in research for renewable alternatives to address the global energy crisis. Among the promising candidates, solar technology is at the forefront of the field. Solar cells permit for the sun's photons to be converted into electricity through the photovoltaic effect, **Figure 1**, providing clean energy. To mitigate some challenges solar cells face, more emphasis has been placed on chemically and structurally robust but cost-effective materials to make up the light harvesting photoanode.
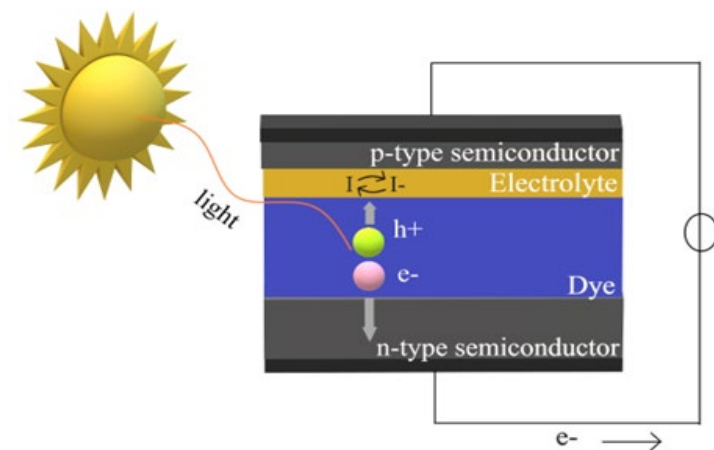

Figure 1: Depiction of the photovoltaic effect

Promising results have been shown by utilizing polyoxometalates (POMs) as photoanodes, given their semiconductor-like properties, exceptional electron accepting abilities, and inherent structural characteristics that promote excited state charge separation and tunable solar utilization. However, polyoxometalates suffer from poor visible light absorption. Given this, POMs may be sensitized with dyes to promote greater visible light absorption. Porphyrins offer high molar absorptivity of the solar spectrum which makes them optimal candidates as photosensitizers. Additionally, introduction of 3d transition metals to the polyoxometalate structure permits for orbital matching with the porphyrin, which may promote efficient charge transfer from the dye to the POM. Not only does this hybrid material promote optimal solar spectrum utilization but the physical distance between the photo-generated electron and hole, upon charge injection from porphyrin and POM, may reduce detrimental charge recombination. This may promote the conversion of the solar energy to usable power.

Approach

The approach of the project is to first, synthesize a series of 3d transition metal containing polyoxometalates (POMs) where M = Mn(II), Fe(III), Cu(II), and Co(II). These POMs are then characterized using a series of spectroscopic and electrochemical techniques to confirm the identity and stoichiometry of each of the POMs. Following, the POMs will each be covalently bound to a porphyrin photosensitizer, monocarboxyphenyl triphenyl porphyrin. The efficiency of the photoinduced charged transfer will be evaluated using electrochemical means. The photocurrent of the POM-porphyrin hybrid material will be measured. To do this, a bias potential will be applied and the resulting current will be measured as a function of white light irradiation. The current produced when the light is on compared to off will indicate whether photocurrent has been produced. This requires that the porphyrin transfers photogenerated electrons to the POM moiety and the POM injects the electrons to the ITO substrate allowing for the production of current which is essential for the function of a dye-sensitized solar cell (DSSC). The POM-porphyrin hybrid that produces the optimal photocurrent and displays the longest charge separation will be chosen to be used in a test DSSC.

Accomplishments

- Synthesis of a series of 3d-transition metal polyoxometalates with the formula: $[X_4(H_2O)_2(PW_9O_{34})_2]^{z-}$ where X = Mn(II), Fe(III), Cu(II), and Co(II).

- The composition of the synthesized polyoxometalates were confirmed using inductively coupled plasma optical emission spectroscopy (ICP-OES) **Table 1**. This method confirmed the targeted stoichiometry shown above.

POM	M	P	W
POM	n/a	2	18
4Mn-POM	4	2	20
4Fe-POM	4	2	10
4Cu-POM	4	2	21
4Co-POM	4	2.4	18

Table 1: ICP-OES results for all synthesized polyoxometalates

- All POMs were characterized using energy dispersive X-ray spectroscopy (EDS) which supported the results of the ICP-OES. This furthered the conclusion that the target formula was obtained.

- Synthesized POMs were characterized using UV/Vis spectroscopy and Fourier transform infrared spectroscopy (FT-IR), **Figures 2-3.**
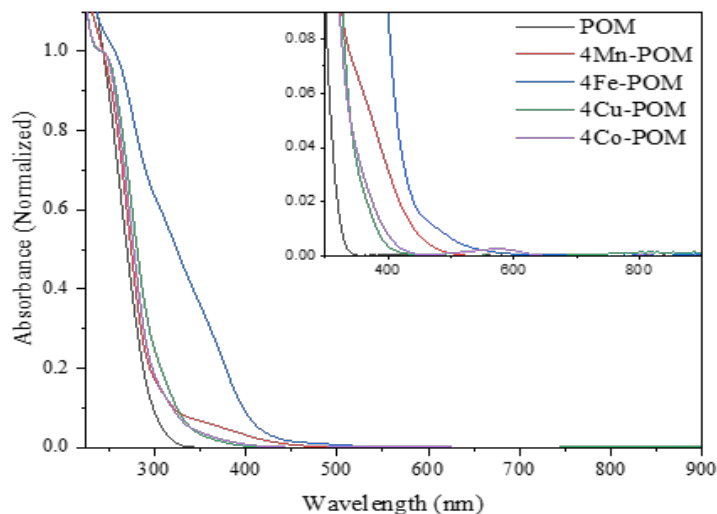
Figure 2: UV/Vis spectroscopy of all synthesized polyoxometalates measured in water
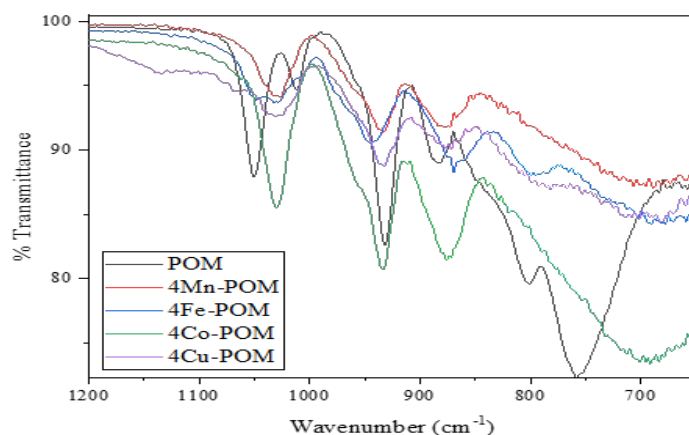

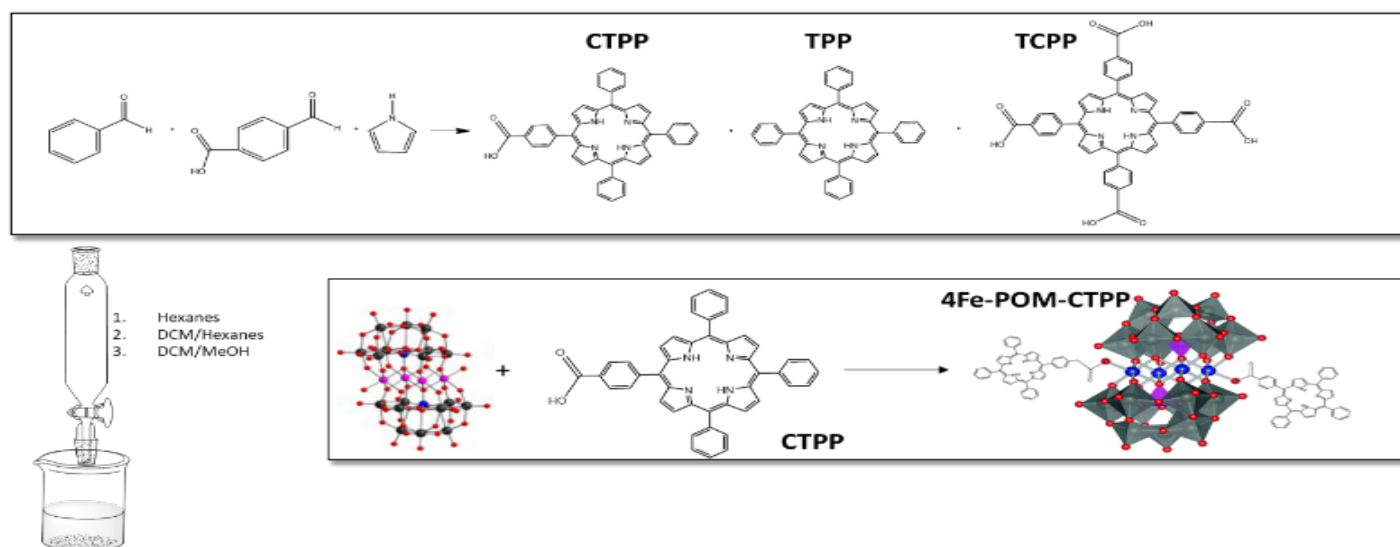**Figure 3:** FT-IR of all synthesized polyoxometalates

Figure 4: Synthesis of monocarboxyphenyl triphenyl porphyrin and POM-porphyrin hybrid material

- Two, porphyrin-POM hybrid materials were obtained by reacting a polyoxometalate with the synthesized porphyrin. Samples were confirmed using FT-IR, **Figure 5**, UV/Vis spectroscopy, **Figure 6**, cyclic voltammetry, **Figure 7**, and EDS, **Figure 8**.
- Initial fluorescence measurements suggested possible fluorescence quenching of a preliminary porphyrin-POM hybrid material
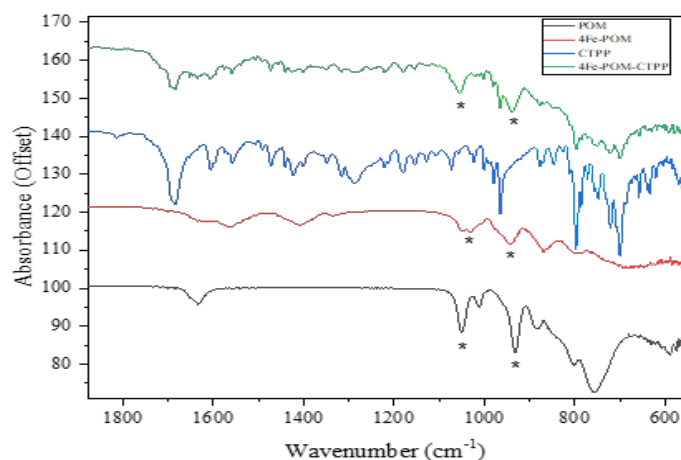

Figure 5: FT-IR of POM (black), 4Fe-POM (red), monocarboxyphenyl triphenyl porphyrin (TCPP) (blue), and POM-porphyrin material (4Fe-POM-CTPP) (green). Selected POM-based modes indicated with an asteris

Team Members

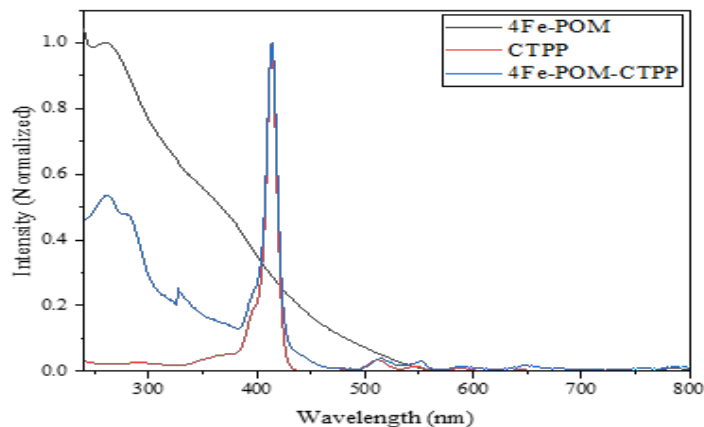Jenny Lockard[a], Kori McDonald

[a] *Rutgers University-Newark*

Figure 6: UV/Vis spectrum of 4Fe-POM, monocarboxyphenyl triphenyl porphyrin (TCPP) (red), POM-porphyrin material (4Fe-POM-CTPP) (blue) measured in acetonitrile
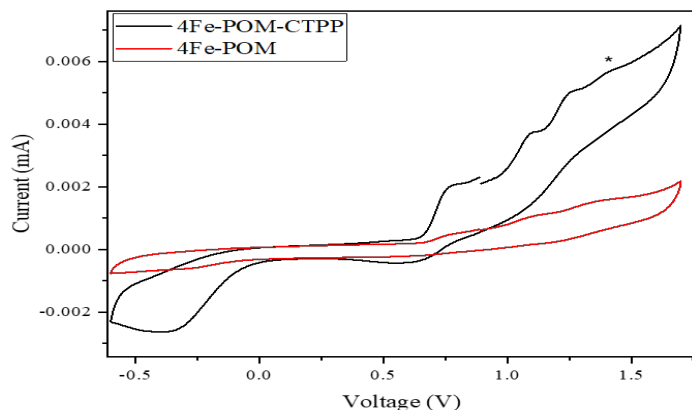

Figure 7: Cyclic voltammogram of 4Fe-POM (red) and 4Fe-POM-CTPP (black) with 0.1 M TBAPF$_6$ measured in degassed acetonitrile. The porphyrin oxidation is indicated with an asterisk.
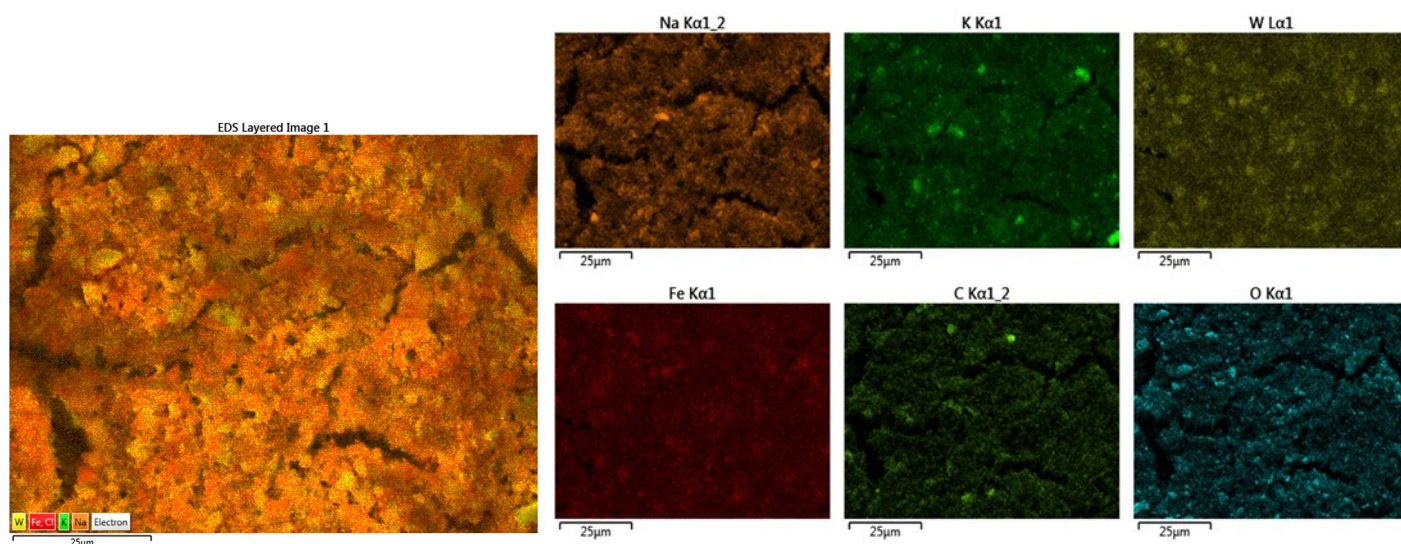

Figure 8: EDS maps of 4Fe-POM-CTPP material

CIIC & SCOPE Power System Co-Simulation

Ian Webb

With the onslaught of recent infrastructure hacking, the ability to remotely and securely control advanced/prototype power electronics that drive renewable energy resources will prove to be a vital capability in future development in the field of grid resiliency. The interconnection of the two power system simulator capabilities between Savannah River National Laboratory (SRNL) and University of South Carolina (USC) will enable both labs to perform research pertaining to distributed energy resource cyber security.

Introduction

Power electronic-based distributed energy resources (DER) connected to distribution networks are beginning to affect the transmission system in operations and planning. Advanced power electronics are often deployed in settings with high amounts of variable renewable energy, which allows for a high degree of control over power flow and stability on the distribution level of a power system. Advancements in information and communication technologies now make it possible to command and control power electronic-based DER from supervisory control and data acquisition (SCADA) networks, allowing for a high level of remote control and monitoring over a wide area. DERs have been demonstrated to be exceptionally vulnerable to network-based attacks, requiring minimally sophisticated cyber-attack frameworks to inflict system shutdown, cause instability, and physically damage power system components. To address the rising issue of DER-based cyber security, R&D solutions need to be developed to secure connected power grid control systems. To this extent, a geographically distributed VPN network was developed between the real-time power system simulators at SRNL and University of South Carolina. This allows for realistic network latency between simulated power systems and physical power system components, namely power electronic-based DERs. The unique capability of both the power electronic prototyping and hardware-in-the-loop capabilities at USC coupled with the VPN connectivity to the hardware-in-the-loop capabilities at SRNL enable researchers at USC to connect physical hardware to power system simulations at USC which directly interact with power system simulations at SRNL.

Approach

SRNL and USC interconnected power hardware-in-the-loop (HIL) and controller hardware-in-the-loop capabilities between the two campuses through connecting the real time digital simulator (RTDS) system at SRNL and the OPAL-RT system at USC. To do so, an IPsec tunnel was established between the SRNL Critical Infrastructure, ICS and Cyber Security (S-CIIC) lab at SRNL and a server at the USC campus. After the IPsec tunnel was established, the VILLAS framework was utilized to interface the power system simulators to one another, shown in **Figure 1**. The VILLAS framework is a toolset that translates the socket information from the power system simulator into UDP packets, which are then transferred across the IPsec tunnel to the other instance of VILLAS. Through this interconnection, transmission simulations developed at SRNL were connected to microgrid simulations and hardware developed at USC. Once connectivity was confirmed, the SRNL VILLASnode instance was configured to transmit information from the RTDS (power system simulator) to VILLAS, and then through the IPsec tunnel to the USC VILLAS instance, which was configured to transmit information between the SRNL VILLASnode and USC's OPAL RT (power system simulator). At that point, power system simulations were created and loaded onto each simulator, and the connection went through the final testing of co-simulation.

Accomplishments

- Successfully deployed VILLASnode locally within S-CIIC and sent information back and forth from simulator to VILLAS
- Obtained SRS Governance Review Board approval to operate over the Juniper SRX cellular gateway
- Established IPsec tunnel between CIIC cellular gateway and USC VILLAS device

Figure 1: Functional Network Diagram of Co-Simulation Network
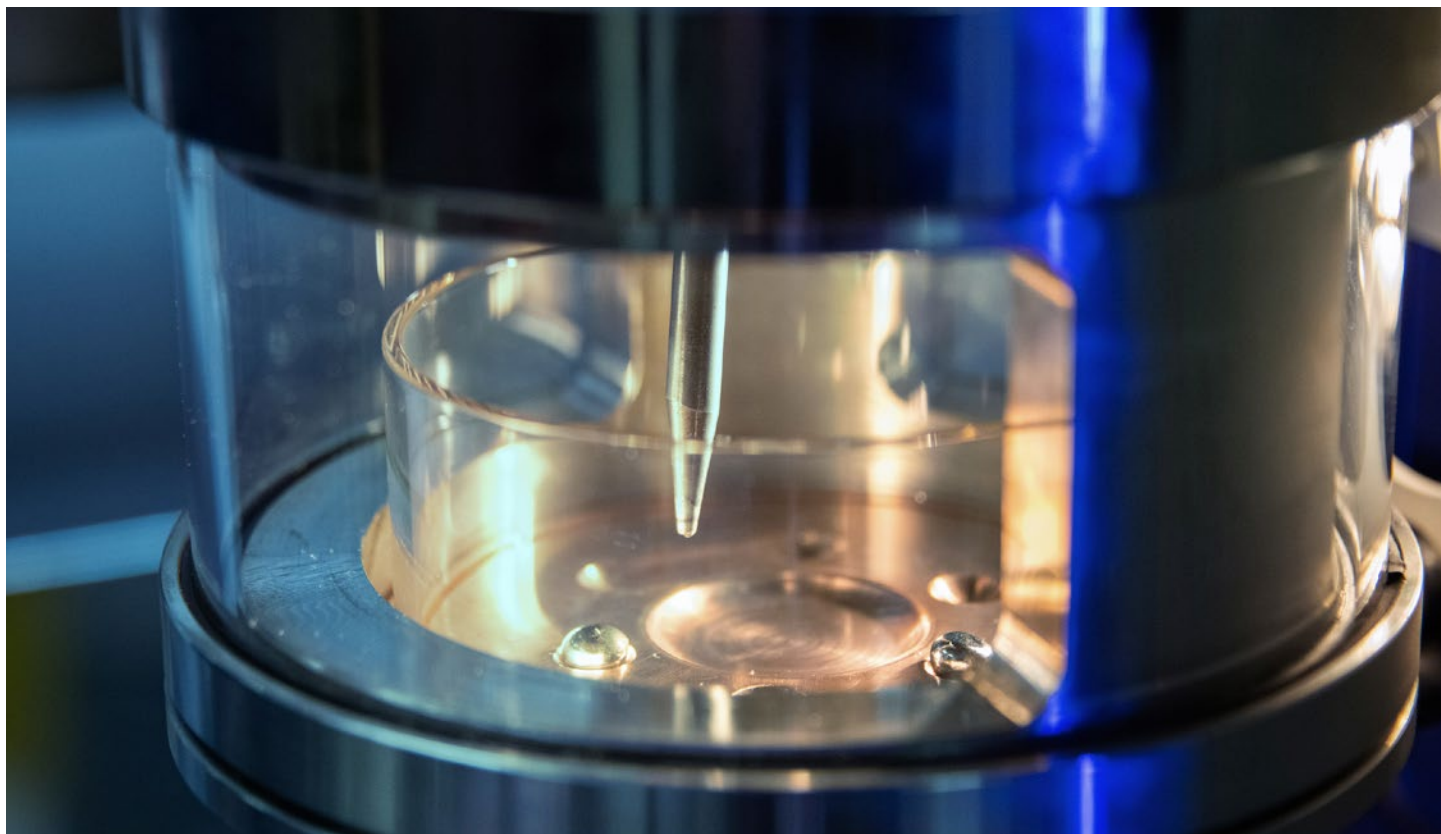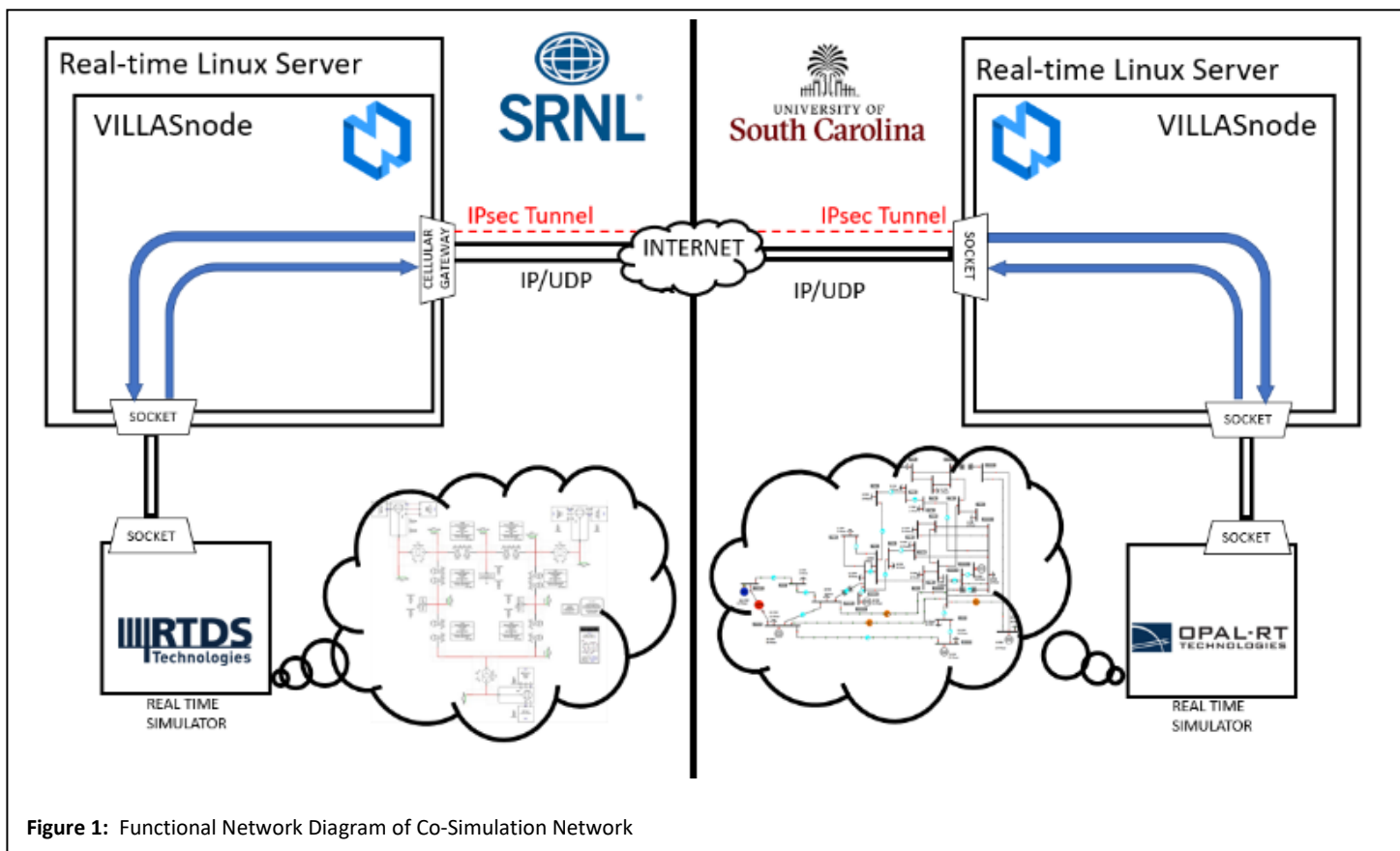
Microscopic Characterization of Pu-bearing Compounds with Diffuse Reflectance Spectroscopy

Eliel Villa-Aleman

The spectra of $Pu_2(C_2O_4)_3$ and its thermal degradation products were measured with diffuse reflectance spectroscopy. PuO_2 was studied at several calcination temperatures. Principal component analysis of diffuse reflectance spectra classified the samples based on calcination temperature producing information on the production history of PuO_2.

Introduction

Retrospective determination of the process history, age, and storage conditions of interdicted nuclear materials is a key goal in the fields of nuclear forensics and nuclear nonproliferation. To accomplish this goal, it is necessary to gain a holistic understanding of the chemical and structural properties of nuclear materials. Despite nearly eighty years of plutonium production and processing, the fundamental chemical and structural properties of most plutonium process materials is largely understudied due to a combination of safety and regulatory considerations, plutonium's inherent chemical complexity both in metal and compound forms, and a historical focus on plutonium for weaponization and fuel applications. Thus, within the category of compounds that are important in the nuclear fuel cycle, plutonium and its chemical compounds are arguably some of the most understudied from a fundamental science point-of-view.

In industrial scale fuel and waste reprocessing plants, plutonium dioxide (PuO_2) is routinely produced via thermal decomposition of hydrated plutonium (IV) and plutonium (III) oxalate. Despite the longstanding utility of this chemical process, only a few studies have utilized optical spectroscopy to study the chemical compounds involved in this process, primarily diffuse reflectance Fourier transform infrared spectroscopy (DRIFTS) and Raman spectroscopy. Hobart et. al reported diffuse reflectance spectroscopy (DRS) for high-fired PuO_2 from the visible to NIR spectral region. This research focuses on the production history of PuO_2 by applying principal component analysis to diffuse reflectance spectra in the short-wave infrared (SWIR)

spectral region of PuO_2 calcined at eight different temperatures.

Approach

While both DRIFTS and Raman vibrational spectroscopy have a high utility in studying metal-containing complexes, like PuO_2 and Pu oxalate, neither technique is particularly sensitive towards assessing metal-ligand electronic interactions, which are poorly understood and not easily modelled for most *f-block* metals. DRS in the SWIR (900–1600 nm) energy range is a spectroscopic tool that can provide detailed information about metal-ligand electronic interactions based on splitting of the crystal field energy levels of the metal. Raman spectroscopy and X-ray diffractions studies have shown that higher calcination temperatures result in a more order crystal lattice; therefore, the highly sensitive DRS technique will be able to discriminate between small changes within the crystal lattice.

In general, room temperature DRS spectra of Pu-bearing compounds are quite complex in the SWIR region, and spectra are usually composed of broad bands due to overlap of numerous absorption bands. In comparison to Raman spectroscopy, DRS is up to an order of magnitude faster enabling the collection of substantial data sets for statistical analysis. Principal component analysis (PCA) can simplify complex data by revealing trends within the data. PCA has been demonstrated to successfully discriminate samples which possess visually similar spectra. PCA combined with DRS can discriminate PuO_2 calcination temperatures yielding information on the production history of PuO_2.

Accomplishments

- Produced $Pu_2(C_2O_4)_3$ and its thermal degradation products, PuO_2, at a total of twelve temperatures.
- Contained Pu samples in a double walled cell to analyze in a clean lab.

- Performed DRS on $Pu_2(C_2O_4)_3$ and PuO_2 at twelve calcination temperatures as shown in **Figure 1**. Spectra were recorded at 10 different spots on each sample for statistical data analysis.
- PCA was applied to the DRS of PuO_2 at eight calcination temperatures. PCA discriminated between each calcination temperature yielding information on the production history of PuO_2 as shown in **Figure 2**.

Team Members

Jason Darvin, Bryan Foley

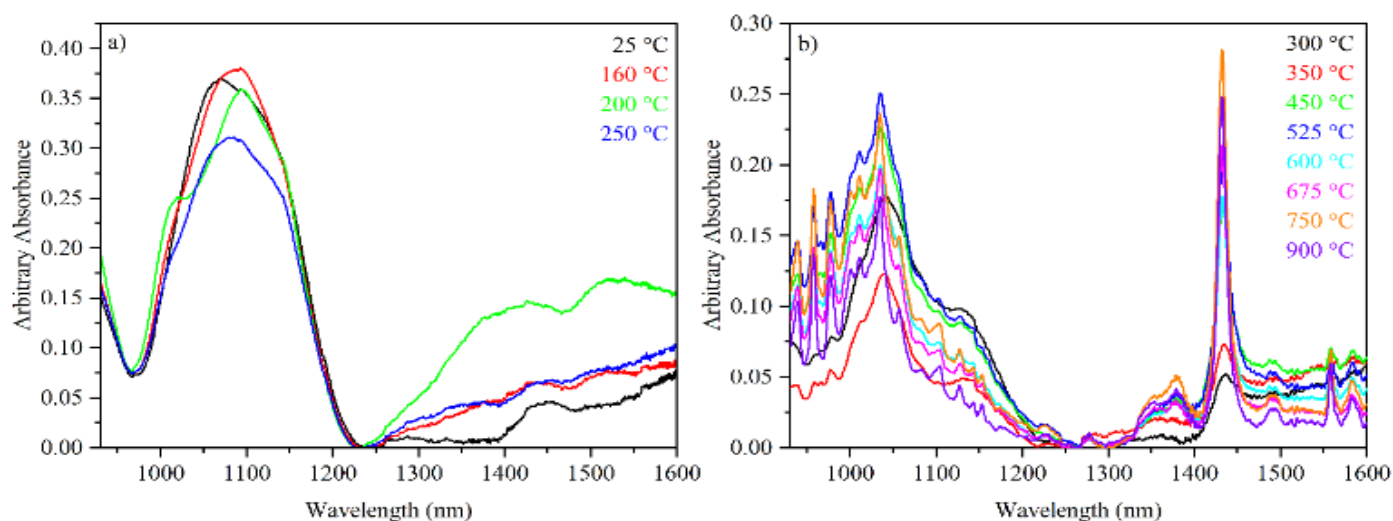**Figure 1:** Diffuse reflectance spectra in the short-wave infrared for a) $Pu_2(C_2O_4)_3 \cdot 9H_2O$, and b) PuO_2 generated from calcination of $Pu_2(C_2O_4)_3 \cdot 9H_2O$ at temperatures ranging from 300 °C to 900 °C.
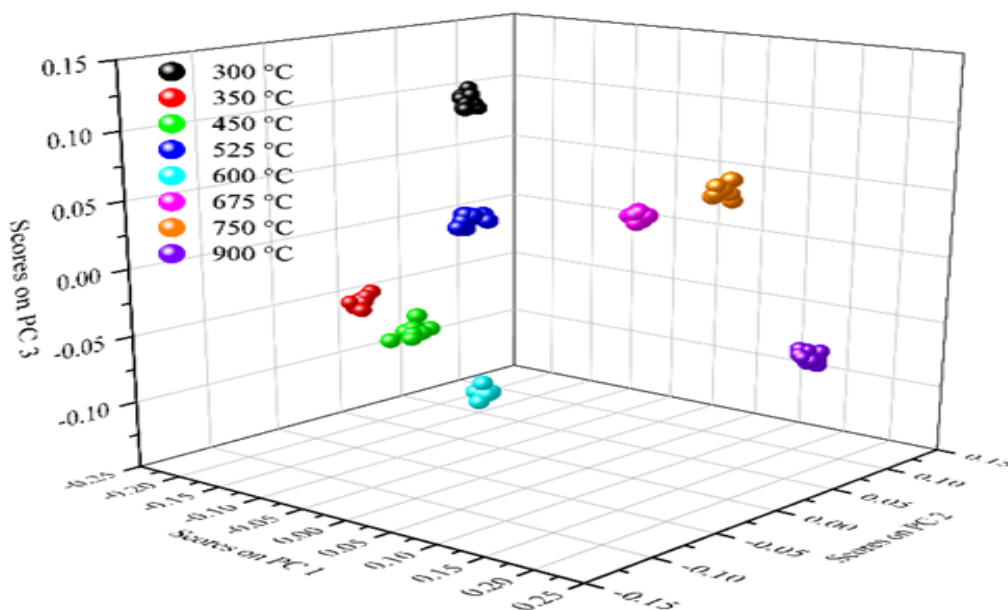

Figure 2: The scores of PC3 vs. PC2 vs. PC1 are shown for the SWIR DRS of PuO_2 calcined at temperatures 300 – 900 °C.

Bipolar Plates Design and Testing for Alkaline Electrochemical Systems

Hector Colon-Mercado

The overall objective of this project is to develop next generation alkaline electrochemical systems by designing low cost, high efficiency bipolar plates (BPs) meeting current DOE technical targets. These BPs will result in lowering commercialization barriers of cost and ease of manufacturing associated with electrochemical systems.

Introduction

Performance, cost, and durability of alkaline electrochemical systems are the key factors that govern the commercialization of H_2-based energy devices such as unitized regenerative fuel cells (URFCs), fuel cells (FCs), and electrolysis cells (ECs). While alkaline systems offer advantages of high energy density vs. existing energy conversion systems, their cost prevents commercialization. Bipolar plates influence many of the system barriers such as cost, lifetime, and performance. While the development of BP is recognized by funding agencies, the research is at its early stage of development and is not a saturated field. This project seeks to address the major obstacles in BP design to develop commercially friendly BP for alkaline electrochemical systems. In this project, SRNL, in collaboration with the University of South Carolina (USC), are working on the development of the next generation BPs that address most of the metrics outlined by funding agencies such as the Department of Energy-Energy Efficiency and Renewable Energy (DOE-EERE). Our research focused on the development of low-cost thin BPs that perform equal to or better than research grade BPs. We (i) developed surface finishes and high-performance thin films for corrosion protection applications, (ii) designed new flow fields with improved mass transport and heat rejection, and (iii) enhanced component test capability for the evaluation of new experimental components being developed at Savannah River National Laboratory (SRNL).

Approach

SRNL utilized its expertise in electropolishing and electroplating to coat different substrates considered as alternate alloy materials such as aluminum and stainless, for preparing BPs. **Figure 1** shows the Scanning Electron Microscope (SEM) image and the energy dispersive X-ray analysis (EDAX) elemental analysis of Ni-coated Al substrate.
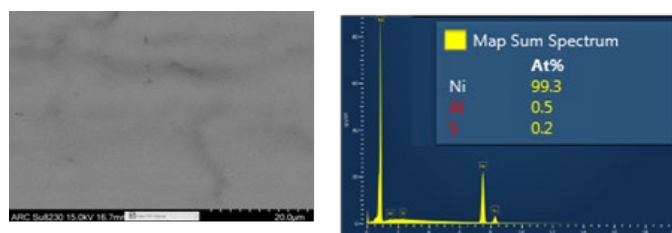

Figure 1: SEM and elemental EDX analysis of Ni-coated Al substrate.

Defect free and smooth surface with a surface roughness (S_a) value of 0.842 μm is achieved which meets our target of S_a <1 μm. **Figure 2** compares the potentiodynamic polarization curves of different metal substrates and Ni-coated Al1100 in 4.0M NaOH solution at room temperature. Pure Ni shows the best corrosion resistance properties and Ni-coated Al shows similar corrosion resistance with 70% weight reduction in construction weight. The corrosion current achieved for the Ni-coated Al substrate meets our target of <1 μA/cm^2.
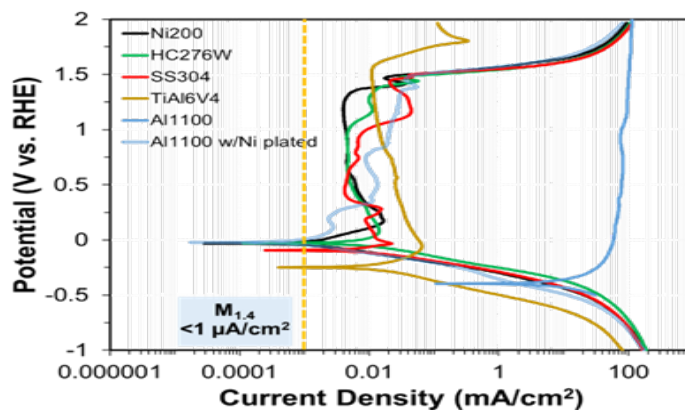

Figure 2: Comparison of potentiodynamic polarization curves of different substrates measured in 4 M NaOH at room temperature.

Figure 3 compares the bare Al substrate before and after the corrosion test. Contact resistance is minimal for Ni and nickel-based alloys, **Figure 4,** and their electrical conductivity, **Figure 5,** meets the target of >100 S/cm.
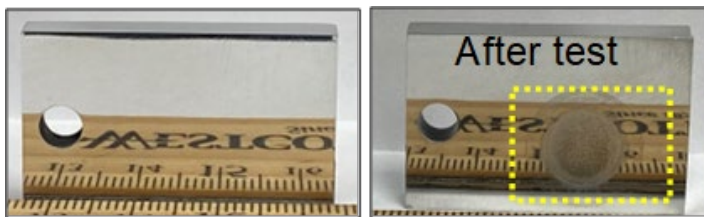

Figure 3: Before and after corrosion test of bare Al6061 coupons. Highlighted area shows post-test electrochemical damage
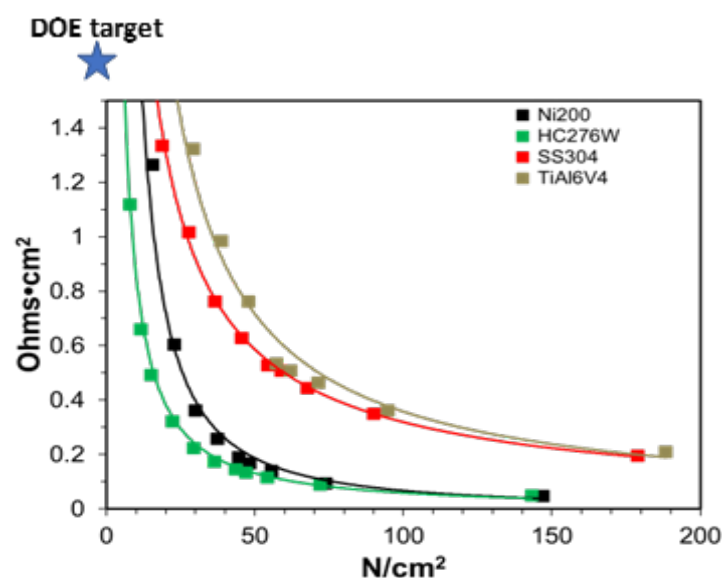

Figure 4: Contact resistance is minimal for Ni and nickel-based alloys, meeting DOE targets
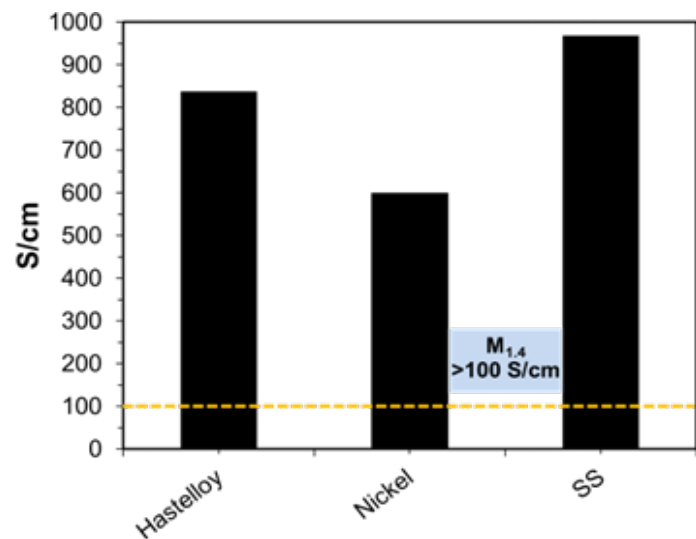

Figure 5: Electrical conductivity for all materials tested meets milestone

The water and heat management issues in BPs were studied at USC by developing and testing new flow-field designs, **Figure 6**, specifically designed for alkaline electrochemical systems where water management is more demanding than in acid systems. Improvements on the flow field design helped reduce mass transport limitations. As shown in **Figure 7**, serpentine (S) and parallel (P) flow-field designs show the best FC performances as they lack the noise observed in the performance curves which is indicative of poor water management.
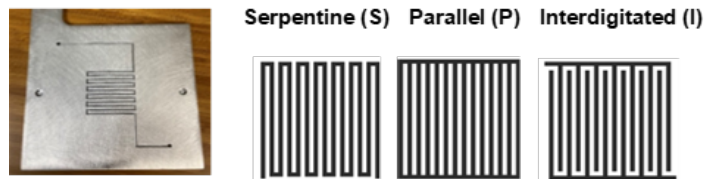

Figure 6: Flow-field designs developed and tested in alkaline environment
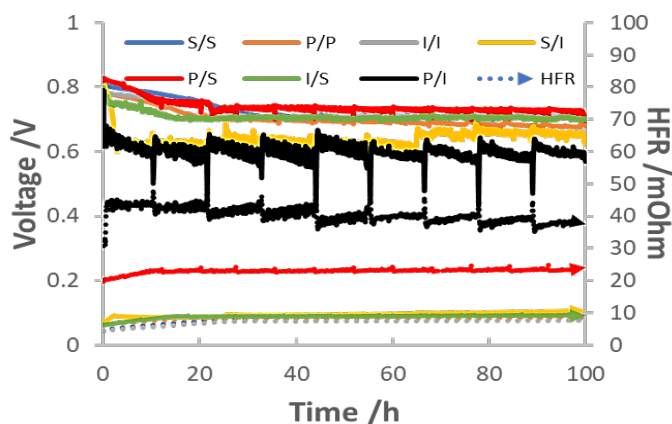
Figure 7: Alkaline fuel cell testing using various flow-field designs.

Accomplishments

- Identified and developed a suitable coating for Al substrates which showed defect-free and smooth surface meeting the proposed milestones for surface roughness, corrosion current, and electrical conductivity.
- Designed and tested three different flow-fields and identified two possible flow-fields for alkaline electrochemical systems.

Team Members

Noor Ul Hassan[a] , William Mustain[a]

[a]University of South Carolina

Defining Qubit Properties in Pa4+ Complexes

Lindsay Roy

This research seeks to develop a detailed understanding of the chemical and electronic properties of protactinium (Pa) complexes in the hopes of controlling its spin-orbit and crystal electric field effects with potential as an actinide qubit. SRNL has a unique opportunity to not only describe the interplay between the d and f orbital occupations, but also make significant contributions to the community using recently found Pa material.

Introduction

The realization of a quantum computer would change our world by boosting computation times and cracking highly safe encryption algorithms. In quantum information processing (QIP), f-element systems have shown exceptional promise. Specifically, as the actinide series traverses from left to right the relativistic effects cause the energetics of the 5f and 6d orbitals to change, imparting a rich and complex chemistry wherein the control of a quantum bit (qubit) could be possible. Protactinium is the most interesting element in the early actinide series because of its near degeneracy of the 6d/5f orbitals, making it behave more like a transition metal. This proposal will delineate the chemically engineering of high-valent 5f1 protactinium complexes as qubits by evaluating how its unique atomic properties, including spin-orbit coupling (SOC), crystal electric field (CEF), and nuclear spin, can be exploited through coordination chemistry to observe long-lived coherence times. The research will leverage both experimental and theoretical findings to generate a set of features to enhance quantum coherences in actinide molecules.

Approach

Our approach can be broken down into two overarching objectives: Purification, synthesis, and characterization of Pa^{4+} complexes and development of first-principles derivation of spin-orbit coupling and crystal electric field parameters for Pa^{4+}.

Purification:

- Identify: Using radiolysis, analyze legacy material for unique radiological signature. This is used to not only understand the bulk element but also its decay daughters/granddaughters.
- Purify: Develop a method to extract the materials from the source.
    - Dissolution: Find a suitable acid/solvent to isolate the sample from the source.
    - Separation: Extract the products from the fission elements using solvent exchange, precipitation, or exchange resins.
- Documentation/Storage

Exploration of the Pa-Ligand chemical space:

- Exploration: Develop ab initio methods to evaluate the metal-ligand chemical space for Pa^{4+} systems.
    - Test Systems: Evaluating Walsh Diagrams for MCl_4, MCl_6^{x-} and MCl_3 (M = Th, Pa, U, Np)
- Spin-Phonon Coupling: Establish a methodology to quantify the intensity as well as mechanisms and processes for relaxation pathways in actinide qubit complexes.

Accomplishments

As mentioned earlier, project work was divided into four tasks to show progress in all areas, outlined below along with their milestones in FY22. Results and accomplishments are presented under each milestone.

- Task 1: Purification of 100 mg legacy protactinium (Pa) material
    - M1: Identified purification method of 231-Pa (August 2022)
        - The Pa sealed source was isolated, **Figure 1**, and various acid dissolution processes were used to separate Pa from the fission products. Additionally, actinium was found in the product

stream and attempts are underway to separate Ac from Pa.

Figure 1: A sealed legacy source at SRNL was found to contain Protactinium-231 and a significant amount of decay daughters.

- Task 2: Synthesis and characterization of Pa^{4+} (ongoing through August 2023)
- Proposed scheme for isolation of a protactinium product has been devised. The proposed synthesis will proceed as an amide salt to then allow for ligand metathesis with a protactinium chloride starting material, **Figure 2**.
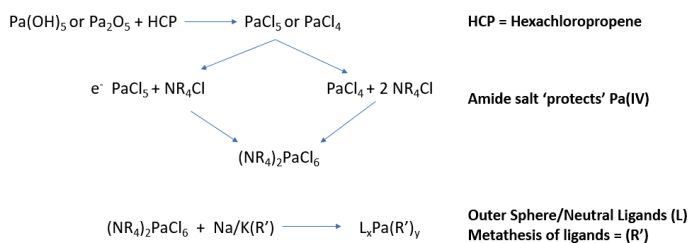

Figure 2: Proposed scheme for protactinium synthesis.

- Task 3: Exploration of the Pa-Ligand chemical space
- M3: Validation of theoretical methods via experiment of Pa^{4+} known complexes (August 2022)
- Complexes
- M2: Determination of new Pa^{4+} complexes

- Calculations were performed on MCl_6 and MCl_4 (M = Th-Np) to evaluate the amount of d/f orbital character when breaking from high symmetry complexes, **Figures 3 – 5**. The results show that as you decrease the symmetry of the system, the overall energy remains flat until a higher degree of symmetry breaking occurs in turn leading to higher d orbital character in the highest occupied molecular orbital. There are several commercial-off-the-shelf ligands available to explore the extent of d-character mixing as a result of symmetry breaking.
- Task 4: Spin-phonon coupling calculations
- M4: Derivation of spin-phonon coupling in 5f1 single ion magnets (ongoing August 2023)
- Spin- the ORCA software in FY22. Initial calculations focus on computing the magnetic properties of the early actinide chlorides.

Peer-reviewed Presentations

"Defining qubit properties in early actinide complexes," Stephanie Gamble, Lindsay Roy, Pete La Pierre, Julie Niklas, Tom Shehee and Garret Gotthelf, MRS Spring Conference, May 2022. (Oral presentation)

"Defining qubit properties in Pa4+ complexes," Stephanie Gamble, Lindsay Roy, Pete La Pierre, Julie Niklas, Tom Shehee and Garret Gotthelf, Rare Earth Research Conference, July 2022. (Poster presentation)

Team Members

Stephanie Gamble, Garret Gotthelf, Megan Hoover, Thomas Shehee, Henry La Pierre[a], Julie Niklas[a]

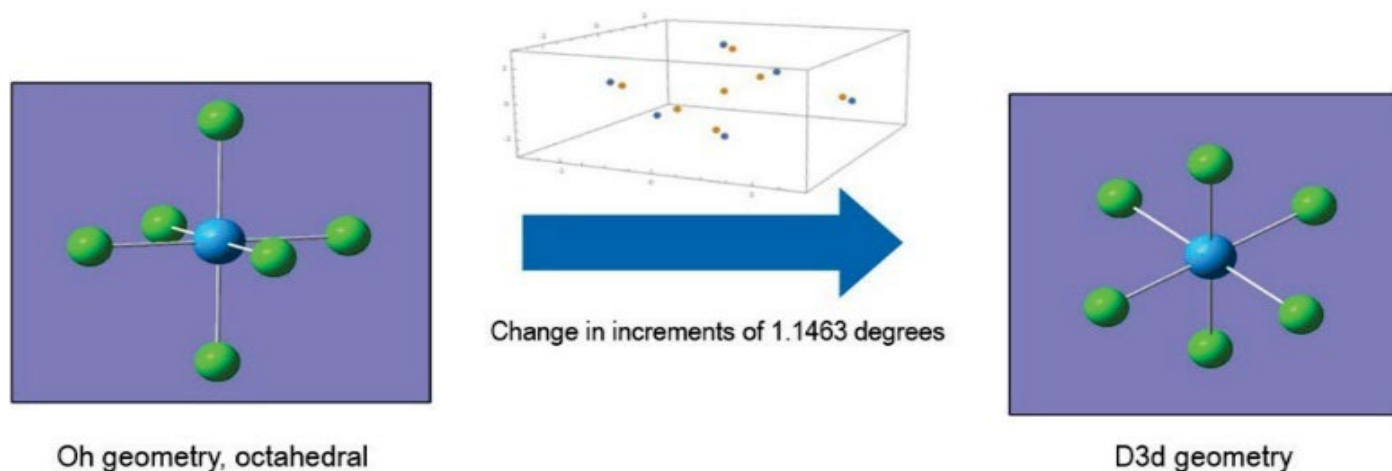[a] *Georgia Institute of Technology*

Figure 3: (*Left*) The actinide hexachloride molecule ([AnCl6]$^{2-}$, An = Th, Pa, U, Np) began with octahedral (*Oh*) symmetry. (*Right*) Small incremental changes to the molecular structure result in dihedral (*D3d*) symmetry. An^{4+}: blue atoms, Cl$^-$: green atoms.

(a)

(b)

Figure 4: The bond energy is plotted for the series of early actinide hexachloride molecules (An = Th, Pa, U, and Np) with (*a*) an overall charge of 2-, [AnCl$_6$]$^{2-}$ and (*b*) a single 5f electron (*i.e.,* 5f^1).
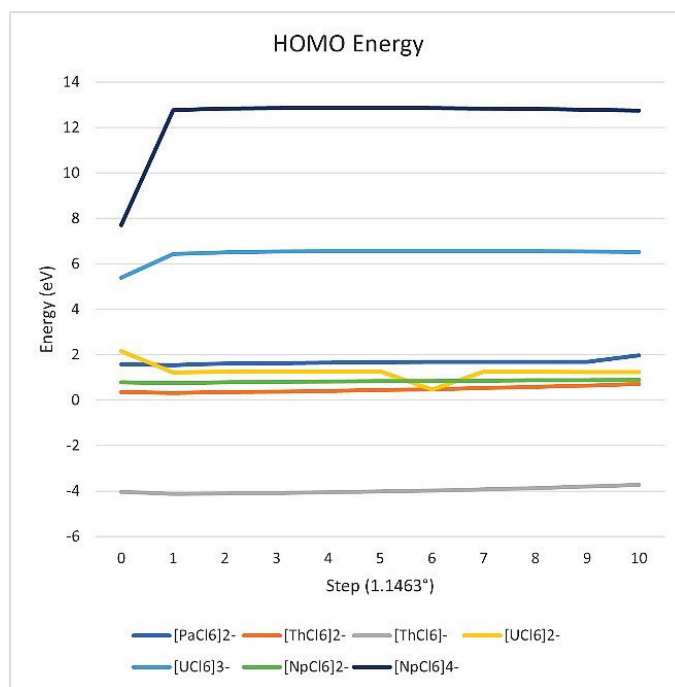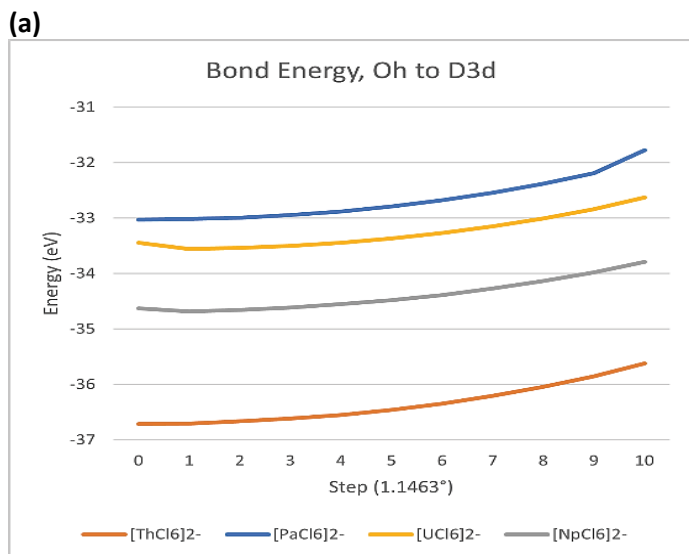

Figure 5: The Highest Occupied Molecular Orbital (HOMO) energy levels are plotted for the early actinide (An = Th, Pa, U, and Np) hexachloride compounds with an overall charge of 2- (*e.g.*, [AnCl6]$^{2-}$) and a single 5f electron (*e.g.*, [ThCl$_6$]$^-$, [PaCl$_6$]$^{2-}$, [UCl$_6$]$^{3-}$, [NpCl$_6$]$^{4-}$).

Leveraging Magnetic Field Coupling for Extended Charge Separation Lifetimes

Patrick Ward

Photovoltaics operate by light induced generation of negative electrons and positive electron holes, which are separated to generate electricity. These charges can recombine before electricity can be generated resulting in lower solar conversion efficiencies. Herein, we study the impact of magnetic fields on mitigating charge recombination to increase photovoltaic efficiencies.

Introduction

Perovskites are well established as one of the most promising candidates for next generation photovoltaics due to their reasonably high solar conversion efficiencies and low-cost production potential. One of the factors which limits photovoltaic efficiencies, is the recombination of positive electron holes and negative electrons before they reach their respective electrodes. Our intention is to demonstrate enhancement in the performance of these materials through the application of a magnetic field to induce Lorentz forces on these charged particles. When a moving charged particle is subjected to a magnetic field, that charged particle experiences a force called the Lorentz force according to the following equation:

$$\vec{F} = q(\vec{V} \times \vec{B})$$

The Lorentz force ($\vec{F}$) depends on the strength of the magnetic field ($\vec{B}$), the velocity of the charged particle ($\vec{V}$), and the charge of the particle (q). Since the direction of the applied Lorentz force is the result of the cross product of the velocity, magnetic field strength, and the sign of the charge q, positive and negative particles will have an induced Lorentz force in opposite directions. **Figure 1** provides a simplified illustration of the concept. Herein, we develop methodologies to carryout fundamental studies and a deeper understanding on the potential that applied magnetic fields can have on the overall enhancement of photovoltaic efficiencies. Novel variable magnetic field sample cells were constructed to pair with transient absorption spectroscopy measurements to systematically evaluate the influence of magnetic field strength and

direction on the lifetimes and degree of charge separated states.
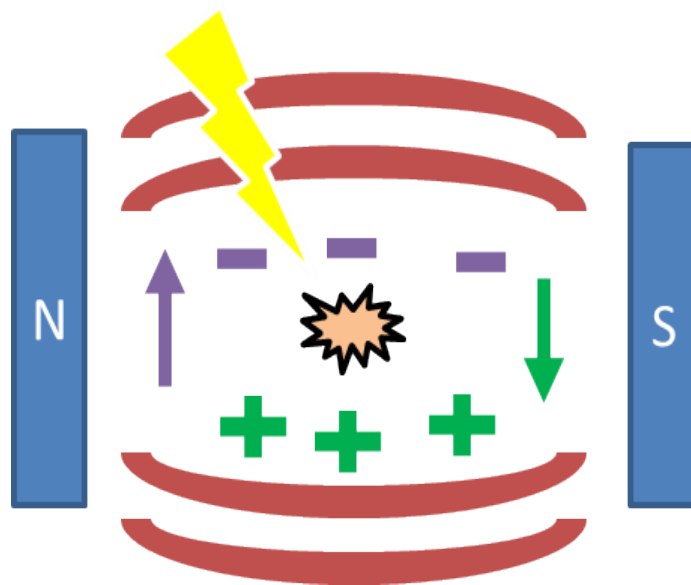

Figure 1: Simplified illustration of Lorentz force on photoinduced charge carriers.

Approach

In our work, we aim to quantify the influence of the magnetic field strength and direction on charge recombination mitigation to increase the solar conversion efficiency of perovskite solar cells. By evaluating various perovskite thin films under fixed illumination and under various external magnetic field strengths and directions, the influential factors and magnitude of performance enhancement can be ascertained. Additionally, slight differences in enhancement between different perovskite solar cells provide insight into the influence of electron transfer pathways and interfaces on the recombination of electrons and electron holes within an applied magnetic field. Furthermore, the alteration of the charge transfer pathway by the influence of an externally applied magnetic field can be evaluated to provide more fundamental insight into these systems, **Figure 2**. We leveraged a custom built variable magnetic field sample cell in conjunction with

UV/visible transient absorption spectroscopy (UV/Vis TAS) to monitor electronic state absorption differences on the femtosecond time scale. This information provides an understanding of the electron transfer pathways, quantity of electron transfer, and lifetimes of charge separated states.
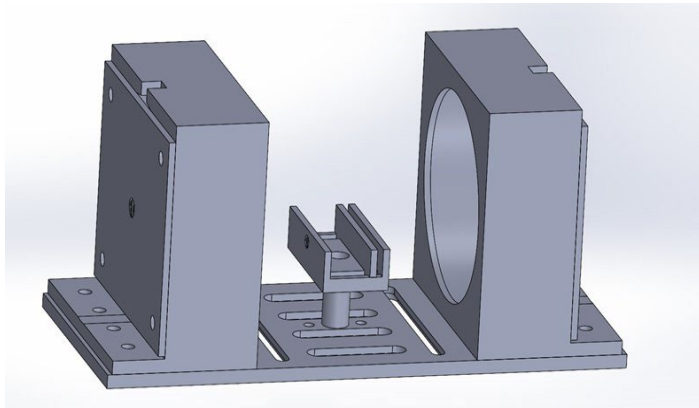

Figure 2: Illustration of applied variable magnetic field sample cell.

To assist in identifying spectral features found in the transient absorption spectroscopy measurements, time domain density function theory (TD-DFT) calculations will be performed to predict the energy of different electronic transitions within the materials. To enable transient absorption measurements, thin film perovskite materials are needed to provide systems for study. Various methodologies are employed, including electrophoretic deposition, spray casting, magnetron sputtering, and spin casting to produce viable samples for evaluation. **Figure 3** illustrates one of these samples.

Figure 3: Perovskite thin films with various concentrations of $CsPbBr_3$.

Accomplishments

- Designed and produced a novel variable magnetic field sample cell for transient absorption spectroscopy measurements
- Synthesized core shell perovskite nanoparticles for transfer dynamic measurements
- Established spray coating techniques to produce homogenous and phase pure perovskite thin films
- Developed electrophoretic deposition techniques for the evaluation of perovskite thin films
- Submitted invention disclosure on a novel photovoltaic device
- Characterized photovoltaic cell performance in applied variable magnetic fields

Intellectual Property

Ward, P.; SRS-22-008, BSRA-228-S

Team Members

Zachary Duca, Rachel Lindvall[a], Chris Pakhanyan[a], Nicholas Porcellino[a], Joseph Teprovich[a], Alex Robb

[a] *California State University Northridge*

Development of an Advanced Compact Nuclear Detector with Ultra-High Energy Resolution

Utpal Roy

The presence of a high density of performance-limiting defects along with compositional inhomogeneity in $Cd_{1-x}Zn_xTe$ restricts the materials ability to achieve ultra-high-resolution germanium-like detector performance. CdZnTeSe successfully mitigates these "killer" defects and provides improved homogeneity. Our goal is to achieve <0.6% energy resolution for 662-keV gamma rays by purifying the material.

Introduction

The development of $Cd_{1-x}Zn_xTe$ (CZT) has been revolutionary in the semiconductor industry, especially for X-ray and gamma-ray radiation detector applications. However, due to the presence of high concentrations of performance-limiting intrinsic defects, such as Te inclusions and sub-grain boundary networks, along with compositional inhomogeneity, CZT has been unable to achieve ultra-high-resolution detector performance. The newly discovered material, CdZnTeSe, was found to be free from sub-grain boundary networks with reduced density of Te inclusions and possess better compositional homogeneity. These properties ensure spatial charge collection homogeneity, which is an essential parameter to achieve ultra-high energy detector resolution at lower production cost. Because of the excellent material quality, the detectors produced from as-grown CdZnTeSe ingots showed an energy resolution of 1±0.1% at 662 keV for 10-mm-thick Frisch grid geometries. The best energy resolution obtained was 0.77 % at 662 keV. However, the material showed the presence of a high concentration of performance-limiting deep level impurities responsible for degrading the detector energy resolution. The starting material CdSe was found to be the main source of the impurities in the resulting CdZnTeSe. To study the effects of point defects, we performed Photo-Induced Current Transient Spectroscopy (PICTS) for estimating the energy levels, concentrations and capture cross-sections of electrically active carrier traps present in CdZnTeSe. The goal is to grow CdZnTeSe with higher purity starting material (CdSe). We have already acquired higher purity CdSe from an established vendor based on a special request. Such purity of CdSe is not otherwise available in the commercial marketplace.

Approach

The approach to achieve ultra-high energy resolution CdZnTeSe detectors is to grow the crystals with higher purity starting material. Most of the present day CdZnTeSe material contains high concentrations of extrinsic impurities, which are responsible for deep levels within the band-gap of the material and represent the foremost cause for degradation in detector performance. The high concentrations of impurities are mainly from the CdSe starting material and have been encountered by crystal growers around the globe. We have been successful in acquiring high-purity CdSe from an established vendor based on a special request. The results of Glow Discharge Mass Spectroscopy (GDMS) of CdSe showed higher purity as compared to conventional Traveling Heater method (THM) grown CdZnTeSe, as shown in **Table 1**.

6N purity $Cd_{0.9}Zn_{0.1}Te_{0.98}Se_{0.02}$ grown by THM	Ingot #1		Ingot #2	
	Element	Concentration [ppb at]	Element	Concentration [ppb at]
	Cr	<20	Cr	36
	Fe	42	Fe	42
	Ni	<4	Ni	16
	Cu	22	Cu	<4
	Sn	<100	Sn	<100
	Pb	10	Pb	11

CdSe raw material	Element	Concentration [ppb at.]
	Cr	<9
	Fe	34
	Ni	3.3
	Cu	<2
	Sn	<80
	Pb	<2

Table 1: Impurity concentrations of THM grown CdZnTeSe and CdSe raw material

The THM is a self-purifying technique since Te is known to be an effective agent for gettering impurities, and it is expected to absorb many impurities from the feed material. Thus, the purity level of THM-grown CZTS is expected to be much higher as compared to the purity of CdSe raw material. It is worth noting that high-purity CdZnTe starting materials are available and standard even for industrial production of CdZnTe detector material. The energy levels, concentrations, and capture cross-sections of different electronically active defect levels for THM grown and vertical Bridgman grown CZTS samples have been quantified using the PICTS technique in collaboration with the University of South Carolina. **Figure 1** shows a typical PICTS spectrum of a THM-grown CZTS detector grade sample and Arrhenius plots of the two dominant detected levels named T_1 and T_2. A straight-line fitting to the plots revealed activation energies of 0.16 eV and 1.14 eV measured with respect to the conduction band minimum corresponding to the peaks T_1 and T_2, respectively. The concentration and capture cross-section of the shallow defect T_1 is found to be 1.61 $\times 10^{10}$ cm^{-3} and 5.91 $\times 10^{-20}$ cm^2, respectively. For the deep level T_2, the values are 1.08 $\times 10^{11}$ cm^{-3} and 6.42 $\times 10^{-12}$ cm^2, respectively. The values will be compared for THM-grown CZTS ingots using higher purity starting material and will be correlated with the detector performance.
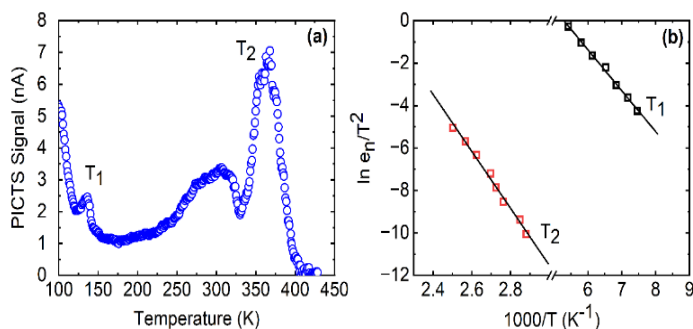

Figure 1: *(a)* A PICTS spectrum obtained for a THM-grown Cd$_{0.9}$Zn$_{0.1}$Te$_{0.98}$Se$_{0.02}$ detector. *(b)* Arrhenius plots corresponding to peaks T_1 and T_2. The solid lines are the linear fits to the Arrhenius plots.

Accomplishments

- Prepared high-purity CdSe in collaboration with an external vendor on special request. The stated purity of CdSe is not available commercially.
- Estimated the energy levels, concentrations and capture cross-sections of electrically active defects present in both vertical Bridgman and THM grown CdZnTeSe.

- Fabricated two-inch diameter quartz ampoules for THM growth of detector-grade CdZnTeSe.
- Developed a convolutional neural network to analyze individual pulses from room-temperature CdZnTeSe radiation detectors.

Peer-reviewed Publications

Rejhon, M.; Dědič, V.; Grill R.; Roy, U.N.; Franc, J.; James, R.B.; Low-Temperature Annealing of CdZnTeSe under Bias. *Sensors* 2021, *22*, 171. https://doi.org/10.3390/s22010171.

Chaudhuri, S.K.; Kleppinger, J.W.; Karadavut, O.F.; Nag, R.; Panta, R.; Agostinelli, F.; Sheth, A.; Roy, U.N.; James, R.B.; Mandal,K.C.; Synthesis of CdZnTeSe single crystals for room temperature radiation detector fabrication: mitigation of hole trapping effects using a convolutional neural network. *J. Mat. Sc.: Materials in Electronics* 2022, *33*, 1452. DOI 10.1007/s10854-021-07623-6.

Roy, U.N.; Baker, J.N.; Camarda, G.S.; Cui, Y.; Yang, G.; James, R.B.; Evaluation of crystalline quality of traveling heater method (THM) grown Cd$_{0.9}$Zn$_{0.1}$Te$_{0.98}$Se$_{0.02}$ crystals. *Appl. Phys. Lett.* 2022, *120*, 242103. (Selected as Featured Article). https://doi.org/10.1063/5.0093255.

Dedic, V.; Franc, J.; Moravec, P.; Grill, R.; Elhadidy, H.; Sima, V.; Cieslar, M.; Roy, U.N.; James, R.B.; Electro and Electro-Photo Plasticity of CdZnTeSe and CdZnTe", *Materials Today Communications*, submitted August 15, 2022 (under review).

Roy, U.N.; Camarda, G.S.; Cui, Y.; Yang, G.; James, R.B.; Study of the growth interface for CdTeSe crystals grown by the THM technique", *Crystals*, submitted September 2, 2022 (under review).

Roy, U.N.; Camarda, G.S.; Cui, Y.; Yang, G.; James, R.B.; "Performance Study of virtual Frisch grid CdZnTeSe detectors", *Instruments*, submitted August 28, 2022 (under review).

Team Members

Jonathon Baker, Giuseppe Camarda[a], Sandeep Chaudhuri[b], Yonggang Cui[a], Vaclav Dedic[c], Jan Franc[c], and Ritwik Nag[b] and Krishna Mandal[b], Ge Yang[d]

[a] Brookhaven National Laboratory
[b] University of South Carolina
[c] Charles University, Czech Republic
[d] North Carolina State University

Austin Stanfield

Advanced Plasticity Theory and Machine Learning Technology for Determining Burst Strength of High Pressure Vessels

Xiankui Zhu

This work developed an advanced strength theory, obtained an exact solution, performed sixty finite element analyses, and created machine learning models of burst pressure from a combined experimental and numerical database. New models can predict more accurate burst strength of pressure vessels, improve their design and operation, and ensure safety and reliability of these energy infrastructures.

Introduction

Pressure vessels and pipelines, made of steels and subject to high internal pressure, are critical infrastructures for storage and transportation of hazardous liquid, natural gas, or other fluids for energy systems. Their maximum pressure bearing capability characterized by burst strength is essential in the structural design, safe operation, and integrity management in practices. Current industry codes or standards were empirically developed from limited experiments on particular steels or a simple strength theory and did not accurately determine the burst strength. This includes ASME Boiler and Pressure Vessel Code, ASME B31.G, Modified B31.G and RSTRENG® models. However, those codes use either the classical Tresca or von Mises strength theory without considering plastic flow effect of metals. Thus, a significant error can be resulted from an estimation scheme in these codes.

An advanced plasticity theory is desired for developing a more accurate burst pressure solution with consideration of the plastic flow or strain hardening effect. Alternatively, the plastic flow theory should be used to determine an exact burst pressure solution, but some complicated mathematical calculations and integrations have to be overcome. In addition to theoretical modeling, elastic-plastic finite element analysis (FEA) may be carried out for a case-by-case investigation or for a parametric study on different pressure vessels or line pipes. With the FEA results, supplemented by existing full-scale burst test data for pressure vessels, machine learning modeling may be explored for a wide range of pressure vessels with various geometries and materials using the artificial neural network (ANN) technology.

Approach

This work adopted a combined technical approach of theoretical, numerical, and experimental analyses with a goal to achieve the project objectives. Full-scale burst test data were collected from literature, and three small tubes for Grade-B steel are prepared to pressure test at Savannah River National Laboratory (SRNL). An advanced strength theory was developed in terms of Zhu-Leis yield criterion, and the associated burst solution was obtained for thin and thick-walled pressure vessels. In the meantime, an exact solution of burst pressure was obtained using the flow theory of plasticity for pressure vessels in power-law hardening materials. Both theoretical solutions were evaluated using burst test data for large-diameter pipes and small-diameter tubes. To supplement the test database, numerical burst data were determined using the commercial software ABAQUS from 2D and 3D elastic-plastic finite element analyses (FEA, see **Figure 1**) for a well-designed matrix of 60 vessel cases covering a wide range of pipeline geometries and steel grades, where Python and Matlab codes were written to generate FEA input files and extract/analyze FEA burst pressures, see flowchart in **Figure 2**.

Based on the large database containing measured and numerical burst pressures, machine learning models were explored using ANN architectures, **Figure 3**, for predicting burst strength. Microsoft Excel Solver was used to create ANN models with one or two hidden layers, while Matlab was utilized to create and optimize ANN architectures with multiple hidden layers through deep learning. Typically, an ANN may have multiple input variables, but only one output variable, i.e., burst pressure. **Figure 4** compares three machine learning predictions with regression results, exact burst solutions and measured test data.
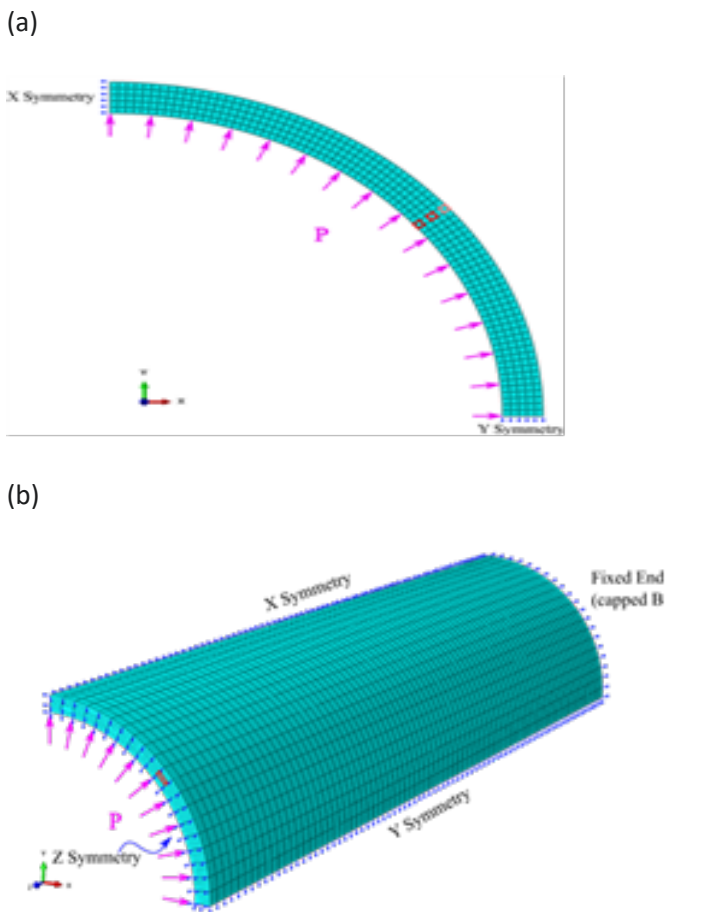
(a)

(b)

Figure 1: Finite element models of end-capped pressure vessel: (a) 2D model, and (b) 3D model
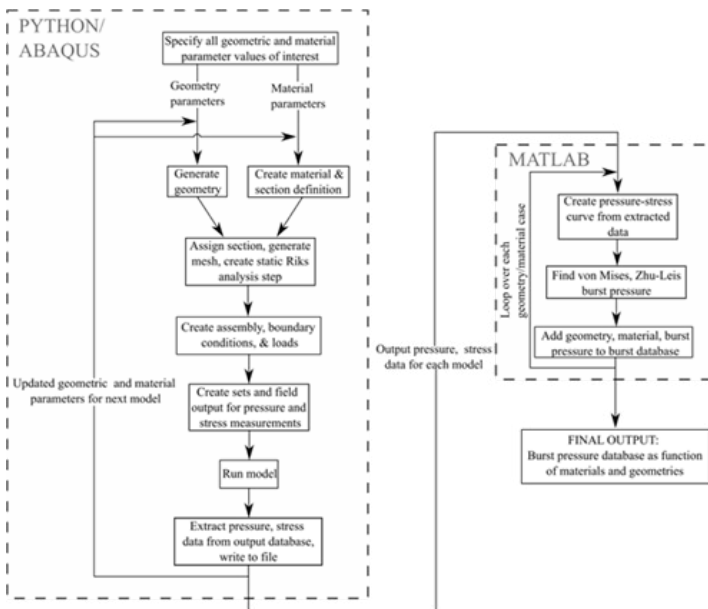

Figure 2: Flowchart of Python and Matlab codes to generate ABAQUS input files and extract/analyze burst pressure data
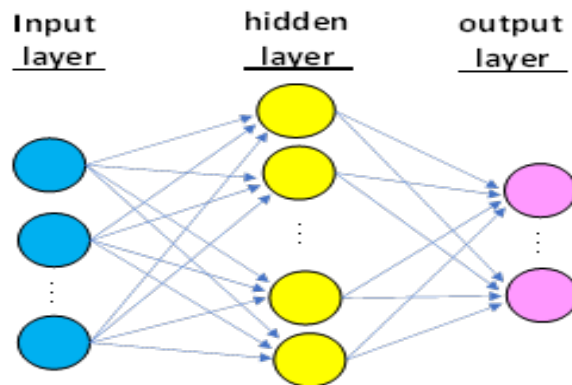

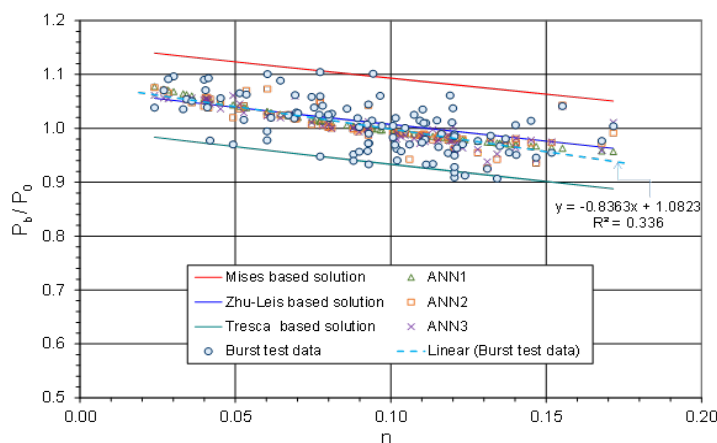**Figure 3:** Illustration of a typical artificial neural network model

Figure 4: Comparison of machine learning predictions with regression results, exact burst solutions and measured test data (ANN1 has 1 input variable and 1 hidden layer with 3 hidden neurons; ANN2 has 3 input variables and 1 hidden layer with 5 hidden neurons; ANN3 has 3 input variables, two hidden layers with 3 hidden neurons for the first hidden layer and 2 hidden neurons for the second hidden layer)

Accomplishments

- Collected a large database of about 300 burst pressure tests for a wide range of pressure vessels from small diameter tubes to large diameter line pipes in carbon steels.
- Developed an advanced strength theory and determined a more accurate burst strength solution for both thin and thick-walled pressure vessels. This new solution filled the technical gap and provided an improved formula for structural design and integrity assessment.
- Obtained an exact solution of burst strength for thick-walled pressure vessels in a power-law hardening material using the flow theory of plasticity for ductile metals. This exact solution verifies the proposed

advanced strength theory and the associated burst pressure solution.

- Developed a Python script-based FEA code and obtained the FEA results for 60 matrixes of thin and thick-walled pressure vessels and pipes in various pipeline steels. The FEA results are consistent with those predicted by the existing thin-wall model and the proposed thick-wall model.
- Developed machine learning models of burst strength for large-diameter defect-free pipelines using Microsoft Excel Solver. Machine learning models improve the existing analytical models.
- The machine learning models of burst strength are to be optimized using Matlab with combined test and numerical database for a variety of pipelines. Compared to a regression tool, Matlab is easy to use to develop a deep learning prediction model for a large database with multiple variables.
- Burst pressure tests are underway for small-diameter (2 inches) tubes with three different thick-walls (D/t = 5.8, 9.2, 13.0) in Grade B steel. Its tensile properties will be also measured.
- Published five conference papers and two journal papers with two other journal papers submitted.

Peer-reviewed Publications

Zhu X.-K.; Wiersma B.; Sindelar B.; Johnson W.R. New Strength Theory and Its Application to Determine Burst Pressure of Thick-Wall Pressure Vessels, *Proceedings of ASME Pressure Vessel and Piping Conference*, July 18-22, 2022, Las Vegas, USA. PVP2022-84902.

Zhu X.-K.; Johnson W.R.; Sindelar B.; Wiersma B. Machine Learning Models of Burst Strength for Defect-Free Pipelines, *Proceedings of ASME Pressure Vessels and Piping Conference*, July 18-22, 2022, Las Vegas, USA. PVP2022-84908.

Zhu X.-K.; Zhu J.B.; Duncan A. Data-Driven Stress Intensity Factor Solution for Axial Outside Surface Cracks in Thick-Wall Cylinders, *Proceedings of ASME Pressure Vessels and Piping Conference*, July 18-22, 2022, Las Vegas, USA. PVP2022-86164.

Zhu X.-K.; Wiersma B. Progress of Assessment Model Development for Determining Remaining Strength of Corroded Pipelines, *Proceedings of ASME International Pipeline Conference*, September 25-30, 2022, Calgary, Canada. IPC2022-86922.

Zhu X.-K. Improved Fracture Toughness Test Method for Single Edge Notched Tension Specimens in Clamped-End Conditions, *Proceedings of ASME International Pipeline Conference*, September 25-30, 2022, Calgary, Canada. IPC2022-86927

Zhu X.-K., Lam P.S.; Chao Y.J. Constraint-dependent CTOA determination for stable ductile crack growth, *Engineering Fracture Mechanics*, 271, 2022: 108651.

Zhu X.-K.; Johnson W.R.; Sindelar B; Wiersma B. Artificial neural network models of burst strength for defect-free pipelines, *Journal of Pipeline Science and Engineering*, 2, 2022: 100090.

Zhu X.-K.; Wiersma B.; Sindelar B.; Johnson W.R. Burst pressure prediction of thin-wall and thick-wall pressure vessels, submitted to *Journal of Pressure Vessel Technology*, in review.

Johnson W.R.; Zhu X.-K.; Sindelar B. A parametric finite element study for determining burst strength of thin and thick-walled pressure vessels, submitted to *International Journal of Pressure Vessel and Piping*, in review.

Team Members

William Johnson, Bruce Wiersma, and Robert Sindelar

FY22
LABORATORY DIRECTED
RESEARCH & DEVELOPMENT
ANNUAL REPORT

SRNL®
SAVANNAH RIVER NATIONAL LABORATORY

www.srnl.doe.gov